INSTITUTO POLITÉCNICO NACIONAL

Centro de Investigación en Ciencia Aplicada y Tecnología Avanzada

Unidad Querétaro

"Modeling of hybrid fusion/fission systems for development of advanced nuclear fuel cycles."

TESIS

QUE PARA OBTENER EL GRADO DE

DOCTOR EN ENERGÍAS ALTERNATIVAS

P R E S E N T A:

José Humberto Salazar Cravioto

DIRECTOR DE TESIS:

DR. MARTÍN DE JESÚS NIETO PÉREZ

QUERÉTARO, QRO. MÉXICO. **Septiembre, 2020.**

SIP-13
REP 2017

INSTITUTO POLITÉCNICO NACIONAL
SECRETARIA DE INVESTIGACIÓN Y POSGRADO

ACTA DE REGISTRO DE TEMA DE TESIS
Y DESIGNACIÓN DE DIRECTOR DE TESIS

Ciudad de México, a 3 de septiembre del 2020

El Colegio de Profesores de Posgrado de **CICATA Unidad Querétaro** en su Sesión **ordinaria** No. **200902** celebrada el día **2** del mes **septiembre** de **2020**, conoció la solicitud presentada por el alumno:

Apellido Paterno:	Salazar	Apellido Materno:	Cravioto	Nombre (s):	José Humberto

Número de registro: B 1 6 0 9 8 9

del Programa Académico de Posgrado: Doctorado en Tecnología Avanzada

Referente al registro de su tema de tesis; acordando lo siguiente:

1.- Se designa al aspirante el tema de tesis titulado:

Modeling of hybrid fusion/fission systems for development of advanced nuclear fuel cycles.

Objetivo general del trabajo de tesis:

El objetivo general de este trabajo es modelar un sistema de reactor híbrido fusión-fisión, capaz de enriquecer en 18 meses o menos al menos 64 ensambles de combustible de un reactor PWR, inicialmente cargados con torio (ThO_2) a un isotopo de uranio (^{233}U) al 4%, manteniendo la auto alimentación de tritio para la fuente de neutrones.

2.- Se designa como Directores de Tesis a los profesores:

Director: Dr. Martín de Jesús Nieto Pérez

2° Director:

No aplica: ☐

3.- El Trabajo de investigación base para el desarrollo de la tesis será elaborado por el alumno en:

Centro de Investigación en Ciencia Aplicada y Tecnología Avanzada, CICATA-Unidad Querétaro

que cuenta con los recursos e infraestructura necesarios.

4.- El interesado deberá asistir a los seminarios desarrollados en el área de adscripción del trabajo desde la fecha en que se suscribe la presente, hasta la aprobación de la versión completa de la tesis por parte de la Comisión Revisora correspondiente.

Director de Tesis

Dr. Martín de Jesús Nieto Pérez

Aspirante

José Humberto Salazar Cravioto

2° Director de Tesis

Presidente del Colegio

Dr. Juan Bautista Hurtado Ramos

INSTITUTO POLITÉCNICO NACIONAL
CENTRO DE INVESTIGACIÓN EN
CIENCIA APLICADA
Y TECNOLOGÍA AVANZADA
UNIDAD QUERÉTARO
DIRECCIÓN

SIP-14
REP 2017

INSTITUTO POLITÉCNICO NACIONAL

SECRETARÍA DE INVESTIGACIÓN Y POSGRADO

ACTA DE REVISIÓN DE TESIS

En la Ciudad de Queretaro siendo las 14:00 horas del día 24 del mes de agosto del 2020 se reunieron los miembros de la Comisión Revisora de la Tesis, designada por el Colegio de Profesores de Posgrado de: CICATA QRO para examinar la tesis titulada:

Modeling of hybrid fusion/fission systems for development of advanced nuclear fuel cycles

del (la) alumno (a):

Apellido Paterno:	Salazar	Apellido Materno:	Cravioto	Nombre (s):	José Humberto

Número de registro: A 1 6 0 9 8 9

Aspirante del Programa Académico de Posgrado: DOCTORADO EN TECNOLOGÍA AVANZADA

Una vez que se realizó un análisis de similitud de texto, utilizando el software antiplagio, se encontró que el trabajo de tesis tiene __4__ % de similitud. **Se adjunta reporte de software utilizado.**

Después que esta Comisión revisó exhaustivamente el contenido, estructura, intención y ubicación de los textos de la tesis identificados como coincidentes con otros documentos, concluyó que en el presente trabajo **SI** [ ] **NO** [X] **SE CONSTITUYE UN POSIBLE PLAGIO.**

JUSTIFICACIÓN DE LA CONCLUSIÓN: *(Por ejemplo, el % de similitud se localiza en metodologías adecuadamente referidas a fuente original)*

El porcentaje de 4 de similitud es debido a las referencias citadas por concepto de figuras o tablas que apoyan el desarrollo del programa de posgrado, respetando la autoría de los mismos haciendo la referencia correspondiente en la sección de referencias dentro de la tesis.

**"Es responsabilidad del alumno como autor de la tesis la verificación antiplagio, y del Director o Directores de tesis el análisis del % de similitud para establecer el riesgo o la existencia de un posible plagio.

Finalmente, y posterior a la lectura, revisión individual, así como el análisis e intercambio de opiniones, los miembros de la Comisión manifestaron **APROBAR** [X] **SUSPENDER** [ ] **NO APROBAR** [ ] la tesis por **UNANIMIDAD** [X] o **MAYORÍA** [ ] en virtud de los motivos siguientes:

El trabajo de posgrado con la finalización de la tesis escrita es motivo para la aprobación y la solicitud de fecha de examen para la obtención del grado de doctor en Energías Alternativas.

COMISIÓN REVISORA DE TESIS

Dr. Martin de Jesús Nieto Pérez
Director de Tesis
Nombre completo y firma

Dr. Gonzalo Alonso Ramos Lopez
Nombre completo y firma

Dr. José Joel González Barbosa
Nombre completo y firma

Dr. Swadesh M. Mahajan
2° Director de Tesis (en su caso)
Nombre completo y firma

Dr. Raul Alejandro Avalos Zúñiga
Nombre completo y firma

Dr. Alejandro Alfredo Torres Guzmán
Nombre completo y firma

PRESIDENTE DEL COLEGIO DE PROFESORES

CENTRO DE INVESTIGACIÓN EN CIENCIA APLICADA Y TECNOLOGÍA AVANZADA
UNIDAD QUERÉTARO
DIRECCIÓN

INSTITUTO POLITÉCNICO NACIONAL

SECRETARÍA DE INVESTIGACIÓN Y POSGRADO

CARTA CESIÓN DE DERECHOS

En la **Ciudad de México, D.F.** el día **3** del mes de **septiembre** del año **2020**, el que suscribe **José Humberto Salazar Cravioto** alumno del Programa de **Doctorado en Tecnología Avanzada**, con número de registro **A160989**, adscrito al **Centro de Investigación en Ciencia Aplicada y Tecnología Avanzada unidad Querétaro**, manifiesto que es el autor intelectual del presente trabajo de Tesis bajo la dirección del **Dr. Martín de Jesús Nieto Pérez** y cede los derechos del trabajo titulado "**Modeling of hybrid fusion/fission systems for development of advanced nuclear fuel cycles"**, al **Instituto Politécnico Nacional** para su difusión, con fines académicos y de investigación.

Los usuarios de la información no deben reproducir el contenido textual, gráficas o datos del trabajo sin el permiso expreso del autor y/o director del trabajo. Este puede ser obtenido escribiendo a la siguiente dirección **m.nieto@ieee.org**. Si el permiso se otorga, el usuario deberá dar el agradecimiento correspondiente y citar la fuente del mismo.

Nombre y firma del alumno(a)

Abstract.

Two main critical applications of fast neutrons can be performed over nuclear industry, in one hand the necessity of spent fuel´s burning minor actinides and in the other, the possibility of breeding fissile material of fertile isotopes. In a fusion reaction between deuterium and tritium, among other reactions, nuclei yields a 14.5 MeV energy neutron. These very energetic neutrons can easily convert for instance 238U and 232Th isotopes (fertile material) into 239Pu and 233U isotopes (fissile material), and also the destruction of minor actinides such as Pu, Np, Am and Cm which are present in the spent fuel, reducing significantly its radiotoxicity. Nevertheless, economy of neutrons becomes critical as per each neutron generated in the fusion reaction, one neutron is consumed by tritium, 6Li nucleus and a neutron are required to generate tritium in the nuclear reactions, that is why an effective hybrid reactor model is necessary. MCNP and SCALE codes are widely used around the world and in this work are used in conjunction characterizing the flux of neutrons that are generated from a low aspect ratio machine known as tokamak to the rest of zones of the hybrid reactor. A transport code such as ASTRA is also part of this hybrid reactor modeling tasks which can be used in the determination of densities and temperatures of the volume plasma profiles. MCNP main task is about the evaluation of the flux of neutrons given this external neutron source. Once the neutron flux is known, ORIGEN, part of the SCALE code suite for model and simulation of nuclear safety design and analysis, is used to evaluate the creation and destruction of isotopes given the cross sections, an initial composition and the energy-resolved neutron flux.

An internal tool was developed to link the nuclear codes used for this purpose with all nuclear data and to build a hybrid reactor model for the simulation. Fusion-Fission HYBrid (FFHYB) is the tool that helps to build an MCNP input reactor model, geometry, data specification, material specification, neutron source definition, and tally specification. The ORIGEN inputs are also built by the tool. Linking and communicating inputs and outputs between these codes is an integral part of the simulation of fuel assemblies irradiated by fast neutrons coming from a fusion plasma. This fusion and fission concept as a hybrid reactor, with a plethora source of fast neutrons, can be performed as a qualitatively tool opening “new” cycles for the transmutations of nuclear fertile material into fissile fuel and for the spent fuel burning actinides. One of the advantages of this concept is the possibility of having a total reprocessing free (ReFree) conversion fuel cycle. ^{232}Th–^{233}U is selected as the case study for this thesis. Virgin fuel assemblies are exposed to tokamak neutron source in the hybrid rector filled with fertile fuel rods, these same assemblies can be then burned into a traditional thermal water reactor, avoiding violating the fuel rods integrity. This “new” technic with a highly capacity to be a proliferation-resistant mode for the production of nuclear fissile fuel, which is a different way from dominated reprocessing path via the standard UREX/PRUREX processes, this can be of a great acceptance to the nuclear industry for the production of fissile material, helping with scarcity of ^{235}U naturally available, augmenting nuclear fuel reserves without throttling the nuclear energy expansion.

Summary

This thesis is an exploratory study on the concept of Hybrid Nuclear Reactors as advanced Nuclear Cycle, i.e. how a model simulation changes materials compositions in different levels of its performance and its abstraction. The main idea of this analysis is the important effect of change in neutron fluxes abstraction in the hybrid reactor zones allowing a good understanding of how the affectation of these changes might affect then the materials compositions in a simulation scheme model. The thesis consists of eight chapters, representing both results theoretical and simulations (case of studies) conjointly. The thesis is classified in five parts (introduction, the chapters, conclusion, future work, references and annexes), each of which is described in the following paragraphs.

Acknowledgement

Firstly, to my advisor Prof. Martín de Jesús Nieto Pérez, I am glad to express my gratitude and sincere recognition of the continuous support working in my Ph. D. program with its related research, Dr. Martin is so patience, always motivated, and he has an immense knowledge in the subject. He is also a good leader because his guidance all the time in the research and writing of the thesis was so helpful.

Secondly, but not less important to my co-advisor Prof. Swadesh M. Mahajan for his enormous contribution to the realization of this project. As a student exchange program, I was working several months at the University of Texas at Austin, where Dr. Mahajan is a professor at the Institute for Fusion Studies. During this time, Dr, Mahajan provided me with all the tools and knowledge required to start the Ph. D. program, as well as all the kindness in my first visit to Austin.

I also have to thank the members of my PhD committee, Professors Gonzalo A. Ramos López, Raúl A. Ávalos Zúñiga, José. J. González Barbosa and Jorge Pineda Piñón for their helpful career advice and suggestions in general.

Of course to the Instituto Politécnico Nacional, at CICATA Querétaro for all the facility support to make possible the realization of this project. All the professors, academics, administrative, and all personnel support in general.

To the Consejo Nacional de Ciencia y Tecnología (CONACyT) for the scholarship budget that was crucial for the tasks developed in the Ph. D. program.

Finally to all my family and friends, their love and understanding really help me to continue in this awesome adventure and endeavor.

Keywords

Nuclear Hybrid Reactors, Advanced Nuclear Cycle, Nuclear Fusion, Nuclear Fission, Light Water Reactors (LWRs), Pressure Nuclear Reactors (PWRs), Boiling Water Rectors (BWRs), Minor Actinides, Tritium Breeding Materials, Isotope Decay Chains, Spent Nuclear Fuel, Neutron Irradiation, Spherical Tokamaks, Fuel Assemblies.

Table of Contents

List of Figures

List of Tables

Abbreviations and Acronyms

AB	Actinide-Burning
ANL	Argonne National Laboratory
ATW	Accelerator transmutation of waste
BWR	Boiling water reactor
CD	Current drive
CFNS	Compact fusion neutron source
CICATA	Centro de Investigación en Ciencia Aplicada y Tecnología Avanzada
CS	Center stack
CTF	Components test facilities
DEMO	The DEMOnstration power plant
DOE	Department of Energy
DOE/NE	Department of Energy/Nuclear Energy Office
D-T	Deuterium Tritium
DT	Density and Temperature
EDTA	Ethylenediaminetetraacetic acid
FBR	Fast breeder reactor
FFHYB	Fusion Fission Hybrid
FFTF	Fast Flux Test Facility
FP	Fission Product
GCDF	Greater Confinement Disposal Facility
HEU	High enriched uranium
HLW	High-level waste
HWR	Heavy-water reactor
IEA	International Energy Agency
IAEA	International Atomic Energy Agency (U.N.)
ILW	Intermediate-level waste
INEL	Idaho National Engineering Laboratory
IPCM	Internal poloidal coil module
IR	Inferred resources
ITER	International Thermonuclear Experimental Reactor
LANL	Los Alamos National Laboratory
LEU	Low enriched uranium
LLW	Low-level wastes
LMFBR	Liquid-metal fast breeder reactor
LMFR	Liquid-metal fast reactors
LMR	Liquid-metal reactor
LWR	Light-water reactor
MA	Minor actinide
MHD	Magnetohydrodynamic
MGD	Mined Geologic Disposal
MOX	Mixed oxide
MSRE	Molten Salt Reactor Experiment
MTU	Metric tons of uranium
NEA	Nuclear Energy Agency
NM	Neutron multiplier
NPT	Nuclear Nonproliferation Treaty (1978)
NRC	Nuclear Regulatory Commission

ORNL	Oak Ridge National Laboratory
PBR	Particle bed reactor
PDF	Probability density function
PFC	Poloidal field coil
PUREX	Plutonium and uranium recovery by extraction
PWR	Pressurized water reactor
RAR	Reasonable assured resources
ReFree	Reprocessing-free
ST	Spherical Tokamak
TBR	Tritium breeding ratio
Tokamak	Toroidal chamber with axial magnetic field
TFC	Toroidal field coil
TRU	Transuranic (wastes/elements)
TRUEX	Transuranic extraction
UOX	Uranium oxide
UT – A	University of Texas at Austin

1 Introduction.

1.1 Background.

1.1.1 Nuclear energy and its importance as an energy source.

A healthy and productive practice in energy policy is the diversification of primary energy source utilization. The planet and its star provide to humankind a broad primary energy sources portfolio: solar energy, wind, internal Earth heat, sea waves, fossil fuels, biomass and nuclear energy. The last one is very young, since it was only discovered less than 100 years ago when Italian scientist Enrico Fermi showed back in 1934 [1] that free thermal neutrons could split many heavy atomic nuclei, liberating large amounts of energy (200 MeV per event, equivalent to 18 GJ/mol). Since its discovery and its unfortunate use for weapons development, nuclear engineering found its way into civilian applications, specifically electric power generation, back in the decade of the 1950s [2].

At present, there are about 440 nuclear power reactors around the world which represent ~10 % of the electricity generated, some 50 more reactors are under construction, 30 countries have at least one nuclear reactor, and some other countries generate at least one quarter of their electrical capacity by nuclear means. In 2018, world nuclear power reactors produced 2563 Terawatt-hour (TWh) of electricity, with a rising trend each year. Nuclear power is ranked 4th among the electricity production technologies in terms of quantitative electrical power produced (TWh), as shown in Figure 1.1.

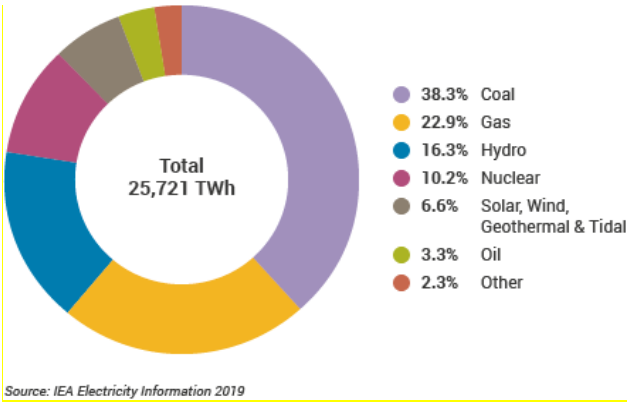

Figure 1.1. 2019 primary power sources used to generate electricity around the world [3].

Generally speaking, nuclear power plants have been considered as base load generating units because of their low fuel cost and the technical limitations on load responsive operation. As world electricity demand rises each year, more base load capacity will be needed. This will have significant implications for the cost of electricity, since it is cheaper to generate base load capacity than having both loads peak and intermediate, so the averaging costs then it is going to be lower than taking into

account the pattern of use nowadays. Besides, if there are increases in the capacity of base load, this will likely must be covered by nuclear power if there are more constrains on carbon emissions in the future. Figure 1.2 represents a possible scenario where base load capacity can replace intermediate and peak load power capacity.

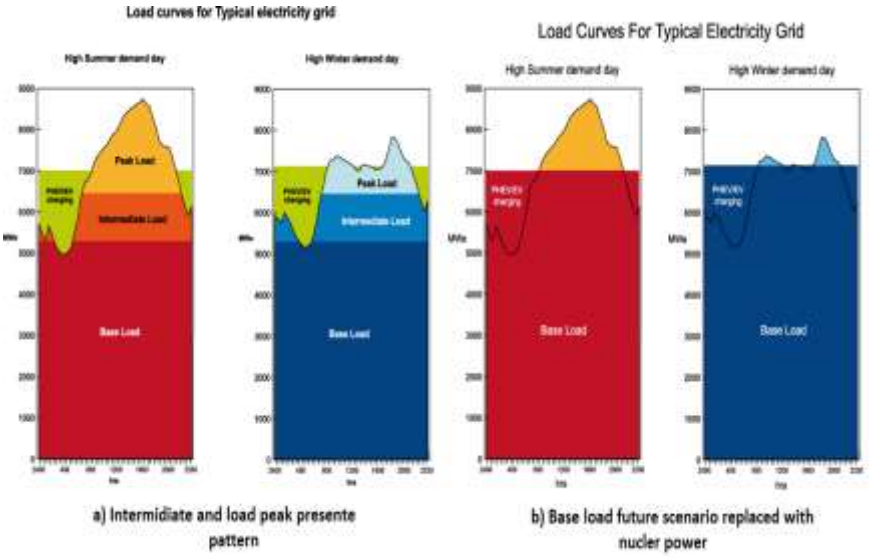

Figure 1.2. a) Present electric grid load pattern, intermediate and load peak use. b) Future possible scenario where base load replaces actual pattern [4].

Since its insertion in the energy production landscape, nuclear power has faced two important challenges: 1) what to do with the highly radioactive nuclear waste [5], and 2) how to transform the natural metals into nuclear fuel capable of "burning" in a nuclear reactor [4]. Other challenges, such as social risk perception associated with the technology and the geopolitical implications on the production and handling of nuclear material are also very relevant [6] but fall outside the scope of the present work. In the next two sections, the challenges associated to fuel availability and waste management will be briefly discussed to contextualize for the reader the goal of the present work within those two challenges.

1.1.2 Nuclear fuel: reserves, production and consumption.

The main natural resource currently used to produce nuclear fuel is uranium metal. The worldwide reasonable assured reserves of uranium mineral are currently on the order of 6 million tons; Table 1.I presents the breakage of these reserves by country. Natural uranium contains two isotopes of uranium: ^{235}U and ^{238}U, with the latter one having an abundance of 99.3%. Of these two isotopes, only one can be split by the impact of a free thermal neutron (a process known as *nuclear fission*), and unfortunately it is the least abundant: ^{235}U. It should be noted here that this isotope is the ONLY natural isotope that is *fissile*, that is, an isotope that can undergo nuclear fission when exposed to thermal neutrons. The other isotope of uranium, ^{238}U, is relevant because it is a *fertile* isotope: this

means that, when exposed to neutrons, this isotope does not undergo fission directly, but it can absorb a neutron and generate a new isotope, which may be fissile. In the particular case of ^{238}U, the process is as follows:

$$^{238}U + n \longrightarrow {}^{239}U \xrightarrow[23\ min]{\beta^-} {}^{239}Np \xrightarrow[2.35\ d]{\beta^-} {}^{239}Pu \tag{1.1}$$

The end product, ^{239}Pu, is an artificial fissile isotope. It is artificial because to exist, the natural ^{238}U isotope needs to be irradiated with neutrons. Upon absorption of one of these neutrons, the resulting ^{239}U undergoes two beta decay events and finally yields ^{239}Pu. In a similar fashion, another abundant natural isotope which is fertile, ^{232}Th, yields a fissile isotope, ^{233}U, when bombarded with neutrons.

Table 1.I. Uranium reserves by country, updated to 2017 [7].

Country	U inventory (tons)	Percent
Australia	*1,818,300*	*29.6*
Kazakhstan	*842,200*	*13.7*
Canada	*514,400*	*8.4*
Russia	*485,600*	*7.9*
Namibia	*442,100*	*7.2*
South Africa	*322,400*	*5.2*
China	*290,400*	*4.7*
Niger	*280,000*	*4.6*
Brazil	*276,800*	*4.5*
Uzbekistan	*139,200*	*2.3*
Ukraine	*114,100*	*1.9*
Mongolia	*113,500*	*1.8*
Botswana	*73,500*	*1.2*
Tanzania	*58,200*	*0.9*
USA	*47,200*	*0.8*
Jordan	*43,500*	*0.7*
Other countries	*280,600*	*4.6*
TOTAL	*6,142,600*	

Now that some important facts about the natural resource associated with the nuclear elements are known, let's draw a parallel with the gasoline in our car. Is it found underground and ready to use upon extraction? No, the gasoline in the car is the product of the transformation of crude oil via a process called refining. Very early in the history of the automobile, engines were able to run with crude oil, but these engines were very inefficient, polluting and did not last as long. Over time, it was found that pre-processing the oil to obtain a better-quality fuel for the engine was beneficial. With the nuclear resources, the history is not so different. The main natural resource for nuclear energy production is uranium ores, as crude oil is the main natural resource to produce gasoline. And just like crude oil, uranium ore needs to follow a series of steps to become nuclear fuel that can be fueled in a nuclear power reactor plant.

Open nuclear fuel cycle is depicted in Figure 1.3 (the qualifier "open" will be addressed later). The first step is uranium mining, which is not so different from mining operations for other metals; the same measures for environment and worker protection associated with heavy metal mining operations must be observed. Additional precautions are necessary due to the existence of high levels of radon in uranium mineral deposits. The result of the uranium mining process is a mixture of uranium oxides powder known as *yellowcake*.

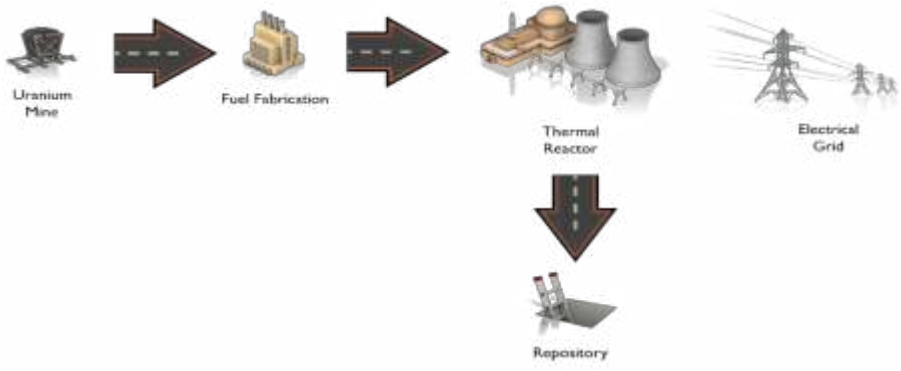

Figure 1.3. The open nuclear fuel cycle.

Although some nuclear reactor designs can operate with natural uranium oxide pellets as fuel, such as the CANDU or RBMK reactors [8], the vast majority of reactors require *enriched* fuel. This means that the uranium oxide needs to have its content of ^{235}U increased from the 0.7% it naturally has, to a level of 3-4%. Since would involve an isotopic separation (selectively remove ^{238}U) chemical processes will not work, so the only alternative are physical separation processes based on mass difference. Currently, the enrichment process involves converting the yellowcake into a gaseous substance containing the metal; uranium hexafluoride, UF_6, is the compound utilized for this purpose. The UF_6 is then passed through a long train of gas centrifuges which accomplish the mass separation by removing some of the gas containing the ^{238}U isotope.

The enriched UF_6 gas is oxidized again to form enriched solid UO_2, which is sintered into ceramic pellets of 1 cm diameter and 1 cm height. These pellets are placed inside zircalloy tubes 4 m in height to form a fuel rod, and square bundles of these fuel rods conform what is called a fuel assembly. Assemblies for pressurized water reactors (PWR) are 17 x 17 rods, while for boiling water reactors (BWR) the fuel assemblies are squares of 9 x 9 rods. This whole process of transforming enriched UO_2 powder into fuel assemblies ready to be placed in the core of a nuclear reactor is known as *fuel fabrication*. A quick calculation tells us that, given the density of 11 g/cm^3 for UO_2, each fuel pellet weights 8.6 g. The 400 pellets on each rod weight 3.5 kg, and a PWR assembly, with its 289 rods, will have approximately 1 ton of fuel. Each PWR reactor has between 150 and 250 assemblies, depending on the power it is designed to produce. This means that the fuel load for a single PWR reactor is between 150 and 250 tons of fuel.

Fuel assemblies stay inside the reactor for a period between 18 and 24 months, after which they undergo a process known as refueling. On each refueling, about 1/3 of the assemblies come out permanently, and 2/3 are reshuffled within the core. Deciding how many and which assemblies will come out, and how the remaining ones will be accommodated within the reactor is not an easy task, and it is the domain of a discipline within nuclear engineering known as *fuel management*. The end result is that between 50 and 80 tons of nuclear material are removed from nuclear reactors every 1.5 to 2 years, so the net consumption of fuel is in the range 25 – 50 tons/yr. Based on the IEA BLUE map scenario [8], with a once through open cycle the reasonable assured resources (RAR) are depleted by 2045, as shown in Figure 1.4. The inferred resources (IR) would be depleted by 2055, when the annual uranium demand is projected to be on the order of 210,000 tons/yr. If the level of usage remains at its present value (no growth), RAR and IR resources will be depleted by 2100.

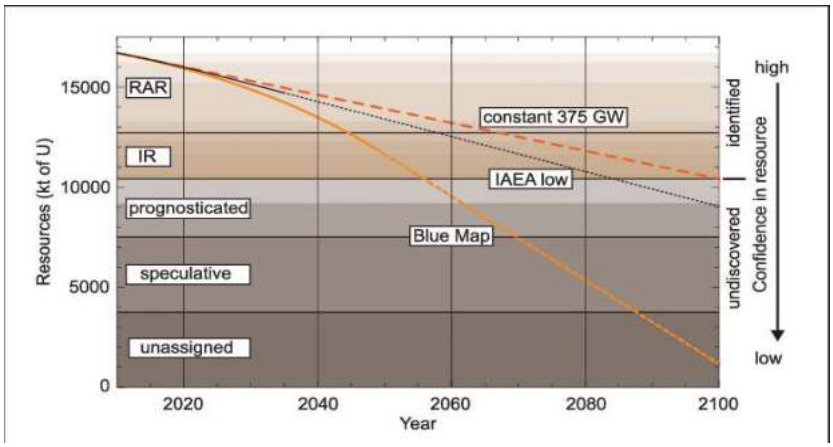

Figure 1.4. Estimated usage of different categories of uranium resources under different scenarios: IEA Blue Map (solid orange), no growth (orange dashed) and IEA low growth (black dashed) [9].

The fate of the fuel material that leaves the reactor after a recharge marks the difference between what is called a *closed cycle* and *open cycle*. Open cycle: spent fuel coming out of the reactor is regarded as waste that needs to be disposed of, hence the term "open cycle". But not everything in the spent fuel is waste: Figure 1.5 shows the composition comparison between fresh fuel and fuel that has been in the reactor for 3 years. It is clear that 94% of the waste mass is inert ^{238}U; to top it off, 2% of the residue is fissile material, which could be used to produce new fuel. In reality, only 4% of the spent fuel is residue, composed primarily of fission products (FP) and actinides that are not fissile.

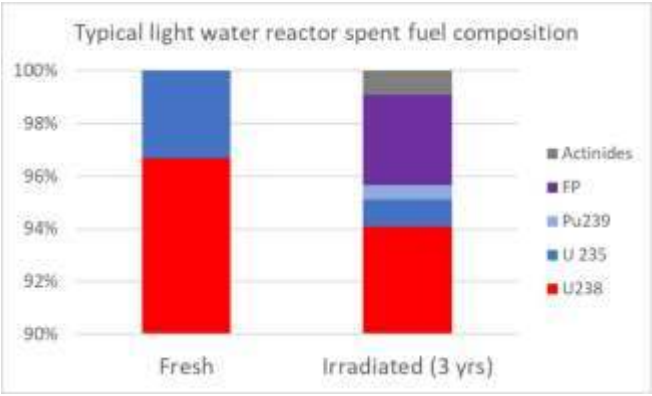

Figure 1.5. Typical composition of spent fuel from light water reactors after 3 years of irradiation.

A closed nuclear fuel cycle, shown in Figure 1.6, involves a step called reprocessing, aimed at extracting the material that may still be useful for the nuclear industry, either fertile or fissile. In this process, the pellets of the fuel assemblies are extracted from the fuel rods and dissolved in nitric acid to obtain all the metals in an aqueous solution. Special solvents, which are chelating agents for U and Pu, are added and mixed with the aqueous solution. Upon separation of organic and aqueous phases, the organic phase will contain most of the uranium and plutonium, and the phase of aqueous contains fission products and any other actinides. The aqueous phase is the real residue on the nuclear

fuel closed cycle, reducing the emission of nuclear material in 96% at the cost of large amounts of water consumption and the risk of additional nuclear material handling after the irradiation. Civilian nuclear reprocessing capacity worldwide is 5,000 tons/year shared among 5 countries (UK, France, Japan, Russia and India), below the 20,000 tons/year generated in the 400 nuclear reactors worldwide.

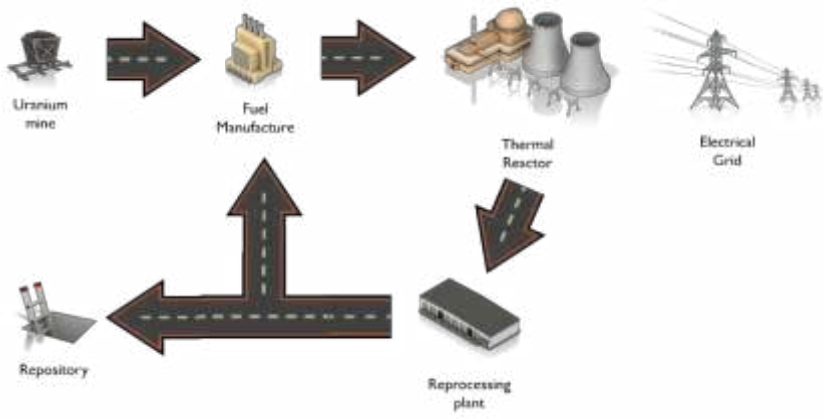

Figure 1.6. Nuclear fuel closed cycle. Cycle is closed by introducing a spent fuel reprocessing facility.

1.1.3 Spent fuel: production and disposition.

As mentioned in the previous section, 94% of the mass in the spent fuel is harmless ^{238}U, which is abundant in nature. An additional 2% is fissile material in the form of ^{235}U and ^{239}Pu, also stable isotopes. This means that most of the energy liberated in form of radiation in the spent fuel comes from 4% of the mass in the spent fuel. Here, that fraction of the spent fuel will be looked at in more detail. Two main groups make up the actual waste in nuclear spent fuel: the minor actinides and the fission products. The minor actinides are any isotopes with atomic number greater than 92 and are a product of successive neutron absorptions, coupled with alpha and beta decay radioactive processes. Table 1.II shows the main minor actinides present in nuclear spent fuel [10]. Most minor actinides are alpha radiation emitters or produce long-lived alpha emitters along their decay chains.

Table 1.II. Main minor actinides present in nuclear spent fuel.

Isotope	*Main decay mode*	*Half-life (y)*	*Energetic γ emitter?*
^{238}Pu	α	87.7	Yes
^{239}Pu	α	24110	No
^{240}Pu	α	6560	Yes
^{241}Pu	β^-	14.4	No
^{242}Pu	α	3.73×10^5	Yes
^{237}Np	α	2.14×10^6	No
^{241}Am	α	432.6	Yes
^{242m}Am	β^-	141	No
^{242}Cm	α	0.5	No
^{243}Cm	α	28.5	Yes
^{244}Cm	α	18.1	No

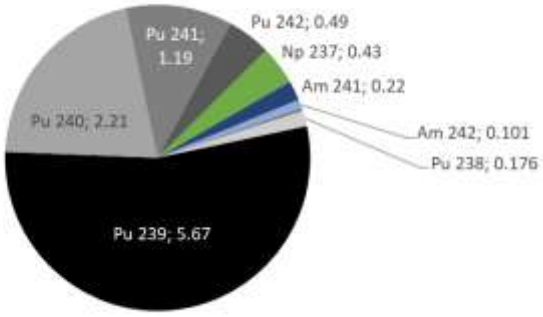

Figure 1.7. Mass in kg of minor actinides present in 1 ton of spent fuel after 3 years of irradiation in a 2 GW PWR reactor [11].

Plutonium accounts for 97.5% of the radioactivity in the spent fuel, with all isotopes except ^{241}Pu contributing significantly. If the plutonium is left in the spent fuel, it will become the main source of toxicity when most fission products have already disappeared. If removed, the residual radioactive toxicity of the waste (due to minor actinides) is reduced by a factor of 7. Figure 1.7 shows the typical mass of each minor actinide in 1 ton of spent fuel, while Figure 1.8 presents the four decay chains associated to the minor actinides present in spent fuel.

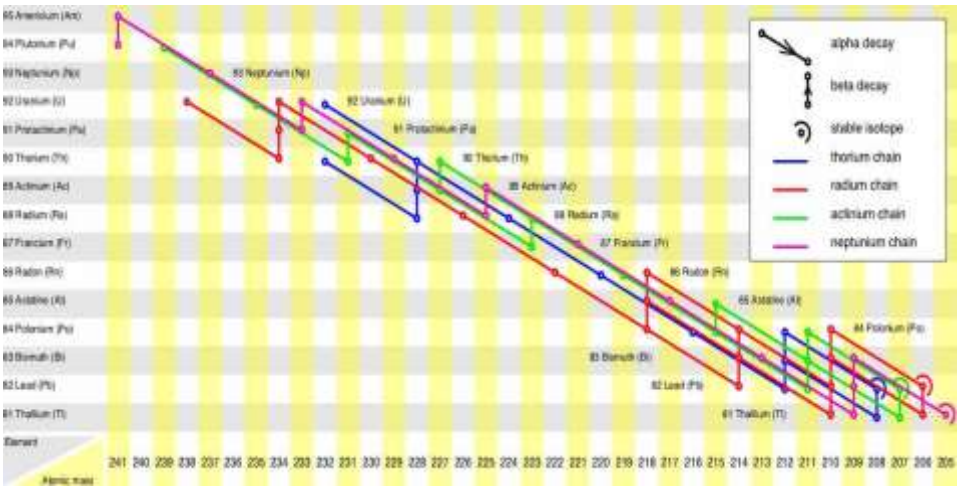

Figure 1.8. Decay chains for the principal actinides typically present in nuclear spent fuel [12].

Fission products are the other part of the real waste in nuclear spent fuel, representing roughly 4% of the total mass. These isotopes arise from the process of breaking up a fissile nucleus upon impact of a neutron:

$$^{235}U + n \longrightarrow ^{139}Ba + ^{94}Kr + 3n \qquad (1.2)$$

The breakage of the fissile nucleus when it is hit by a neutron is not deterministic; therefore, a probability distribution of fission products results from fissions occurring in nuclear fuel, which

converges to a continuous function if many fission events occur. Figure 1.9 presents the distribution of fission products for a thermal reactor with 4% enriched UO_2 as fuel, while Figure 1.10 presents the distribution of fission products for ^{233}U in a fast (100 eV peak neutron energy) reactor.

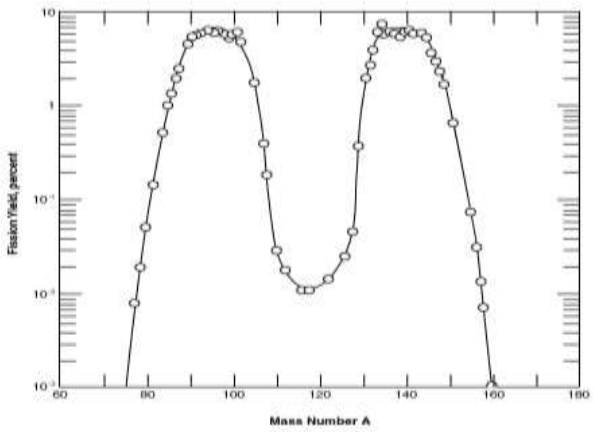

Figure 1.9. Fission products yield for U-235 in at thermal reactor.

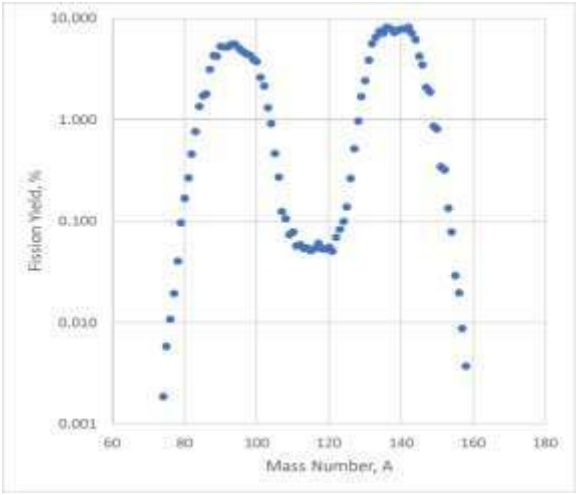

Figure 1.10. Fission yield for U-233 in a fast reactor.

Fission yields will depend on both the nucleus undergoing fission and the neutron energy spectrum. Half-lives shorter than 90 years have most fission products; however, half-lives exceeding 100,000 years have a handful of fission products. These long-lived fission products and their typical yield for thermal reactors and ^{233}U in a fast reactor are shown in Table 1.III.

Table 1.III. Long-lived fission products and their yield for ^{235}U fission in a thermal reactor and ^{233}U fission in a fast reactor.

Isotope	*Half-life (10^5 years)*	*% Yield in thermal reactor*	*Yield for ^{233}U in fast reactor*
^{99}Tc	*2.11*	*6.14*	*3.95*
^{126}Sn	*2.30*	*0.11*	*0.264*
^{79}Se	*3.27*	*0.045*	*0.096*
^{93}Zr	*15.3*	*5.46*	*5.54*
^{135}Cs	*23.0*	*6.91*	*7.19*
^{107}Pd	*65.0*	*1.25*	*0.125*
^{129}I	*157*	*0.84*	*1.69*

After this discussion, it is clear that the radiotoxicity of nuclear spent fuel has two main sources: fission products and minor actinides. Fission products emit primarily beta and gamma radiation, while actinides emit primarily alpha and beta radiation. The contributions of each of these groups of isotopes is shown in Figure 1.11. Two fission products, ^{137}Cs and ^{90}Sr, contribute the most to the activity in the spent nuclear fuel for the first 100 years. After that, the main contribution is the α decay of ^{241}Am (see the Neptunium series in Figure 1.8), which comes from the β decay of ^{241}Pu. The elimination of these three isotopes would put the activity of the spent nuclear fuel al levels below the activity of natural uranium ore.

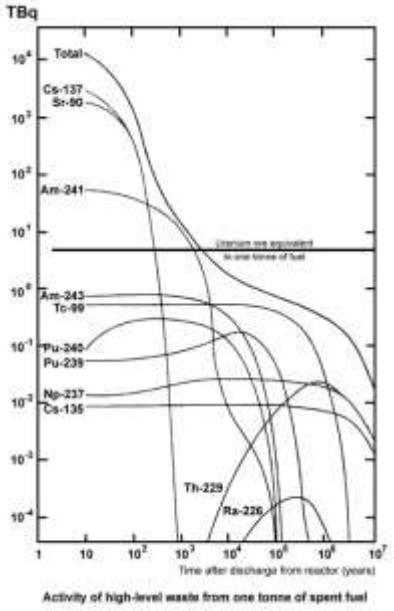

Figure 1.11. Evolution of the radioactivity in spent nuclear fuel, broken down by the main isotopes (minor actinides and fission products). Horizontal line shows radioactivity level of natural uranium ore for comparison [13].

Once taken out of the reactor after partial burning, nuclear assemblies are generally stored in spent fuel pools at site power plants; these are typically 12 meters or more deep, about 4.3 meters at the bottom is equipped with racks of storage to hold fuel assemblies designed when they are removed from nuclear reactors. This is done mainly because the fuel assemblies keep releasing “decay heat” for up to 18 months, making the fuel handling difficult. Figure 1.12 shows spent fuel pool of the Caorso Nuclear Power Plant an example of. Pool is used for immediate "cooling" of the nuclear fuel assemblies, where short-lived isotopes decay reducing ionization radiation that comes from the

nuclear fuel rods. Water also makes a cooling function of the nuclear fuel providing shielding from their radiation as radiological protection .

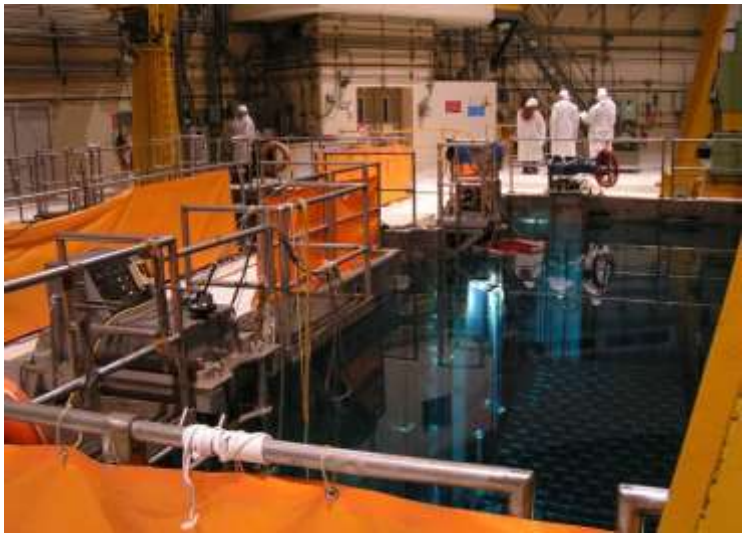

Figure 1.12. Example of a spent fuel pool from the shut-down Caorso Nuclear Power Plant [14]. This pool is not holding large amounts of material.

Depending on polices, rules, laws or objectives of countries and/or companies, the strategies for interim storage, reprocessing and final disposition of fuel elements varies significantly. Since no long-term geological repository has been implemented, most nuclear power plant operators rely on dry cask storage technology once the fuel has cooled down in the storage pools. Figure 1.13 shows typical dry cask storage containers for nuclear spent fuel in a nuclear power plant. The container is specifically designed to shield humans from the harmful radiation, but the accumulation of this highly radioactive material represents a misuse risk nonetheless and needs to be heavily guarded. Dry cask storage is regarded as a short-term solution while permanent disposition sites are constructed and become operational.

Figure 1.13. Dry cask storage of spent nuclear fuel at Vermont Yankee nuclear power plant [15].

Final disposition is related to the construction of massive nuclear waste geological repositories, such as the one shown in Figure 1.14. In the case of United States, the development and construction of the Yucca Mountain Repository was cancelled in 2010. This issue complicates even

more the strategies for interim storage and reprocessing steps in the nuclear fuel cycle. Due to the Yucca Mountain project cancellation, interim repository represents a risk because the nuclear fuel assemblies must be kept at the nuclear power plant site in pools, which have a finite capacity and represent an added cost for the operator.

Figure 1.14. View of a proposed nuclear or radioactive waste disposal, Deep Geological Repository [16].

1.2 Justification.

1.2.1 The need to breed fissile material.

As discussed in Section 1.1.2, the nuclear resource (natural ^{235}U) is a non-renewable kind of primary energy. In 2017, measured resources of uranium are around 6 million tons (see Figure 1.4), and these reserves are used only in thermal reactors. The reserves are enough to sustain nuclear electricity generation for a period between 50 and 100 years depending on how the consumption rate evolves. This window of time may represent a higher level of assured resources, since it allows for further exploration on the basis of present geological knowledge. The reprocessing technology may also contribute marginally to extend the life of nuclear resources, between 20 and 25%. Nonetheless, with a certain type of nuclear manipulation, synthetic fissile isotopes can be created to be a primary source of energy. As mentioned before, neutron bombardment of fertile nuclei such as ^{232}Th or ^{238}U can produce fissile isotopes, ^{233}U and ^{239}Pu, respectively. One of the technologies proposed for producing fissile material in this way are breeder reactors, regarded as an important tool to extend nuclear resources for several thousand years [17]. Breeder reactors are a type of nuclear reactor which produces more fissile material than it consumes to generate electric power, and most nuclear experts around the world regard this technology as the most viable route to extend nuclear energy time horizon beyond 100 years.

Breeder reactors are classified as fast or thermal, depending on the fertile isotope utilized. A fast breeding reactor employs ^{238}U to obtain the fissile isotope ^{239}Pu [18]; the coolant in this type of

fast reactor is liquid metal in order to achieve a fast neutron energy spectrum. Thermal breeder reactors use ^{232}Th to breed ^{233}U [18], and in this kind of breeder reactors ordinary water can be used for the cooling system since the slowing down of neutrons is not only desirable but required. As of February 2020, there are about 20 operational breeder reactors around the world [17], which were introduced into the nuclear power industry as research reactors since the 1950s; some of these research reactors were so successful that they supply electric power commercially. Other breeder reactor projects, such as the Super-Phénix in France, were not so fortunate; this project suffered from technical challenges and strong public opposition that led to its definitive closing in 1998 [19]. Nonetheless, breeder reactors have accumulated 400 years of experience in maintenance and operation.

1.2.2 The need to destroy minor actinides.

Since the start of nuclear power electric generation in 1954, have been storage, from all nuclear power plants around the world, about 370,000 of spent fuel, Pakistan and India are excluded. Of this grand total, about 1/3 (120,000 tons) have been reprocessed. The remaining amount (2/3) is stored waiting for the reprocessing process or its final disposal. Most of this spent fuel is precisely at the pools of the nuclear power plants or in dry storage casks, either in wet storage in the reactor pools or dry storage casks. Lasting for at least 5 years after initial storage in the cooling process into the pools, part of this spent fuel is transferred to dry casks, as well as centralized into wet storage facilities. About 250,000 tons of spent fuel in storage as a total amount [20].

The most important strategy to reduce the mass of spent fuel is reprocessing, which recovers the uranium and the plutonium from the spent fuel, which is 96% of the mass. But even reprocessing and thermal nuclear facilities produce a small fraction of radioactive materials that are released to the environment each year as a result of plant operations, these are named radioactive effluents which are emitted in airborne and liquid form. They originate from several sources within a reprocessing plant. Effluent releases are permitted under regulations promulgated by international agencies and countries, but they must be controlled, monitored, and reported to regulatory authorities.

There are other effluents produced in the reprocessing plant that have a high complexity in their treatment, containing high radioactivity concentrations of long-live nuclides [21]. The liquid of decontamination is a common example, that results as per the general lack of cleaning tasks of plant piping and equipment of the reprocessing process. Some of these effluent substances can contain corrosion products, crud, as well as phosphates, detergents, tartrates, citrates, acidic products and ethylenediaminetetraacetic acid, EDTA. These effluents should be taken into care, segregating and collecting them into containers or small bottles. The option of direct conditioning as the preferred processing waste of this type, generally, with cement in a final geological repository. The same for solvents, liquid, oils, treatment of final waste by minimizing its volume via requiring management treatment processes and reducing potential hazard conditioning the waste immobilizing and containing into a stable solid [22].

1.3 Fusion-fission hybrid systems.

1.3.1 Working principle.

In addition to the fission process used in nuclear power plants to generate energy, already discussed in the previous sections, there is a second alternative for obtaining net energy from nuclear reactions. This process involves fusing light nuclei to produce heavier nuclei, and therefore the process is called *nuclear fusion*. All the stars in the Universe, including our Sun, draw their energy from this process that occurs in their cores. These are some of the nuclear fusion reactions that are known to occur among light nuclei:

$$^{2}H + {}^{3}H \longrightarrow {}^{4}He\ (3.5\ \text{MeV}) + n\ (14.1\ \text{MeV}) \tag{1.3}$$
$$^{2}H + {}^{2}H \longrightarrow {}^{3}H\ (1.01\ \text{MeV}) + {}^{1}H\ (3.02\ \text{MeV})$$
$$^{2}H + {}^{2}H \longrightarrow {}^{3}He\ (0.82\ \text{MeV}) + n\ (2.45\ \text{MeV})$$
$$^{2}H + {}^{3}He \longrightarrow {}^{4}He\ (3.6\ \text{MeV}) + {}^{1}H\ (14.7\ \text{MeV})$$
$$^{3}H + {}^{3}He \longrightarrow {}^{4}He + {}^{1}H + n\ (12.1\ MeV)$$
$$^{3}H + {}^{3}He \longrightarrow {}^{4}He\ (4.8\ \text{MeV}) + {}^{2}H\ (9.5\ \text{MeV})$$
$$^{1}H + {}^{6}Li \longrightarrow {}^{4}He\ (1.7\ \text{MeV}) + {}^{3}He\ (2.3\ \text{MeV})$$

Unlike the fission reactions, which do not have an energy threshold, fusion reactors require a minimum energy to be carried out. This is because the reacting nuclei both have positive charge, so bringing them close enough to each other for the reaction to occur requires overcoming their electrostatic repulsion. Therefore, the interaction cross section for these reactions has a threshold, as can be seen in Figure 1.15. In the Figure, the isotope of hydrogen with atomic mass 2 is denoted deuterium (D) and the hydrogen isotope with atomic mass 3 is called tritium (T).

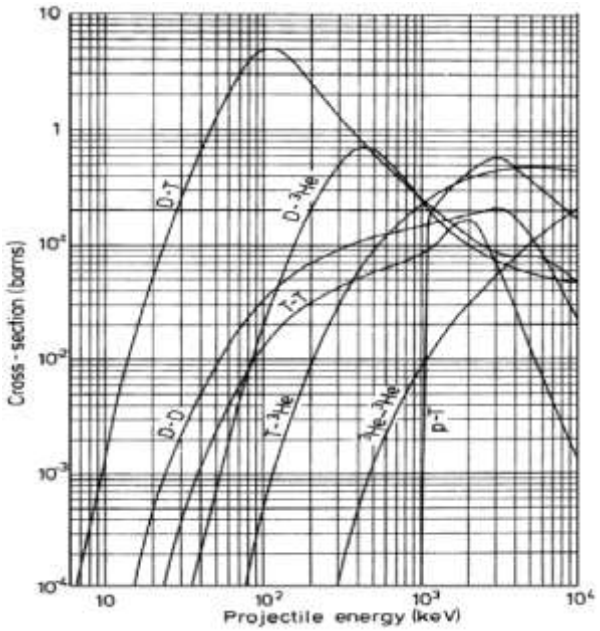

Figure 1.15. Cross sections for several fusion reactions as a function of center-of-mass energy [23].

Although there has been a tremendous international effort to convert fusion energy into a practical energy source, the technology is just not there yet despite the significant advance in the science and technology of nuclear fusion systems over the last 70 years. Some authors have proposed that the way to accelerate the maturity of nuclear fusion technology is by inserting it into the economic cycle of the nuclear industry [24]. And the two previously outlined technological challenges in the present nuclear industry could certainly benefit from fusion-based energetic neutron sources: fast neutrons for converting fertile material into fissile material with limited burning, and destruction of minor actinides which are inert in a thermal neutron spectrum but can undergo fission when exposed to a fast neutron spectrum (see Figure 1.16).

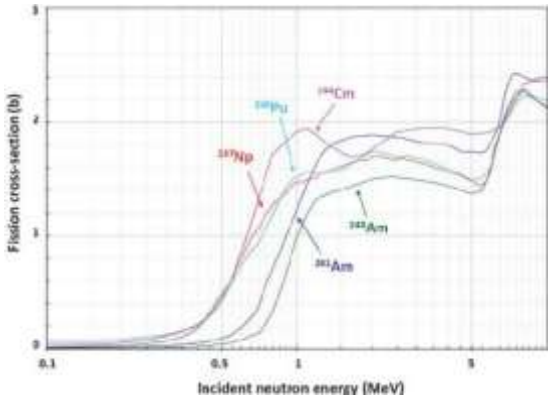

Figure 1.16. Fission cross sections for minor actinides in the fast region of the neutron energy spectrum [25].

The reaction between D and T produces a 14.1 MeV neutron. This fusion reaction also happens to have the highest cross section at the lowest temperature (see Figure 1.15), so it is the easiest one to accomplish. Without the overhead of requiring net energy production, the existing technology for fusion systems based on magnetically confined high temperature plasmas seems to be at the point where it can be used to produce high fluxes of fast neutrons [26].

1.3.2 Previous work.

The idea of a synergy between fusion and fission reactors is not new. The earliest references to a nuclear system making use of fast fusion reactors date back to the early 1950s [27], and the preferred fusion reactor configuration for these early proposals was a magnetic mirror. An excellent review of the early days in fission-fusion systems concept development is given by Lidsky [28]. During the next two decades, the first powerful fusion experiments would be built, but it was soon realized that there were just too many hurdles towards an economically competitive fusion electric power plant. In the 1980s, when it became evident that pure fusion power was not going to happen in the short term, hybrids were proposed as a strategy to accelerate the technology development of fusion systems, while producing an economic benefit at least before a complete developed pure fusion system. Although there are economic detailed studies of these suggested systems, these studies could not be competitive with fission reactors [29].

The hybrid concept was altogether in some way idle for a while, since the fission community had no interest in tinkering with an already well-established fuel cycle, and the fusion community

wanted to stay as far away as possible from fission to allow marketing itself as a clean, safe energy source. A brief revival of the concept occurred around 2009 with a Nature publication [30], but now the studies switched focus from direct energy production devices to bringing competition to the fast breeder reactor for the generation of artificial fissile material, and also on nuclear waste disposal aspects of the design [31].

Manheimer [32], Stacey [33] and Freiberg [34] have remained champions of the concept for many years in the US, despite the fluctuating interest in the concept, and a small group of researchers at the University of Texas has explored the possibility of using a fusion neutron source based on a low-aspect ratio (i.e. spherical) tokamak machine to produce high fluxes of neutrons [35], a concept that has been also developed within the fusion community Abdou [36], Peng [37], Wilson [38] for the purpose of testing fusion relevant materials under high neutron dose environments. The Texas group has even a patent on a fusion-based system aimed at creating a reprocessing-free (ReFree) nuclear fuel cycle. This option has also been studied by groups in China [39], Turkey [40], Brazil [41] and Mexico [42].

Nuclear hybrid fusion-fission systems propose an option to avoid re-processing techniques, because of magnetic confinement advances in fusion technology, nowadays is possible to design and construct fast neutron intense sources, opening the window of this concept of ReFee cycles [43-45]. Of course, fusion technology has had a slow growing, only recently, real fusion reactors for research and development have been built, which makes a real possibility to apply this technology to these hybrid systems concept. Advantages of the concept implies to have an hybrid reactor, which is considered inherently safe as processes can be operated sub-critically in the fission blanket section for all conditions and probably be less susceptible to instabilities [45]. No isotopes separation are considered in this technique, which makes this option optimal to avoid getting Pu-239 and U-233 separated, lowering weapon proliferation risk. ReFee cycle could be the most proliferation resistant of the known fuel management schemes (including FBRs [46] and centrifuges for enrichment utilization [47]), and also has been found to be efficient because a single hybrid reactor would feed fuel about 3.5 to 4 same thermal power light water reactors; which means a good economic option. Advantages are also on the breeding side; fertile Th-232 can be irradiated by neutrons producing a small fissile material percentage appropriately. Without been modified, assemblies are shuffled to an LWR and burn up as fuel. For LWR's utilization, allowing this percentage of synthetic U-233 is sufficient for a critical condition, positioning the hybrid breeding in the faster spectrum, but the assemblies in the sub critical state reactor. Figure 2.1 shows a schematic diagram of a hybrid reactor system.

Previous analysis by CICATA research group [48] have focused on a simple mass balance analysis for a thorium fuel cycle, as well as preliminary evaluation of actinide burning [49, 50]. The purpose of the present work will be the application of more sophisticated tools and a greater level of detail on the simulation activities previously carried out by the group.

1.3.3 Tokamak-based systems.

The most advanced configuration to achieve confinement of a high temperature plasma using magnetic fields is the tokamak, a device invented in the former Soviet Union during the 1950s [51]. The simplified operating principle of those machines is as follows: a high current is somehow injected into a toroidal loop of plasma, and the plasma will heat due to its internal electrical resistance;

additional plasma heating in the form of microwaves or neutral beams can be implemented. As energy is injected into the plasma, its internal pressure will increase and it will try to expand; to prevent the expansion, an external magnetic field in the toroidal direction is added to create a counter pressure due to the Lorenz force, **j** x **B**. External toroidal magnetic field in combination with the self-generated poloidal field due to plasma current circulation results in a helical field, which is able to confine the high temperature plasma.

Figure 1.17 shows a typical tokamak schematic with its main components. The central column contains the return leg of the toroidal field coil, and the solenoid that allows inducing plasma current by means of a magnetic flux swing. The poloidal field coils are there to counteract drifts associated with magnetic field curvature, and also to control position and shape of the plasma column. The divertor is a component where most of the particles that escape confinement end up, and it is designed to handle the high energy flux associated with particle escape.

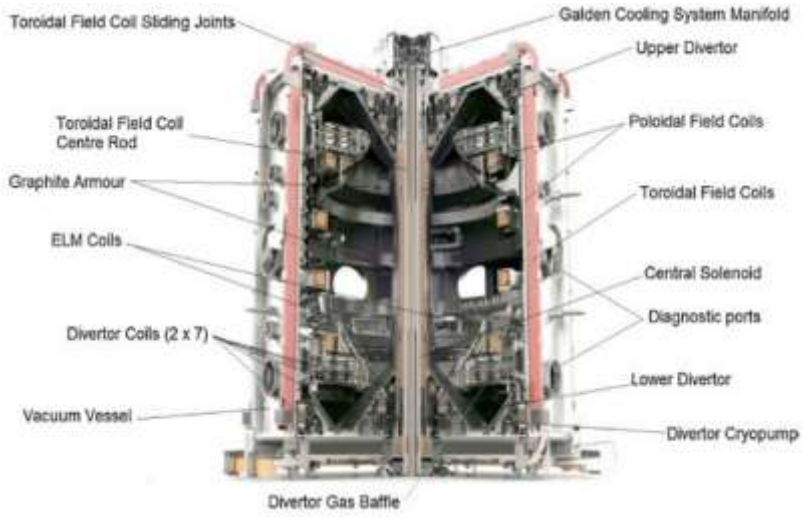

Figure 1.17. Cross section of the Mega Amp Spherical Tokamak (MAST), a low aspect ratio tokamak machine [52].

Within the plasma column, a mechanical equilibrium is established between kinetic forces associated with pressure and temperature, and electromagnetic forces associated with charged particle fluxes and electric/magnetic fields. The equation describing this equilibrium state in toroidal coordinates is known as the Grad-Shafranov equation [53]. The details on the system of equations used to solve the equilibrium and how they are solved are well beyond the scope of the present work; the important thing is that for any geometrical configuration, plasma current, magnetic field and internal transport coefficients, the Grad-Shafranov equation allows for the calculation of temperature and density profiles within the plasma. This topic will be discussed in detail in Sections 3.1.2 and 4.1.2 of this document, pertaining to the description of the volumetric neutron source.

1.4 Relevant features of hybrid systems.

1.4.1 Tritium self-sufficiency.

An important aspect on the operation of hybrid systems is the tritium self-sufficiency. Let´s recall here the fusion reaction between deuterium and tritium:

$$D + T \longrightarrow {}^{4}He\ (3.5\ \text{MeV}) + n\ (14.1\ \text{MeV}) \tag{1.4}$$

For each neutron generated in the system, a tritium nucleus is consumed. This tritium has a half-life of 12 years and is radioactive, it is no surprise that it does not exist in nature. It would then be important to estimate the amount of tritium required to operate a fusion system at a given thermal power. The thermal power *P* is given in terms of the number of neutrons per second generated *S* as:

$$P = E_n S \tag{1.5}$$

where E_n is the energy liberated per neutron, equal to 14.1 MeV, or 2.26 x 10^{-21} GJ. On the other hand, the production rate of tritium mass required to achieve the neutron source strength *S* is given by:

$$\dot{m}_T = \frac{3S}{N_A} \tag{1.6}$$

where N_A is Avogadro's number, 6.02 x 10^{23} mol^{-1} and 3 is the atomic mass of tritium in g/mol. Therefore, the relationship between tritium consumption (in g/s) and the reactor thermal power (in GW) is given by:

$$\dot{m}_T = \frac{3P}{E_n N_A} = \left(0.0022\,\frac{g}{GJ}\right)P \tag{1.7}$$

Meaning that sustaining a 1 GWth fusion reactor in steady state will require 2.2 mg/s, or 190 g/day, of tritium generation in order to provide enough fuel to sustain the reactor. When the fusion reactor generates tritium at the rate specified by eq. (1.7), it is said that the reactor has a *tritium breeding ratio* (TBR) equal to 1. In practice, values of TBR greater than 1 are required to offset tritium recovery inefficiencies.

The tritium in the fusion reactor is expected to come from a blanket that contains lithium, since the reaction of the ^{6}Li isotope with a neutron generates a tritium atom:

$$n + {}^{6}Li \longrightarrow {}^{4}He + T \tag{1.8}$$

This means that for each neutron generated, we have the possibility of creating a tritium atom from a ^{6}Li atom, so the requirement is in reality for 380 g/day of ^{6}Li, assuming all the neutrons can be captured by ^{6}Li atoms. Here, it should be noted that the abundance of ^{6}Li in natural lithium is 7.6%.

The bombardment of ^{7}Li with neutrons can also produce tritium, but the cross section is much smaller and the reaction requires very high neutron energies.

For the case of the hybrid systems, it is clear that if all neutrons in the system are spent on breeding tritium, there will be no leftover neutrons to perform other functions, such as breeding fissile material, or fissioning a minor actinide nucleus. In the old hybrid designs, this problem was solved by mixing the fertile material with a coolant containing a neutron multiplication element, such as lead or beryllium [54], usually in the form of molten salts, liquid metals or solutions. However, since the system envisioned in this work does not allow for that, a careful study on the neutronics within the system is needed to ensure there are excess neutrons to carry out other functions.

1.4.2 Thermal reactor support ratio.

As mentioned in the introduction, thermal reactors retire about 1/3 of their assemblies every 18 -24 months. Depending on the power level, reactor cores can hold between 120 to 193 fuel assemblies. For example, a Westinghouse 3-loop PWR reactor, with a typical power of 2.5 GWth, contain 157 17x17 fuel assemblies, while a 4-loop configuration uses 193 fuel assemblies and delivers 3.8 GWth [55]; the Areva EPR design uses 241 assemblies and delivers 4.6 GWth [56]. A good rule of thumb is that each assembly delivers between 17 and 19 MW of neutron power. A PWR core used as reference within the Nuclear energy Agency has 157 fuel assemblies and it is shown in Figure 1.18.

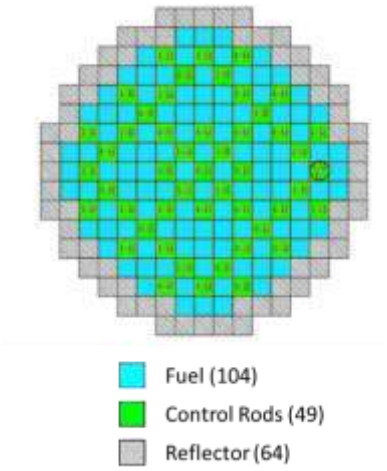

Figure 1.18. NEACRP LWR reference core.

Assuming 193 assemblies per core, a third of that is 64 assemblies, which will need replacement with new fuel every year. This means that the hybrid system needs to provide 64 assemblies of fresh fuel and accommodate the 64 that come out to boost the content of fissile material and destroy some of the minor actinides. The support ratio of the device is said to be equal to 1 if the hybrid device, in 1 year of operation, is able to produce 128 assemblies with adequate enrichment, 50% of them with no fissile material and 50% with some level of fissile material below the desired enrichment.

1.4.3 Nuclear fuel assembly management.

The hybrid fission-fusion system envisioned as part of this project would use nuclear fuel assemblies coming from either thermal reactors (partially burned fuel) or fuel fabrication facilities (to enrich fresh fertile material). Exposure of these assemblies to the fusion neutron flux should breed fissile material. The idea is to use the hybrid device in a reprocessing-free fuel cycle scheme [57], where the fuel assemblies are irradiated in the hybrid device in order to burn some of the minor actinides and, more importantly, replenish the content of fissile material. Once the content of fissile material is back to the nominal value, the fuel assembly would be returned to the thermal nuclear reactor in order to continue burning it. This cycle would be repeated until the accumulation of fission products or minor actinides within the fuel assembly becomes too great, and then the fuel assembly would be disposed of permanently.

The proposed array of assemblies in the hybrid device is in annular concentric rings around the neutron source, following regular polygons with their side equal to the length of a fuel assembly side. Polygons are laid out such that they have an angle of symmetry, given by the number of sides of the base polygon, as shown in Figure 1.19, where fuel assemblies top views are shown as a gray square. The figure illustrates four different fuel assembly arrangements, corresponding to four different symmetry angles of the polygon sequence: when the base polygon has 4 sides, the symmetry angle is $\pi/2$; when the base polygon has 6 sides, the symmetry angle is $\pi/3$; if the base polygon has 8 sides, the symmetry angle is $\pi/4$, and so on. Having a small symmetry angle is advantageous because it reduces the volume of the system that needs to be modeled. Consecutive polygons have a number of sides (shown in Figure 16 as small numbers over the polygons) equal to the base polygon multiplied by an integer factor. For instance, the sequence of polygons with symmetry angle $\pi/2$ have 4, 8, 12, 16, 20,..,4n sides; polygons with symmetry angle $\pi/3$ have number of sides 6, 12, 18, 24,…, 6n. Care should be taken, because the difference in the radius of the inscribed circles between consecutive polygons needs to be larger than the side length of the polygon, since the fuel assemblies have a square cross section; Figure 16a for the case of symmetry $\pi/4$ is an excellent example of that situation.

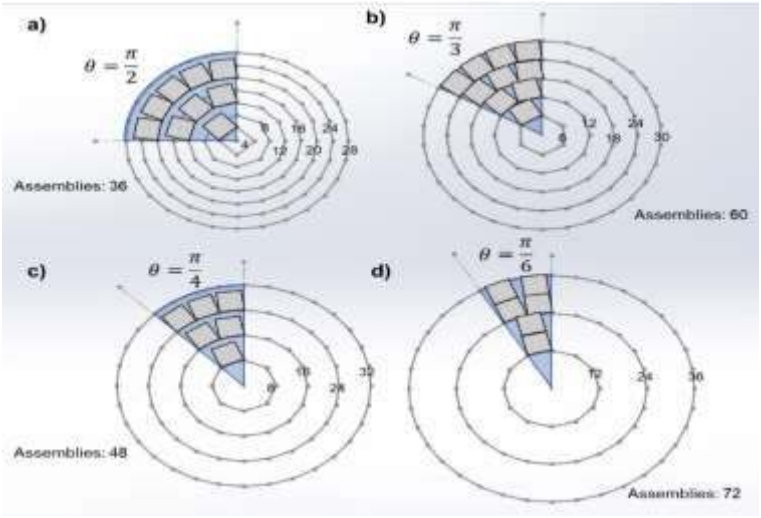

Figure 1.19. Layout of fuel assemblies in concentric rings defined by a sequence of polygons with different angles of symmetry: a) $\pi/2$, number of sides multiple of 4; b) $\pi/3$, number of sides multiple of 6; c) $\pi/4$, number of sides multiple of 8; and d) $\pi/6$, number of sides multiple of 12.

Since the assemblies are arranged in concentric circles, it is expected that the assemblies in the innermost ring will be exposed to the highest neutron flux, while the outermost ring will be exposed to a much lower neutron flux. The development of a shuffling strategy for the assemblies considering a mixture of bot fresh and used fuel is beyond the scope of the present work; however, a simple shifting strategy will be discussed in Section 4.3.3 of this document.

2 Scope of work.

2.1 General Objective.

The general goal of this work is to model a fusion-fission hybrid system capable of enriching at least 64 PWR fuel assemblies initially filled with pure ThO_2 with 4% ^{233}U isotope in a time frame of 18 months or less, while maintaining tritium self-sufficiency for the fusion neutron source.

2.2 Specific Objectives.

- Achieve familiarity with the two main computational tools to be used during this project: MCNP and ORIGEN.
- Develop a software system capable of automatic generation of adequate input files for MCNP and ORIGEN based on user input on geometry, initial material composition and simulation parameters, also capable of post-processing the information obtained from the simulations to aid in its analysis.
- Perform simulations of nuclear fuel assemblies irradiated by a spherical tokamak based on the CFNS design, exploring the effect of material selection for tritium breeder, neutron multipliers and neutron reflectors.
- Determine the effect of material selection of fuel support ratio and tritium self-sufficiency for the hybrid system.

2.3 Work Hypothesis.

The right combination of neutron power, tritium breeding material and neutron multiplying material will produce a hybrid fission-fusion system with a fuel support ratio greater than 1 and self-sufficient in terms of tritium production.

3 Methods and Materials.

3.1 Systems view of the simulation environment.

Within the framework of systems modelling, a system is defined as a collection of interacting entities which interconnect to form a mechanism capable of performing a complex function [58]. For an advanced nuclear fuel cycle incorporating fission-fusion hybrid systems, this high-level function is to provide every 12 months the necessary number of nuclear fuel assemblies for a thermal nuclear reactor containing enriched fuel at 4%, minimizing the waste produced. At the highest level, we have four main actors interacting in this advanced fuel cycle:

- A supplier of fresh fuel assemblies, filled with fertile material at zero or very low enrichment level, with a steady output fuel assemblies containing UO_2 or ThO_2 without enrichment.
- A high-energy, high-flux neutron irradiation facility, which receives fresh fuel assemblies from the fertile material supplier to be enriched from 0 to 4 %, and/or partially spent fuel assemblies from the thermal reactor that will have a non-zero enrichment below 4% depending on the burnup.
- A thermal reactor, containing a certain number of fuel assemblies and exchanging 30% of them every 12 months.

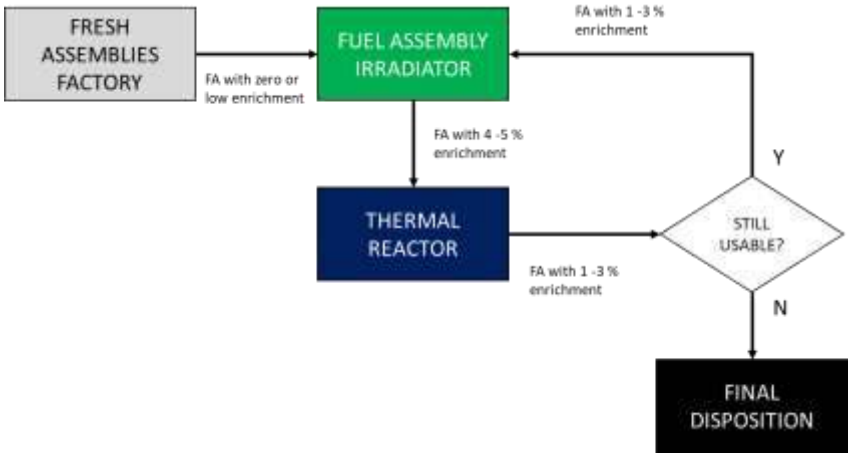

Figure 3.1. High-level interaction between the fresh fuel fabrication, fuel irradiation and fuel burning blocks in a semi-close nuclear fuel cycle without reprocessing.

Figure 3.1 presents a high-level interaction diagram between these three actors in terms of material exchange. Right away, this nuclear fuel cycle can be identified as three actors exchanging fuel assemblies, and each actor modifying an attribute of these fuel assemblies (the enrichment) in order to pass it to another block. The fresh fissile block is only in charge of replenishing the fuel assemblies that go to final disposal. And this number will be minimized if the criteria for reuse is met over multiple cycles of a fuel assembly; that criteria might have to do with material damage to the

fuel assembly due to extended neutron irradiation, or accumulation of undesirable material such as fission products or minor actinides.

The main focus of this work will be the characterization of the fuel assembly irradiation block, in particular developing a tool for understanding its behavior as its attributes are modified. The fuel irradiation block can also be broken down into individual elements. For the particular case of a tokamak-based fusion neutron source, the fuel irradiator has the following components:

- A high temperature plasma, which produces 14.56 MeV neutrons in a volume from the fusion reaction between deuterium (D) and tritium (T).
- A set of magnetic field coils (toroidal and poloidal) which generate the confining magnetic field.
- A system for energy injection into the plasma for keeping it at high temperature.
- A central column, which induces the plasma current necessary for the confinement.
- A neutron multiplier, in charge of generating more than 1 neutron per neutron produced in the plasma to allow for fuel irradiation and tritium self-sufficiency simultaneously.
- A tritium breeder tasked with producing tritium from the nuclear reaction between ^{6}Li and a neutron.
- A fuel irradiation chamber, where the fuel assemblies are placed.
- Neutron reflectors and shields to prevent neutron leakage from the system and protect components from neutron irradiation.

Figure 3.2 presents a high-level interaction diagram of the components that make up the fuel irradiator block, and in the following sections some of the most important blocks are discussed in detail.

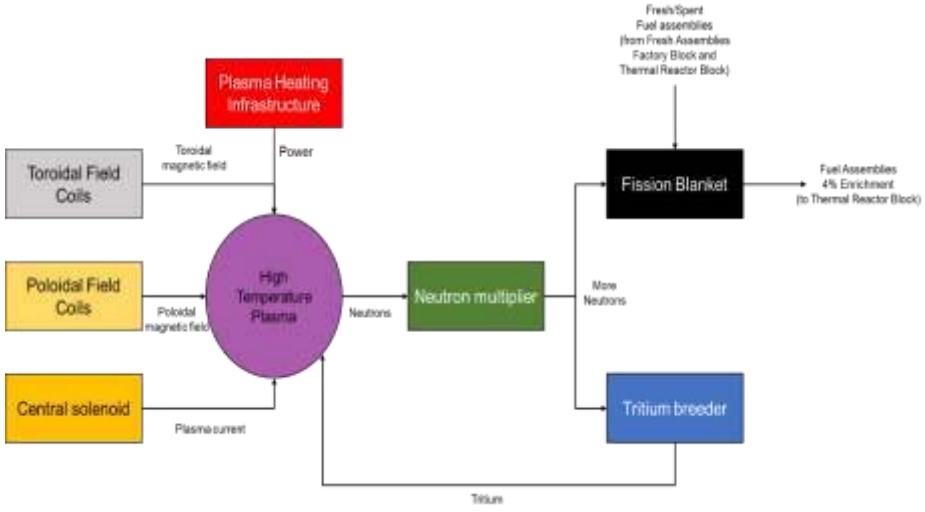

Figure 3.2. Block diagram of the fuel irradiator based on a tokamak fusion neutron source.

3.1.1 Central solenoid, poloidal and toroidal field coils.

These subsystems are related to three aspects of tokamak operation:

- Plasma current induction.
- Toroidal field generation.
- Plasma positioning and shaping

These systems for the ITER tokamak are shown in Figure 3.3. These three systems, in addition to the power injection (which will not be discussed in detail for this work), have a profound impact in the shape and the neutron emission profile of the volumetric plasma source. They will be discussed briefly here, but the reader is referred to more specialized literature [59, 60] for a detailed description of these systems and their impact on the neutron source characteristics.

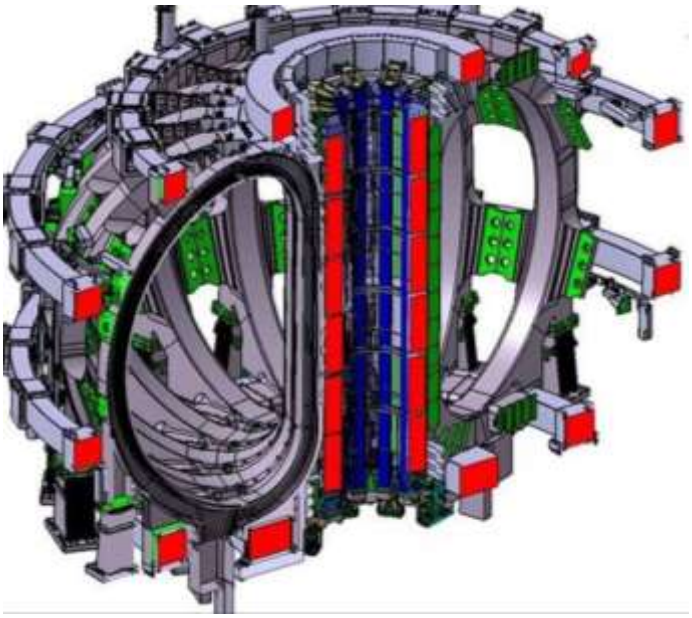

Figure 3.3. Magnetic systems for the ITER Tokamak [61]. Poloidal coils are the red squares, toroidal coils have a "D" shape and the segmented solenoid is in the center of the device.

The central solenoid acts as the primary winding in a transformer, while the single-loop secondary winding is the plasma ring. A time-changing current is circulated in the central solenoid, producing a magnetic field variation $d\mathbf{B}/dt$ in through the area enclosed by the plasma loop, which in turn induces a current in the plasma loop. Since the solenoid has many more turns than the single plasma turn, the result is an elevation in current circulating on the plasma, proportional to the number of turns in the central solenoid. This plasma current, in addition of providing the necessary poloidal field to achieve magnetic confinement, also produces plasma heating via the Joule effect since the plasma has a finite resistivity. Achieving a trapezoidal induced plasma current profile involves the segmentation of the central solenoid, where each segment will independently carry its own current waveform and the total induced current in the secondary winding will be the desired trapezoidal waveform [62]. Schemes of magnetic confinement without the need for a central solenoid are also being explored [63].

The toroidal field coil in a tokamak needs to produce, as the name implies, the toroidal component of the magnetic field, B_T. The intensity of this field is related to a parameter known as the safety factor $q(r)$, given by the ratio of toroidal to poloidal field at the edge of the plasma r_p:

$$q(r) = \frac{r_p\, B_\phi}{R_p\, B_\theta} = \frac{2\pi r_p^2\, B_T}{\mu_0 I_p R_p} \tag{3.1}$$

Here, R_p and r_p are the major and minor radius of the plasma torus, respectively, and I_p is the plasma current. The stability criteria for the plasma magnetic confinement sets a requirement for q of 3 – 4. Therefore, the required toroidal field for confining a plasma with current I_p can be estimated by calculating B_T from 3.1 knowing that $q = 4$.

The poloidal field coils are required in order to control the plasma shape and position. As can be seen in Figure 3.3, ITER has 6 poloidal field coils, but other tokamak machines such as TCV have 16 poloidal field coils [64]. The MAST-U machine, shown in Figure 1.17, has 20 poloidal field coils, with 50% of them dedicated to plasma shaping and the rest for plasma exhaust shaping in the divertor region [65].

Large tokamaks such as ITER, JT-60SA and KSTAR, with a mission towards direct energy production from fusion systems, need to employ superconducting magnets for the construction of the central solenoid and all the tokamak coils. This is necessary given the level of current that circulates in these components in order to obtain very high temperatures and densities in the confined plasma. It has been argued, however, that for the confinement requirements associated with a fusion neutron source, regular copper or aluminum conductors would be sufficient to achieve a high neutron flux when that is the primary purpose of the facility [66].

3.1.2 The plasma fusion neutron source.

An adequate combination of plasma current, external magnetic fields and auxiliary heating will produce a stable fusion plasma. MHD equilibrium computer codes such as ASTRA [67] are capable of solving the transport of mass and energy in toroidal geometry given the transport coefficients, the plasma current, the toroidal field and the geometric parameters of the plasma. If an axisymmetric system is considered (no variations with toroidal angle), the shape of the plasma cross section in an rz plane is given by the following expressions by Turnbull [68]:

$$r = R_p + \rho\, cos(\theta + \alpha sin\theta) \tag{3.2a}$$

$$z = \kappa\, \rho\, sin\theta \tag{3.2b}$$

Here, ρ and θ are polar coordinates with the origin in the center of the plasma cross section. The parameters κ and α give the plasma cross section its "D" shape: κ is known as the *elongation* and α is known as the *triangularity*. These equations describe contours of the plasma where the density and the temperature are constant, and they are therefore called *isobaric lines* or *isobars*, each

value of ρ corresponds to a particular isobar. It is customary to present eq. (3.2) in dimensionless form, normalized to the major radius of the plasma R_p:

$$\frac{r}{R_p} = 1 + \varepsilon\, cos(\theta + \alpha sin\theta) \tag{3.3a}$$

$$\frac{z}{R_p} = \kappa\, \varepsilon\, sin\theta \tag{3.3b}$$

Sweeping of θ between 0 and 2π and ε between 0 and $\varepsilon_{max} = r_p/R_p$ generates the full cross-sectional area of the plasma. Since z =0 is a symmetry plane, the sweeping in θ can be done between 0 and π to generate the upper half of the plasma cross section, which is identical to the lower half. The parameter ε corresponds to the different plasma isobars. Figure 3.4 presents the cross section of different plasmas with different values of κ, α and ε_{max}.

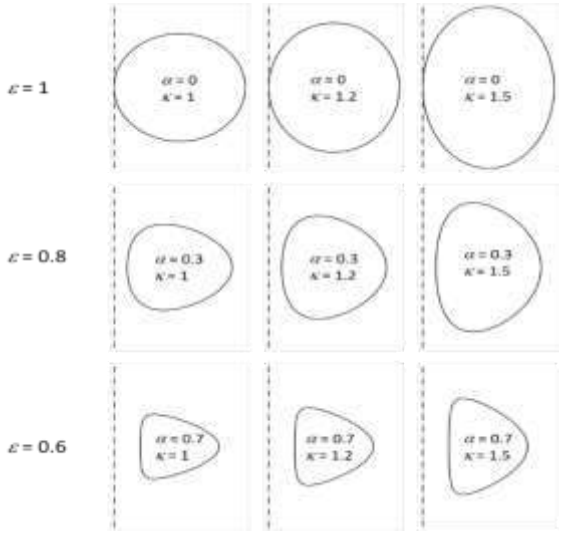

Figure 3.4. Effect of elongation, triangularity and aspect ratio on the shape of the plasma cross section.

Let´s assume that the ion density n and the ion temperature kT are known as a function of ε; that is, assume that values of plasma density and temperature are known at each isobar. The volumetric rate r_{DT} at which fusion reactions occur is given by:

$$r_{DT}(\varepsilon) = k_{DT}(kT)\frac{n^2}{4} \tag{3.4}$$

The factor k_{DT} is known as the *rate constant*, and has units of m^3/s. It is the weighted average of the product between the cross section and the velocity over the energy distribution. For thermalized ions, the energy distribution is of the Maxwell-Boltzmann (MB) type f_{MB} given by:

$$f_{MB}(E) = 2\sqrt{\frac{E}{\pi}}\,kT^{-\frac{3}{2}}\,e^{-\frac{E}{kT}} \qquad (3.5)$$

Therefore, the rate constant can be calculated if the microscopic cross section σ_{DT} for the DT fusion reaction as a function of energy (Figure 1.15) is known:

$$k_{DT}(kT) = \int_0^\infty \sigma_{DT}(E)\, v\, f_{MB}(E)\, dE = \frac{2\sqrt{2}}{\sqrt{m\pi}} kT^{-\frac{3}{2}} \int_0^\infty E\, \sigma_{DT}(E)\, e^{-\frac{E}{kT}}\, dE \qquad (3.6)$$

If the only information available is cross section data at different energies, eq. (3.6) needs to be numerically integrated for different values of kT to obtain the rate constant as a function of ion temperature. An alternative is the use of polynomial fits to the rate constant as a function of temperature; for this work, the numerical fits suggested in [69] for the rate constant are utilized. If the functional relationship between k_{DT} and kT is established, the local volumetric reaction rate can then be calculated using eq. (3.4).

Once the local volumetric reaction rate is known, the total number of neutrons emitted per second by the whole plasma, denoted by S, would be the integral over the plasma volume of the volumetric reaction rate:

$$S = \int r_{DT}\, dV = \frac{1}{4}\int k_{DT}\, n^2\, dV \qquad (3.7)$$

Since both kT (and therefore k_{DT}) and n are functions of the parameter ε, the volume integration in eq. (3.7) needs to be done as:

$$S = \frac{1}{4}\int_0^{\varepsilon_{max}} k_{DT}\, n^2 \frac{dV}{d\varepsilon}\, d\varepsilon \qquad (3.8)$$

Clearly, a parametrization of the plasma volume with ε will be necessary to calculate S. The plasma volume is generated by rotating the plasma cross section in the rz plane, given by eq. (3.2), around the z axis. Appendix A presents the procedure for the parametrization of the plasma volume in detail. Using the results from Appendix A, the integral (3.8) can be written as:

$$S = \frac{\pi R_p^3 \kappa}{2}\int_0^{\varepsilon_{max}} k_{DT}\, n^2\, (4\varepsilon I_1 + 3\varepsilon^2 I_2)\, d\varepsilon \qquad (3.9)$$

The values for I_1 and I_2 are obtained from Figure (A.1) or from numerical integration of eq. (A.6). The cumulative distribution function (CDF) F for neutron emission, defined as the number of neutrons per second emitted up to the plasma isobar ε divided by the total number of neutrons emitted by the plasma, can be derived from eq. (3.9):

$$F(\varepsilon) = \frac{\pi R_p^3 \kappa}{2S} \int_0^{\varepsilon} k_{DT}(\varepsilon')\, n(\varepsilon')^2 \left(4\varepsilon' I_1 + 3\varepsilon'^2 I_2\right) d\varepsilon' \tag{3.10}$$

From the CDF in eq. (3.10), the probability density function (PDF) f can be found:

$$f(\varepsilon) = \frac{dF}{d\varepsilon} = \frac{(4\varepsilon I_2 + 3\varepsilon^2 I_3)\pi R_p^3 \kappa\, k_{DT} n^2}{2S} \tag{3.11}$$

The PDF in eq. (3.11) is fundamental for the definition of the neutron source, since it effectively gives a neutron emission probability map for the plasma volume, which is required for the modeling implementation of the volumetric neutron source.

3.1.3 Tritium breeding.

As mentioned in Section 1.4.1, the production of one neutron in the plasma implies the consumption of one tritium nucleus. Tritium, unlike deuterium, is not a natural hydrogen isotope, and has to be manufactured via the reaction shown in eq. (1.8), between a neutron and a ^{6}Li nucleus. The tritium volumetric production rate r_T will be given by:

$$r_T = n_{Li} \phi \int_0^{\infty} \sigma_{Li-n}\, f(E)\, dE \tag{3.12}$$

Here, ϕ is the *neutron flux* (the product of neutron speed times neutron density) in units of cm^{-2} s^{-1}, n_{Li} is the atomic density of ^{6}Li atoms at the point of calculation, f is the energy PDF for the neutron flux and $\sigma_{Li\text{-}n}$ is the microscopic cross section for the reaction between and neutron and a ^{6}Li nucleus producing a tritium nucleus, shown in Figure 3.5. If the neutrons are monoenergetic, f is a Dirac delta function at the neutron energy and the integral in (3.12) is trivial: the integrand evaluated at the neutron energy; however, most of the times the neutron flux has an energy PDF and the rate needs to be calculated by performing the integral of the cross section weighted by the neutron flux energy PDF.

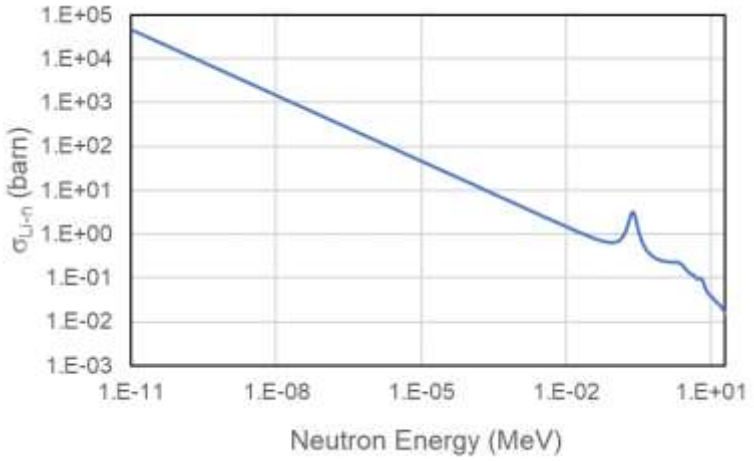

Figure 3.5. Microscopic cross section for the reaction between a neutron and a 6Li nucleus resulting in a tritium nucleus and an alpha particle (1 barn = 10-28 cm2).

If the goal is to increase the amount of tritium produced, the following strategies can be implemented:

- Increase the atomic density of ^{6}Li in the material. Table 3.I presents different compounds containing lithium often cited as potential liquid and solid tritium breeding materials in nuclear fusion devices [70] and their natural atomic densities of ^{6}Li. If the material is "enriched" with ^{6}Li by artificial means, the atom density will increase accordingly. Presence of other atoms in the breeder such as O, C, S or Pb will affect the tritium breeding performance of the material [71].
- Increase the neutron flux. Tritium breeding needs to occur at locations where the flux is high, as close to the neutron source as possible. The plasma inboard and the top and bottom of the plasma are possible areas for locating tritium breeding infrastructure.
- Ensure the neutron energy PDF is high at low energies and low at high energies. Placement of a graphite or water layer before the breeding material can effectively moderate the neutrons and shift the neutron energy distribution towards the low energy spectrum, with the consequent increase in tritium production rate due to the increase in the cross section.

Table 3.I. Natural atomic density of 6Li for some solid and liquid tritium breeding materials.

Material	*State*	*Molar mass (g/mol)*	*Density (g/cm^3)*	*^{6}Li atomic density (10^{21} cm^{-3})*
Li	*Solid/liquid*	*6.94*	*0.534*	*3.52*
Li_2O	*Solid*	*29.88*	*2.01*	*6.15*
LiF	*Solid*	*25.94*	*2.64*	*4.65*
Li/Pb eutectic	*Liquid*	*173*	*10*	*0.45*
Li_2C_2	*Solid*	*37.9*	*1.3*	*3.14*
FLiBe	*Solid/Liquid*	*33*	*1.94*	*2.69*
$LiAlO_2$	*Solid*	*65.92*	*2.62*	*1.82*
Li_2TiO_3	*Solid*	*109.76*	*3.43*	*2.86*
LiOH	*Solid*	*23.95*	*1.46*	*2.79*

3.1.4 Neutron multiplication.

Without the presence of some material able to multiply the number of neutrons in the system, there would only be enough neutrons to breed the necessary tritium used as fuel in the plasma. For systems aimed at extracting energy from the neutrons, their economy is not so relevant as long as they can be converted into tritium and this tritium recovered with high efficiency. And even on pure fusion systems, neutron multipliers are necessary to recover tritium losses and extraction inefficiencies to maintain the tritium self-sufficiency [72]. On a hybrid system, where neutrons need to perform other tasks in addition to tritium breeding, neutron multiplication becomes even more critical.

There are three materials often cited as neutron multipliers in fusion systems: beryllium, lead and zirconium [73]. Their cross sections for the (n, 2n) reactions are shown in Figure 3.6. Unlike the tritium breeding reaction, the neutron multiplication reaction has energy thresholds above 1 MeV, so the neutron multiplier needs to have a fairly unobstructed access to the fusion neutrons, otherwise neutron multiplication may not occur. And although Pb seems to be a better option that Be from the point of view of cross section magnitude, strong neutron absorption and activation issues make Be a more attractive choice. Many blanket designs involve the use of beryllium as the most vital material [54], because of its exceptional properties as an excellent neutron multiplier and moderator, and its low absorption cross section for thermalized neutrons. Using MCNP,

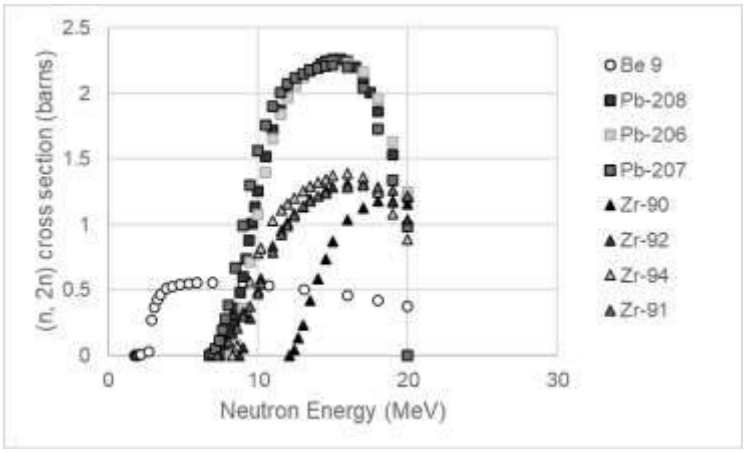

Figure 3.6. Microscopic cross sections for the (n,2n) reaction between and energetic neutron and Be, Pb and Zr natural isotopes.

For the neutron multiplier, the multiplication factor will be a strong function of the thickness. Different scenarios were analyzed, where beryllium layer thickness was changed in order to get an optimal neutron multiplication output. The computer model of this project has a beryllium reflector with an entire circular geometry as shown in Figure 3.7. For example, in green color beryllium layers. At first, neutron multiplication increases rapidly with thickness, until a saturation effect is observed, and eventually losses by scattering and absorption start to dominate and the neutron multiplication factor starts to slowly decrease.

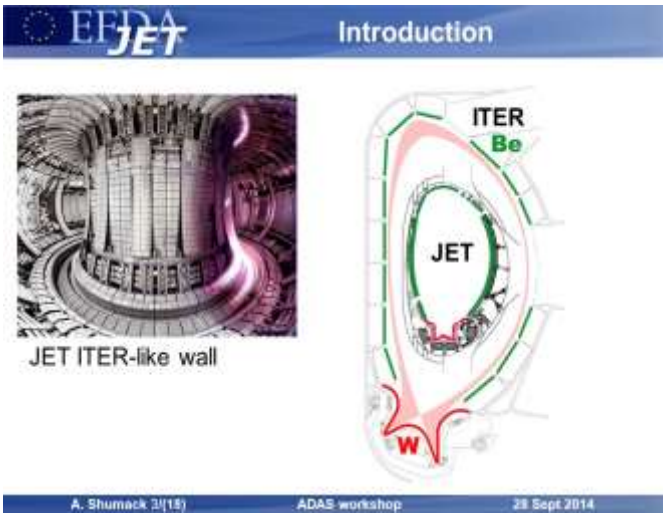

Figure 3.7. JET ITER – like with Beryllium wall in color green indicated [74].

The beryllium nucleus characteristic is that the binding nucleon energy is sufficiently lower than a nuclear reaction such that an energetic particle resulting with a neutron emitted. Figure 3.8 shows this characteristic, in Chain 3, indicating that beryllium can be a neutron multiplier. In fact, chain 3 is recognized as a good neutron multiplier for fusion reactors.

Q-values of (n, 2n) for beryllium reactions has the following magnitudes:

$n + Be \rightarrow 2n + 2^4He$ -1.7 MeV,

Energy balances in this tritium process generation for beryllium case is as follows:

-1.8 MeV + 4.8 MeV = ~3 MeV,

Energy multiplication in the beryllium neutron multiplier is enhanced, energy multiplications are obtained as 1.35 according to increasing beryllium thickness, at the multiplier thickness of about 10 cm. Beryllium has been accepted as the neutron multiplier because of the Q-value and number density greater. The lowest Q-value in a (n, 2n) reaction is in fact of beryllium of all nuclides, and also is chosen for this work based on energy multiplication considerations and TBR. Figure 3.9, shows beryllium as a multiplier, neutron multiplication improves with a thicker beryllium wall until approximately 25 cm.

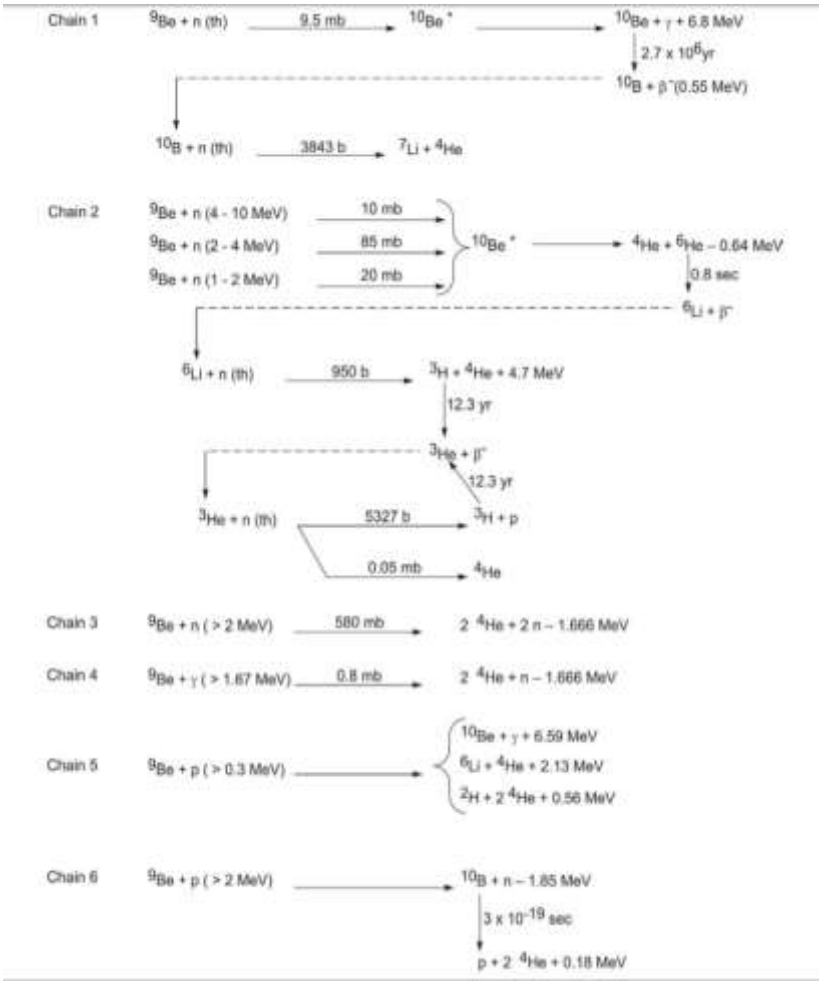

Figure 3.8. Beryllium nuclear reaction chains [75].

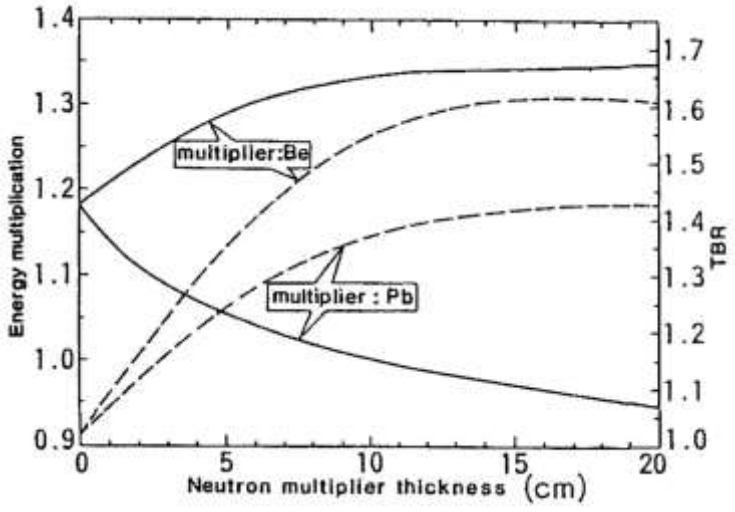

Figure 3.9. Energy Multiplication in High Tritium Breeding Ratio Blanket with Front Breeder Zone for Fusion Reactors [76].

3.1.5 The fission blanket.

Due to the tokamak geometry, it is safe to assume that the neutron source can be enclosed by a straight cylinder of a given height and radius. Sources with the height greater than the radius would be preferred since the neutron flux decays as $1/r$, and therefore plasmas with high elongation and low aspect ratio R_p/r_p would be preferred. Since the present design considers the neutron source a replaceable component for the irradiator, a physical disconnection between the fission blanket and the neutron source would be desirable. The simplest way to accomplish this is to design the fission blanket as a ring container around the tokamak neutron source, as shown in Figure 3.10.

The fission blanket container is characterized by three dimensions: the inner radius, the height and the outer radius. The height is constrained in the sense that it needs to be sufficient to accommodate a 4 m long fuel assembly. The inner radius is also constrained, since it needs to be equal to the outer radius of the neutron source enclosure. The only parameter left to determine the capacity of the fission blanket is the outer radius. And this parameter is also somewhen constrained for two reasons: the neutron flux drops as $1/r$, so assemblies placed near the outer edge of a fission blanket with a large outer radius will get a very small neutron flux; also, the toroidal field coil for the tokamak neutron source may go around the fission blanket in some designs, and a large radius coil would require more current to achieve the desired toroidal field in the plasma region.

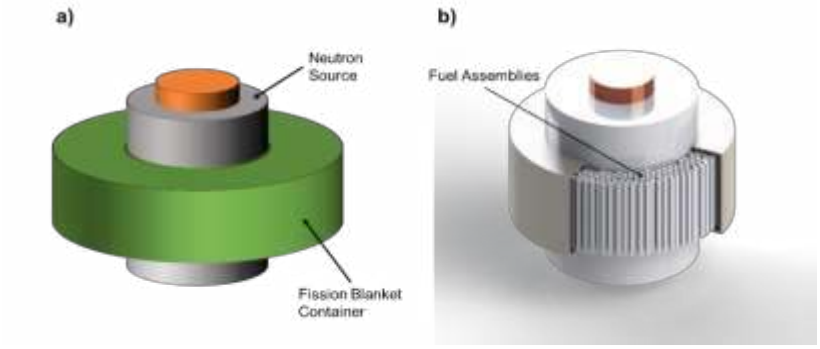

Figure 3.10. a) Sketch showing the proposed geometry for the fission blanket. b) Cutaway of the fission blanket container showing fuel assemblies.

Section 1.4.3 has already touched on some of the geometrical aspects of the fission blanket. As mentioned there, the strategy for placing the fuel assemblies in the blanket is the use of concentric regular polygons with a given symmetry angle. The radius r of the circle inscribed in a regular polygon with n sides of length L is given by the following expression:

$$r = \frac{L}{2}\cot\frac{\pi}{n} \tag{3.12}$$

To preserve the symmetry, the sequence of concentric polygons needs to have integer multiples of a base number of sides n, determined by the desired angle of symmetry θ_{sym} (in radians) for the system:

$$n = \frac{2\pi}{\theta_{sym}} \tag{3.13}$$

It should be noted that n needs to be an integer value, since it represents the number of sides of the base polygon. The inscribed circle radius for the j^{th} concentric polygon can now be found as a function of the polygon side length and the selected symmetry angle:

$$r_j = \frac{L}{2}\cot\frac{\theta_{sym}}{2j} \tag{3.14}$$

The spacing between two consecutive inscribed circles is given by:

$$\Delta r_j = r_{j+1} - r_j = \frac{L}{2}\left(\cot\frac{\theta_{sym}}{2(j+1)} - \cot\frac{\theta_{sym}}{2j}\right) \tag{3.15}$$

When the term in parenthesis on the RHS of eq (3.15) is equal to 2, the spacing between the consecutive polygons is equal to L, and a square of side L can be accommodated; otherwise, the placement needs to be done in the following concentric polygon. Figure 3.11 presents the radius of the inscribed circles and the spacing between consecutive inscribed circles normalized to the side length. The curves in the Figure are for different values of n. As n gets larger, the radius of the concentric polygons grows as well, while the spacing between concentric polygons is constant for $j > 3$. For $n < 7$, the spacing between consecutive polygons is smaller than L ($\Delta r/L < 1$), so a symmetry angle smaller than $\pi/8$ would be desirable for facilitating the placement of the fuel assemblies in the blanket container. If larger angles of symmetry are required, one concentric polygon needs to be skipped in order to accommodate a fuel assembly.

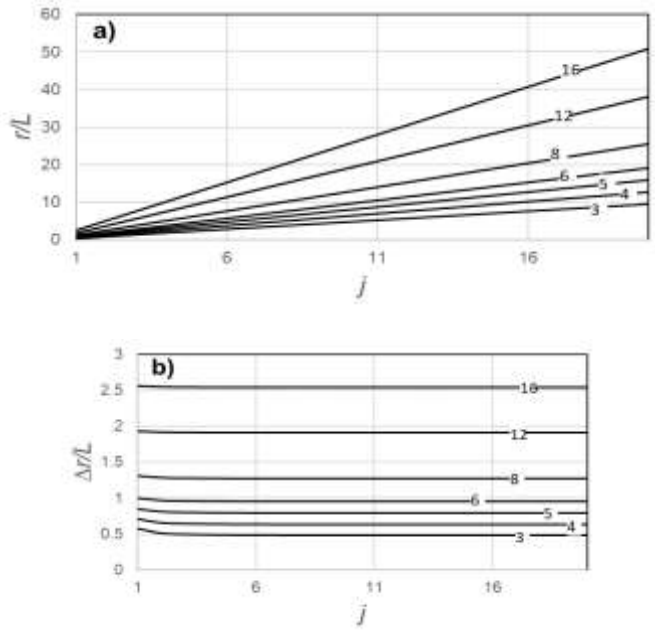

Figure 3.11. a) Radius of the consecutive concentric polygons normalized to the side length; b) space between consecutive concentric polygons. Horizontal axis is the number of the polygon/spacing in the sequence, and curves are for different values of n.

Considering that the dimensions of a PWR reactor fuel assembly are 0.2 x 0.2 x 4 m, Figure 3.12 presents the estimated capacity of assemblies given the tokamak cask outer radius and the outer radius of the fuel assemblies container for symmetry angles of π/8 and π/16. With a tokamak cask outer radius of 2 m and a fission blanket container with 3.75 m of outer radius, up to 560 assemblies can be placed in that space for a symmetry angle of π/8.

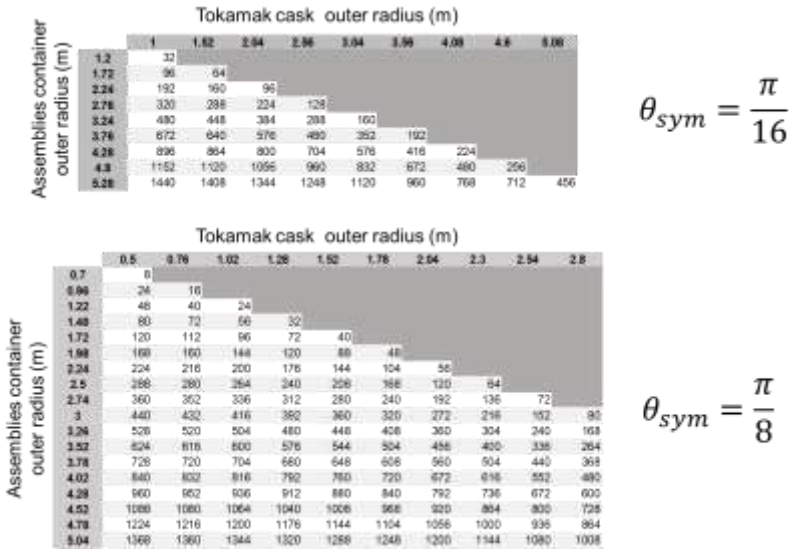

Figure 3.12. Blanket fuel assemblies capacity for two symmetry angles as a function of inner and outer radius. Capacity is found by intersecting the row corresponding to the blanket container outer radius and the column corresponding to the tokamak cask outer radius.

Considering that the dimensions of a PWR reactor fuel assembly are 0.2 x 0.2 x 4 m, Figure 3.12 presents the estimated capacity of assemblies given the tokamak cask outer radius and the outer radius of the fuel assemblies container for symmetry angles of π/8 and π/16. For example, with a tokamak cask outer radius of 2 m and a fission blanket container with 3.75 m of outer radius, up to 560 assemblies can be placed in that space for a symmetry angle of π/8. With those same dimensions, a blanket with a symmetry angle of π/16 can accommodate 576 assemblies.

As mentioned previously, assemblies in the different radial zones of the blanket will be exposed to different neutron fluxes: those closest to the source will receive a higher flux, with an energy spectrum containing a strong high-energy component, and those in the outermost zones will receive a smaller flux and the energy distribution will be different. If the goal is to give the assemblies an homogeneous treatment (i.e. reaching the same level of fissile material or minor actinides in all assemblies, depending on the primary function), shuffling the assemblies between zones will be necessary; the assemblies in the innermost zone will spend a certain amount of time there, and then moved to the outermost zone, the assemblies in the second zone will go to the first, those in the third zone will go to the second, those in the fourth to the third, and so on. The shuffling scheme needs to consider that different zones have different assembly capacities (outer zones tend to have a higher capacity), that different enrichment/destruction targets may be desired, or that assemblies in a single zone are not identical. However, the development of an optimal shuffling strategy is beyond the scope of the present work and needs to be developed as part of future efforts.

In lieu of a formal shuffling strategy, a simpler scheme for the purpose of enriching fuel is presented here. This approximation is adequate to obtain an estimate of the required irradiation time to reach a given level of enrichment. The enrichment X will be defined as:

$$X = \frac{m_f}{m_0 - m_f} \approx \frac{m_f}{m_0} \tag{3.16}$$

Where m_0 is the initial mass of fertile material and m_f is the mass of fissile material at the end of the irradiation cycle, and the approximation is valid for low levels of enrichment.

Consider i radial zones, which will be assumed to hold equal number of assemblies each, so they can be interchanged one-to-one. The fissile material production rate f_i for each zone is given by:

$$\frac{dn_i}{dt} = f_i(n_i, t) \tag{3.17}$$

So the amount of fissile material gained by an assembly sitting in region i from time t to time $t+\Delta t$ can be written as:

$$n_i(t + \Delta t) = n_i(t) + \int_t^{t+\Delta t} f_i(n_i, t')dt' \tag{3.18}$$

Consider now the shuffling strategy, represented by a vector **i** of size m (equal to the number of movements of the assembly) containing a sequence of positions of the assembly in the blanket zones, i_j; for example, if an assembly starts at zone 1, then goes to zone 2, then to zone 3, and then back to zone 1, the *shuffling vector*, which represents the movements of an assembly in the blanket, is given by **i** = (1, 2, 3, 1). In addition to the shuffling vector, an *irradiation time vector* **T** can be defined, indicating the time spent at each position by the assembly. If the assembly from the previous example spends 30 days in zone 1, then 60 days in zone 2, then 90 days in zone 3 and finally 60 days in zone 1, the irradiation time vector is given by **T** = (30, 60, 90, 60). The sum of the components of vector **T** give the total irradiation time of the assembly.

For this simple shuffling scheme, it will be assumed that the fissile material generation rate is a constant, independent of time and composition of the fuel assembly. Under that assumption, the mass of fissile material on an assembly with shuffling vector **i** with components i_j and time irradiation vector **T** with components T_j is:

$$m_f = \sum_{j=1}^{m} f_{i_j} T_j \tag{3.19}$$

This discussion can be extended for the scenario of a blanket that has *n* available zones, with equal number of assemblies on each zone, and with all the assemblies in the blanket spending the same total amount of time in the blanket. If all assemblies in each zone are identical, eq. (3.19) can be written in vector-matrix form:

$$\mathbf{m_f} = \mathbf{F} \cdot \mathbf{T} = \begin{pmatrix} \mathbf{F_1} \\ \mathbf{F_2} \\ \vdots \\ \mathbf{F_n} \end{pmatrix} \mathbf{T} \tag{3.20}$$

The final mass is now a vector $\mathbf{m_f}$, with one component representative for assemblies in the different *n* zones of the blanket in the beginning. The matrix **F** contains the generation rate functions for each zone, arranged to represent on its rows $\mathbf{F_j}$ the shuffling history for a group of assemblies in the blanket that move as a block from zone to zone. If the target final mass for assemblies in the blanket is known, the irradiation time vector can be found:

$$\mathbf{T} = \mathbf{F^{-1}} \cdot \mathbf{m_f} \tag{3.21}$$

A practical example should help to better understand how the required irradiation time is calculated, and this example is shown graphically in Figure 3.13. In this example, consider a blanket with 3 zones, where the fissile material production rates for each zone are f_1, f_2 and f_3, all in g/day. The shuffling strategy is as follows:

- After T_1 days, assemblies in zone 1 go to zone 3, assemblies in zone 2 go to zone 1, and assemblies in zone 3 go to zone 2.
- After T_2 days, assemblies in zone 1 go to zone 3, assemblies in zone 2 go to zone 1, and assemblies in zone 3 go to zone 2.
- After T_3 days, all assemblies are taken out.

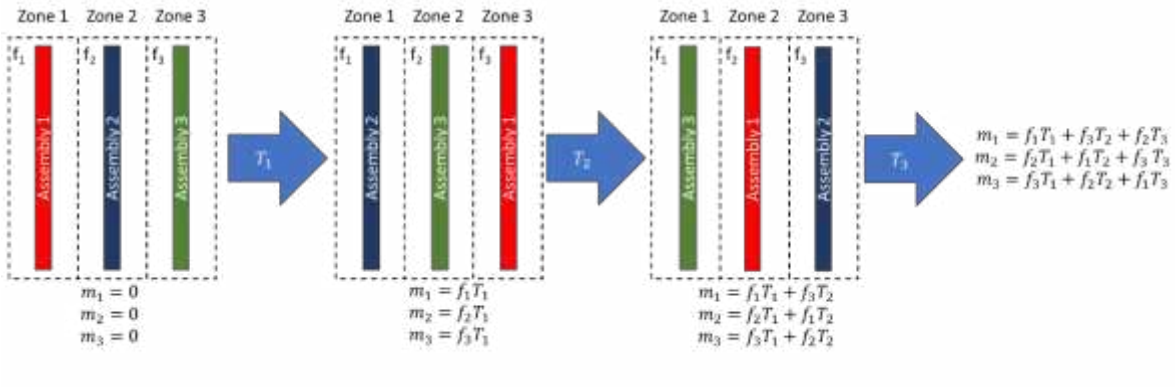

Figure 3.13. Shuffling strategy for fuel assemblies in a fission blanket with 3 zones, each one with fissile material production rate fi.

For the assemblies initially in zone 1, their final mass of fissile material is given by:

$$m_{f,1} = f_1 T_1 + f_3 T_2 + f_2 T_3 \tag{3.22a}$$

Similarly, for the assemblies that were in zone 2 when the irradiation process started, the final mass of fissile material is:

$$m_{f,2} = f_2 T_1 + f_1 T_2 + f_3 T_3 \tag{3.22b}$$

And for those initially in the third zone:

$$m_{f,3} = f_3 T_1 + f_2 T_2 + f_1 T_3 \tag{3.22c}$$

It is easy to see that eqs (3.22a-c) can be combined into a single vector equation:

$$\begin{pmatrix} m_{f,1} \\ m_{f,2} \\ m_{f,2} \end{pmatrix} = \begin{pmatrix} f_1 & f_3 & f_2 \\ f_2 & f_1 & f_3 \\ f_3 & f_2 & f_1 \end{pmatrix} \begin{pmatrix} T_1 \\ T_2 \\ T_3 \end{pmatrix} \tag{3.23}$$

Thanks to eq. (3.23), for a given shuffling strategy (represented by the matrix **F**) and a vector of irradiation intervals between shuffles **T**, the content of fissile material at the end of the irradiation can be found for all the assemblies initially present in the blanket. In consequence, the sequential exposures times for each of the shuffle steps required to achieve a target content of fissile material for each of the assembly groups can also be fount using eq. (3.21).

3.2 The MCNP code.

MCNP is a general purpose nuclear code that computes nuclear particles (neutron, photon) and electron distributions in a continuous energy and generalized geometry, as well as time dependent, using the Monte Carlo calculation technique [77]. It has the characteristic to be used in neutron, photon and electron only transport modes. But also combined neutron with photon transport mode where neutron interactions produce photons, other transport modes are neutron with photon and electron, and photon with electron, or electron with photon. For all isotopes, spectrum energy is from 10^{-5} eV to 20 MeV and for 150 MeV some isotopes. Whereas from 1 keV to 100 GeV spectrum energy of the photon, and from 1keV to 1 GeV, electron energy spectrum. Inputs are created by the user and then MCNP reads such inputs. Basically, inputs information contain data about geometry specification, materials compositions and cross section, as well as the source location and characteristics of particles, definition of tallies required, variance reduction techniques improving efficiency.

It is so difficult to predict neutrons and nuclei behavior. Nevertheless, the whole behavior of a great quantity of neutrons can be simulated effectively with neutron fluxes, having knowledge of its behavior, reaction rates and cross sections. MCNP base its calculations in the transport theory by solving the Boltzmann transport equation which describes neutral particles transport when it collides with an atom to the collision to another. Basically results in a balance equation statement that calculates the sum and rest of several particles in the distribution defined space for certain energy and direction of movement and well as the time dependent variable.

$$\frac{1}{v(E)}\frac{d\Phi(r,E,\Omega,t)}{dt} \quad (3.24a)$$

$$= -\Omega\cdot\nabla\Phi(\mathrm{r},\mathrm{E},\Omega,\mathrm{t}) \quad (3.24b)$$

$$-\sum_t(\mathrm{r},\mathrm{E},\Omega)\,\Phi(\mathrm{r},\mathrm{E},\Omega,\mathrm{t}) \quad (3.24c)$$

$$+\chi(\mathrm{E})\int_{\mathrm{E}'}\mathrm{dE}'\int_{\Omega'}\mathrm{d}\Omega'\nu\sum_{\mathrm{f}}(\mathrm{r},\mathrm{E}',\Omega',\mathrm{t})\,\Phi(\mathrm{r},\mathrm{E}',\Omega',\mathrm{t}) \quad (3.24d)$$

$$+\int_{\mathrm{E}'}\mathrm{dE}'\int_{\Omega'}\mathrm{d}\Omega'\nu\sum_{\mathrm{s}}(\mathrm{r};\ \mathrm{E}'\rightarrow\mathrm{E};\ \Omega'\rightarrow\Omega)\,\Phi(\mathrm{r},\mathrm{E}',\Omega',\mathrm{t}) \quad (3.24e)$$

These equations represent each one a rate term, volume, direction and energy (per unit)

- Term 3.16a = neutrons accumulated rate
- Term 3.16b = leakage rate
- Term 3.16c = interaction rate (total scattering or absorption or energy).
- Terms 3.16d and 3.16e production phenomena from E' and Ω' neutrons reacting with nuclei to generate E and Ω neutrons.
- Term 3.16d = total fission rate; then χ(E) refers to the energy spectrum produced in the fission process.
- Term 3.16e = scattering with initial energy (E') to final (E) initial direction (Ω ') to final (Ω).

The full Boltzmann transport equation has seven independent variables (3 in space, 2 in direction, energy and time). Sometimes the terms vary widely with one or more variables.

Basically to define an MCNP input, it must contain five fundamental components:

a. Regions or volumes bounded are treated by MCNP primarily as a geometry problem of surfaces in first and second degree terms. Definitions of cells are as algebra Boolean operations of complements, unions and intersections of the regions, and user definition of materials contained. Cartesian coordinate 3D (x, y, z) system is used by MCNP. Volumes or cells constitute all the space in composed contiguous fashion. Cells are bounded by surfaces, one or multiple, or infinity as well. No "gaps" are allowed in the geometry definition of a model, i.e., points belonging to no surfaces, no cells are allowed, an execution error message will be indicated. A unique identified number given by user for each surface and cell.
b. Data specification, definition of particle types, sources of radiation, scored results (tallied), interactions of particles, techniques of variance reduction, libraries of cross section, type of output amount.
c. Material composition, cells material compositions with the following elements: (a) material number (unique definition), (b) isotopic composition, (c) utilization of cross section compilations.
d. Neutron source definition, this task should not be as difficult as it could appear, but as for a hybrid reactor concept, neutron source could be a complex model to define, a toroidal shape of the real source must be taken into account to represent a more realistic model of the source corresponding to a tokamak fusion core.
e. Parameters of interest are scoring by the tally definition process, providing for each answer, fractional standard deviation, relative error. Tally definition is an input card with the format Fna, "n" is a unique number and "a" is for a neutron (N), photon (P) or electron (E) type of particle. Instructions to define the scoring of interesedt parameters are shown in table 3. II. It can be noted that multiples of 10 adding keeps the type of tally, i.e. F2, F12, F22 are F2 tallies, specified for different reasons.

Table 3.II. Types of tallies available in MCNP. The type of particle tallied is denoted by *pl* [77].

Mneumonic	*Tally Type*	*particles pl*	*Fn Units*	**Fn Units*
F1:pl	*surface current*	*N or P or N,P or E*	*#*	*MeV*
F2:pl	*average surface flux*	*N or P or N,P or E*	*#/cm2*	*MeV/cm2*
F4:pl	*average flux in a cell*	*N or P or N,P or E*	*#/cm2*	*MeV/cm2*
FMESH4:pl	*track-length tally over 3D mesh*	*N or P or E*	*#/cm2*	*MeV/cm2*
F5a:pl	*flux at a point or ring*	*N or P*	*#/cm2*	*MeV/cm2*
FIP5:pl	*pin-hole flux image*	*N or P*	*#/cm2*	*MeV/cm2*
FIR5:pl	*planar radiograph flux image*	*N or P*	*#/cm2*	*MeV/cm2*
FIC5:pl	*cylindrical radiograph flux image*	*N or P*	*#/cm2*	*MeV/cm2*
F6:pl	*energy deposition*	*N or P or N,P*	*MeV/g*	*jerks/g*
F7:pl	*fission energy deposition in a cell*	*N*	*MeV/g*	*jerks/g*
F8:pl	*pulse height distribution in a cell*	*N or E or P,E*	*pulses*	*MeV*

3.3 The SCALE code.

SCALE is a suit of nuclear codes developed by Oak Ridge National Laboratory, Oak Ridge, Tennessee [78]. The main goal of SCALE is to provide a suite of tools aimed to make calculations reducing user input requirements. SCALE is designed to provide sequences that are standard with modern and advanced capabilities integrated when user defines a simple input file having the control of a seamless calculation. Scale also has other utility modules to make post processing of the data generated from the sequence of analysis for advanced studies. Input sequences are provided in text files [78]. Two codes of the SCALE suit are used in the present work: COUPLE and SCALE.

3.3.1 COUPLE.

COUPLE is a coupling code that prepares the transition matrix A from Eq. (3.12), which contains the decay and cross section transition rate constants. The transition matrix and other important data are stored on an ORIGEN library (f33) file for use by other modules. COUPLE has two distinct modes of operation: 1. to create a new decay-only ORIGEN library from an ORIGEN decay resource, and 2. to add new or to update existing reaction transitions yield resource, reaction resource, and optionally an AMPX working library containing multigroup cross sections. Details on the decay, yield, and reaction resources may be found in the ORIGEN Data Resources chapter in the SCALE user´s manual.

This section briefly highlights some key features in COUPLE and describes how they are used. AMPX multigroup libraries contain multigroup cross sections by nuclide and material-zone identifiers. If the working library is the result of a multiregion transport calculation, then it is important to specify the correct zone identifier, e.g. corresponding to the fuel in a problem with moderator, clad, and fuel zones. The neutron flux is also stored on the AMPX library associated with a nuclide and a zone as are the cross sections. An AMPX library flux can be used to perform the cross section collapse as an alternative to providing a flux spectrum in the COUPLE input. New transitions may be added to the ORIGEN binary library for all reactions for which there are data in the weighted AMPX library if both the target and product nuclides are present in the ORIGEN library.

Nuclide specification in COUPLE, the following nuclide identifier is used: Nuclide identifier = Z * 10000 + A * 10 + I, where Z = atomic number, A = mass number, I = metastable/isomeric state

(0 is ground/1 is first metastable) Examples include 922350 for 235U and 952421 for 242mAm. Note that this varies from the identifiers used in other ORIGEN-related modules in which the isomeric state I comes first, as in 1095242 for 242mAm. Adding new transitions and user-defined transitions. The use of a transition matrix in ORIGEN allows any nuclide to transition to any other nuclide. By default, when the reaction data on the library is updated, then the transition matrix's sparse storage is expanded to include the new reaction transition if both the target and the reaction product nuclide are in the library.

The user may explicitly set one-group transition coefficients by setting Block1 1$$ LBUP=1 and entering Block6 and Block8 data. Unit numbers and Aliases In COUPLE, a unit number is used instead of a full file name to specify files, where unit number XY links to the data file "ftXYf001" in the working directory. For example, unit number 33 means file ft33f001. There are several predefined unit numbers that are controlled by a special "origen_filenames" file, which creates an alias for the local file "ftXYf001" to a file in the data directory. Table 3.7 shows the basic COUPLE unit numbers, their aliases, and a description of the file. An "origen_filenames" list which maps unit number 21 to alias "END7DEC" could link unit 21 to the file "${DATA}/origen.rev04.end7dec," where ${DATA} is the path to the SCALE data directory. To override this association, COUPLE must find a file named "ft21f001" in the working directory. The entire set of unit numbers is given in the ORIGEN Data Resources chapter.

Table 3.III. Couple basic units.

17	*YIELDS*	*ORIGEN Yield Resource*
21	*END7DEC*	*ORIGEN library ENDF/B-VII-based decay transitions only*
27	*DECAY*	*ORIGEN Decay Resource*
80	*JEFF252G*	*ORIGEN Reaction Resource (252 groups)*

COUPLE uses the FIDO input system, except for title entries. The input is arranged in blocks, with each block containing one or more arrays, followed by the FIDO block terminator "t." Each input parameter is named and defined below in the order in which it appears, with the index of the parameter in the array. Some options have been deprecated over time and thus the first available entry may not correspond to index "1" and some indices may be skipped. Default values are given in parentheses. In the SCALE code system, COUPLE input appears between "=couple" and "end." Block1: titles, unit numbers, and case controls. TITLE – Title lines Title lines can provide information about the ORIGEN library created and printed when the library is used. The input Block1 1$$ NUMA allows title lines to be copied from the input library to the output library. The first blank line terminates the title. A maximum of 40 lines can be included in the library. A special title of "DONE" in the first four columns marks the completion of a COUPLE input case. 0$$ Array – Logical Unit Assignments 1.

3.3.2 ORIGEN.

The Oak Ridge Isotope Generation (ORIGEN) has multiple calculation functions as activities, radiation, concentrations of a great number of isotopes that can be depleted or generated simultaneously by the transmutation of neutrons, radioactive decay and fission. ORIGEN has the capability nuclide feed rates included continuously and rates of chemical removal continuously described with constants of rates in reprocessing applications or other nuclide removal or feed system involved. Multi-group cross sections capability is included in ORIGEN from evaluations processed from standard ENDF/B. Modeling user-defined systems can use transport codes within SCALE,

applying COUPLE to calculate neutron-spectrum-weighted problem dependent representing conditions of cross sections in a given fuel assembly or reactor converting these cross sections into an ORIGEN library to be used. During irradiation, to reflect fuel composition variations, time dependent cross section libraries can be produced.

The ORIGEN module drives depletion, decay, and activation calculations, including the conversion of generated powers to fluxes, as well as alpha, beta, gamma, and neutron source calculations. It solves the following set of kinetic equations for nuclear interactions:

$$\frac{dN_i}{dt} = \sum_{j \neq i}(l_{ij}\lambda_j + f_{ij}\sigma_j\Phi)N_j(t) - (\lambda_i + \sigma_i\Phi)N_i(t) + S_i(t) \quad (3.25)$$

The nuclide identifiers in ORIGEN are more flexible than those in other modules of SCALE such as COUPLE. Table 3.IV shows the possible ways to specify nuclides (and elements). One important aspect ORIGEN users must be aware of is that the ORIGEN library (f33) being used dictates the set of nuclides available in a calculation and that there may be more than one version of a nuclide in a library.

Table 3.IV. Nuclide/Element Specification in ORIGEN.

Identifier Form	*Comments*	*Examples* *nuclide → input id*
IZZZAAA *I – isomeric state* *ZZZ – atomic number* *AAA – mass number*	*Standard numeric identifier with one optional digit of isomeric state, three digits of atomic number, three digit of mass number; elements have mass number of 000.*	$^{235}U \rightarrow 92235$ $^{235m}U \rightarrow 1092235$ $^{135}Xe \rightarrow 54135$ $^{1}H \rightarrow 1001$ $^{10}B \rightarrow 5010$ *Fe → 54000*
EAm *E – element symbol* *A – mass number* *m – metastable indicator*	*Standard symbolic identifier with element symbol followed by mas number, followed by optional metastable indicator; can include a dash between E and A (E-Am); case insensitive.*	$^{235}U \rightarrow u235$ $^{235m}U \rightarrow u235m$ $^{135}Xe \rightarrow xe135$ $^{1}H \rightarrow h1$ $^{10}B \rightarrow b10$ *Fe → 5fe*

The duplicates arise in large part from the need to analyze fission products separately. For example, a gadolinia-doped uranium oxide fuel with burnup will have some 155Gd from the initial gadolinia loading and some 155Gd generated as a fission product. Although these fuels physically behave the same way, it is sometimes important to be able to analyze them separately. These groups, versions, or categories are referred to as sub-libraries because in an ORIGEN library, they appear almost like three separate, smaller ORIGEN libraries. The three libraries are for 1. Naturally occurring, light nuclides, sometimes called “light elements” or “activation products,” 2. Actinides and their reaction and decay products, and 3. Fission products. Called “sublibs” for short, they are identified by a number or 2-character specified: 1. light nuclides with “LT” or 1, 2. actinides with “AC” or 2, and 3. fission products with “FP” or 3. The production of fission products from actinides (2/AC, 3/FP) is the only type of transition in a typical ORIGEN library that spans sublibs. The sublib is optional in a nuclide specification and is indicated in parentheses after the identifier—IZZZAAA(S), EAm(S). If the sublib for a nuclide/element is not provided, it is guessed in the following manner: 1. If the nuclide is in fact an element, then it is placed in sublib=1/LT. 2. If the atomic number Z

The ORIGEN input is hierarchical, containing four levels, where level 0 is the "root" level, allowed between "=origen" and "end." The complete set of keywords is shown in Table 5.1.11, with arrays denoted with "=[]", blocks with "{}". There is a "solver" block for changing solver options, a "bounds" block for entering the energy boundaries for various particle emissions, and an "options" block for altering the miscellaneous global options. These blocks may only appear once. The remainder of the input is a sequence of "case" blocks (in the above examples there are two cases with identifiers "A" and "B"), which each case is executed in order, with each case possibly depending on one or more of the previous cases.

The most important three components are the lib, mat, and time/power/flux inputs: 1. an ORIGEN library and the transition matrix data set on it to use (lib), 2. Initial amounts of nuclides (mat), and 3. a power or flux history (time/power or time/flux). The case identifier and case title are echoed in the output file and can be a convenient way to differential cases. Both are optional, with the ID defaulting to the case index, with "1" for the first case, "2" for the second, etc. The "print" and "save" blocks represent two ways to analyze the output from a calculation. The "print" block prints tables directly to the output file, and the "save" block saves the solution in a special ORIGEN binary concentration file (f71), e.g., for later post-processing. Finally, the "alpha," "beta," "gamma," and "neutron" blocks control the emission source calculations for alpha, beta, gamma, and neutron particles, respectively. The remaining subsections will describe the input for each of these blocks.

3.4 Communication layer.

The three computational tools described above (MCNP, COUPLE and ORIGEN) need to interact among them to simulate the neutron irradiation of the fuel assemblies, the multiplication of the original neutrons and the breeding of tritium for the plasma sustainment. Formally, the multi-group cross sections and the rate equations for all nuclides would have to be solved simultaneously. However, that problem may prove impossible to solve or take an impractical amount of time and resources to solve, so the assumption that the updating of the composition and the recalculation of the neutron flux at finite intervals is sufficient to describe the problem. The simulation sequence is as follows:

- Given a geometry, materials assigned to the components of that geometry and an external neutron source, MCNP calculates the energy resolved neutron flux on the geometry sections indicated by the user.
- Given the neutron energy PDF, the COUPLE code generates a reaction matrix with the cross sections for all interactions weighted with the energy PDF, effectively transforming the problem from a multi-group calculation to a single group calculation.
- Given the neutron flux, the one-group cross section reaction matrix, the initial composition of the material and a time step, the ORIGEN code calculates the new composition of the material after the time step has elapsed.

In the problem at hand, both the geometry and the source are invariant, so they are defined at the start of the problem and remain unchanged. Some regions of the geometry (i.e. the toroidal field coil, the neutron reflectors or the center stack) might not be relevant, and they can also be marked as static materials for the purpose of the computation. Regions such as the TBRs, the NMs or the FAs require tracking of the neutron flux and their composition over time, so the regions in the geometry performing those functions are typically marked as dynamic composition regions. An inert coolant

(i.e. He) in the fission blanket can be marked as static, but a coolant with the potential to breed tritium or multiply neutrons (i.e. Li, FLiBe) can be marked as a dynamic composition region.

Although the interaction mechanism described above sounds simple in paper, the information exchange between the user and the codes and among the codes themselves made necessary the development of a communication layer, designed to translate user input into text that can be interpreted by MCNP, COUPLE and ORIGEN. This communication layer should automate the generation of input files for the codes, read the output and extract it, translate information between codes, and even help with the postprocessing of results. Originally, the MONTEBURNS code [79] was envisioned as the tool to perform this task. However, the available MONTEBURNS code was not compatible with the MCNP and SCALE versions that are available to our group.

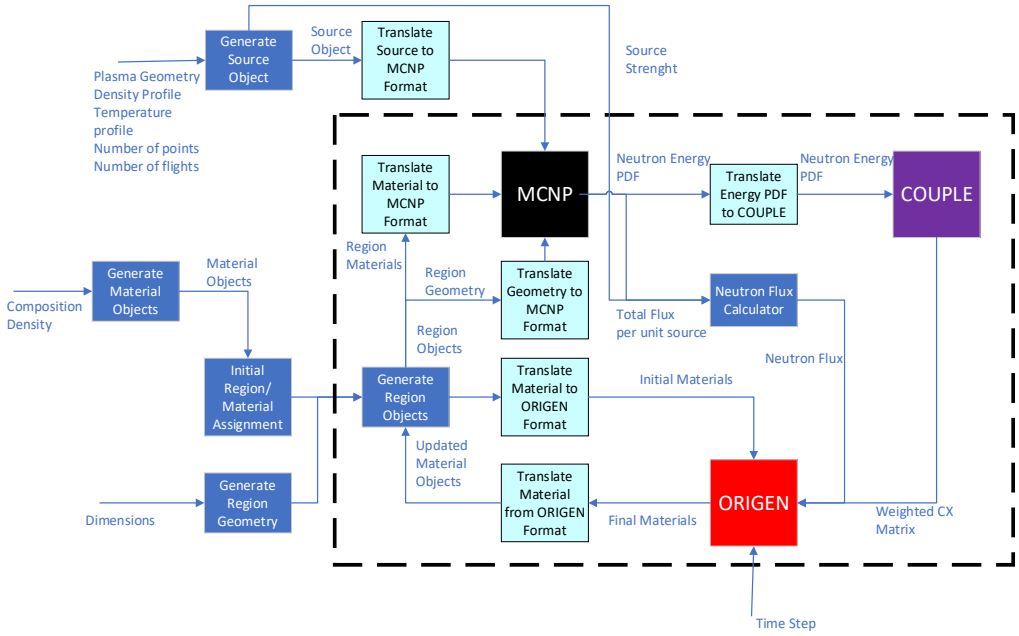

Figure 3.14. Block diagram showing the interaction between the FFHYB management layer and the three computational codes: MCNP, COUPLE and ORIGEN.

Figure 3.14 shows the interaction of the Fusion-Fission HYBrid (FFHYB) management layer and the three codes. The blue blocks are in charge of transforming the user input into internal objects. The green blocks perform internal operations between the objects generated. The cyan blocks perform translations between the internal objects and the MCNP, COUPLE and ORIGEN inputs and outputs. In the following sections, the handling of the data input and the generation of these internal objects will be discussed.

3.4.1 Source.

The neutron source is one of the most important parts of the simulation input. The FFHYB system requires the following input from the user to define the source:

- Plasma major radius (R_p)
- Plasma minor radius (r_p)

- Elongation factor (κ)
- Triangularity factor (α)
- Temperature profile (kT) in the ε (isobar) coordinate.
- Density profile (n) in the ε (isobar) coordinate.
- Number of point sources to construct the source (n_{src}).
- Number of histories for MCNP (N_H)
- The symmetry angle, in radians, to be used in the simulation (θ_{sym}).

From the input, FFHYB defines a bounding region for the plasma, which is a hollow cylinder wedge spanning the angle θ_{sym}, the inner radius is R_p-r_p and the outer radius is R_p+r_p, and the height is κr_p. The code uses three evenly distributed random numbers rnd_1, rnd_2 and rnd_3 to find the cylindrical coordinates of evenly distributed points within the wedge, using the following expressions:

$$\theta = rnd_1 \theta_{sym} \tag{3.26}$$

$$r = \sqrt{\left(R_p - r_p\right)^2 + 4R_p r_p rnd_2}$$

$$z = \kappa r_p rnd_3$$

Once the cylindrical coordinates of the random point are known, the value of ε is calculated based on the coordinates r and z. If the calculated value is greater that ε_{max} (recall that ε_{max} is equal to r_p/R_p), the point is outside the plasma volume and it is dropped. If the point is found to be within the plasma volume, the probability of emission for the given ε is calculated using the PDF for emission, eq. (3.11). A random number is generated, and if it is smaller than the value of the PDF, the point is accepted and its cartesian coordinates are recorded; otherwise, it is rejected, and a new point within the wedge is randomly picked. This process is repeated until the number of points specified by the user has been accepted. Following this procedure, a collection of randomly distributed point sources which follow the neutron emission PDF within the plasma has been constructed. Within MCNP, all these point sources are given equal probability since the emission PDF has already been taken into account for their colocation within the plasma volume. Figure 3.15 shows an example of 300 point sources distribution projected on the rz plane for a given set of plasma parameters.

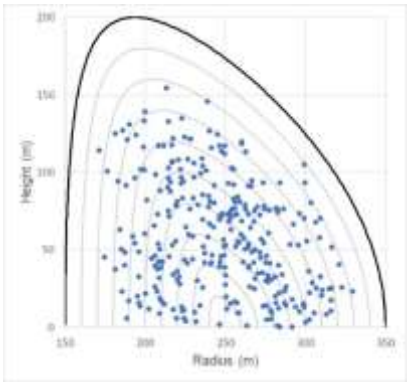

Figure 3.15. Distribution of point sources in the plasma volume. Isobars are shown as thin gray lines, plasma boundary isobar is shown as thick black line.

FFHYB can generate and read a text file for the source. The structure of the file description source is specified in Table B.I in Annex B. The neutron source file does not include the list of point sources because those are generated by the code for each run of the program.

3.4.2 Geometry.

The geometry of the hybrid can be split into two somewhat independent sections: the tokamak geometry and the blanket geometry. The different regions in the tokamak geometry are shown in Figure 3.16. The whole irradiator system is assumed to have equatorial symmetry, so the lower half is a mirror image of the upper half. Although the dimensions for a given tokamak design can be changed, the general structure of the tokamak regions cannot be easily modified. Figure 3.17 presents a similar component map for the blanket part of the irradiator. Regions in white indicate a void (no material).

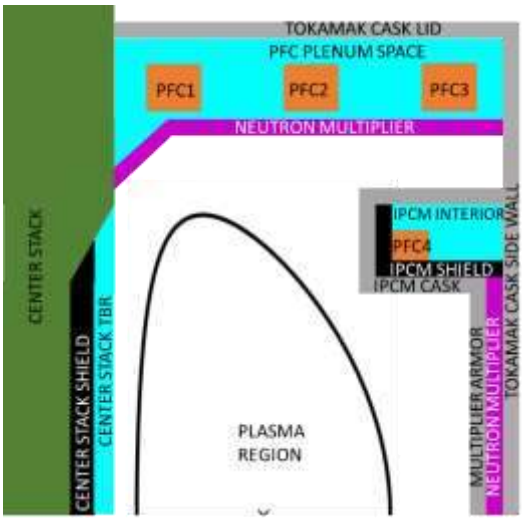

Figure 3.16. Regions and components of the tokamak.

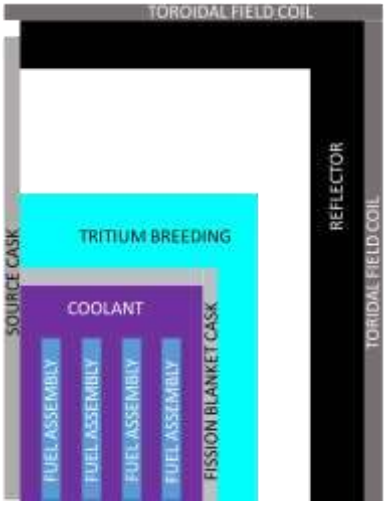

Figure 3.17. Regions and components of the fission blanket.

Figures 3.16 and 3.17 are good to obtain a general sense of what the hybrid system looks like, but the neutronics calculations necessary for the irradiator performance evaluation require a more comprehensive definition. Taking Figures 3.16 and 3.17 as a base, it is found that the geometry is fully specified by providing 29 dimensional values. Figure 3.18 shows those dimensions in a schematic, and Table 3.V lists their physical description. In addition to these dimensions, four parameters are required to specify each poloidal field coil: the inner radius, the outer radius, the height and the z coordinate of the coil center. All these geometrical parameters can be specified to FFHYB either on a graphic user interface or with text files having the structure specified in Tables B.II and B.III in Appendix B. The input of these dimensions into computer aided design (CAD) software allows for the constructions of 3D models of the hybrid such as the one shown in Figure 3.19.

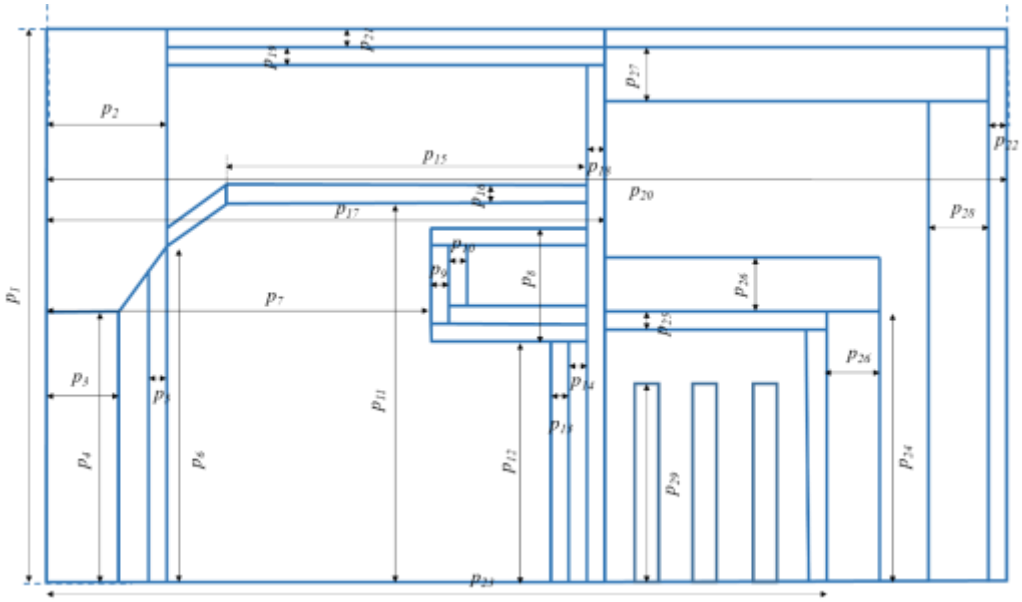

Figure 3.18. Dimensions required for the full specification of the hybrid device geometry guidance.

Table 3.V. List of dimensions required for complete geometry specification of the irradiator.

Dimension	*Description*
Center stack	
p_1	*Overall height*
p_2	*Maximum radius*
p_3	*Minimum radius*
p_4	*Shield inner height*
p_5	*Tritium breeding region thickness*
p_6	*Tritium breeding outer height*
Internal Poloidal Coils Module (IPCM)	
p_7	*Inner radius*
p_8	*Height*
p_9	*Cask thickness*
p_{10}	*Shield thickness*
Neutron Multipliers	
p_{11}	*Top NM z coordinate*

p_{12}	*Side NM height*
p_{13}	*Side NM armor plate thickness*
p_{14}	*Side NM thickness*
p_{15}	*Top NM straight section length*
p_{16}	*Top NM thickness*
Tokamak cask	
p_{17}	*Outer radius*
p_{18}	*Side wall thickness*
p_{19}	*Lid thickness*
Toroidal field coil	
p_{20}	*Outer radius*
p_{21}	*Horizontal limb thickness*
p_{22}	*Vertical limb thickness*
Fission blanket	
p_{23}	*Cask outer radius*
p_{24}	*Cask height*
p_{25}	*Cask wall thickness*
p_{26}	*Tritium breeding region thickness*
p_{27}	*Reflector horizontal limb thickness*
p_{28}	*Reflector vertical limb thickness*
p_{29}	*Fuel assembly height*

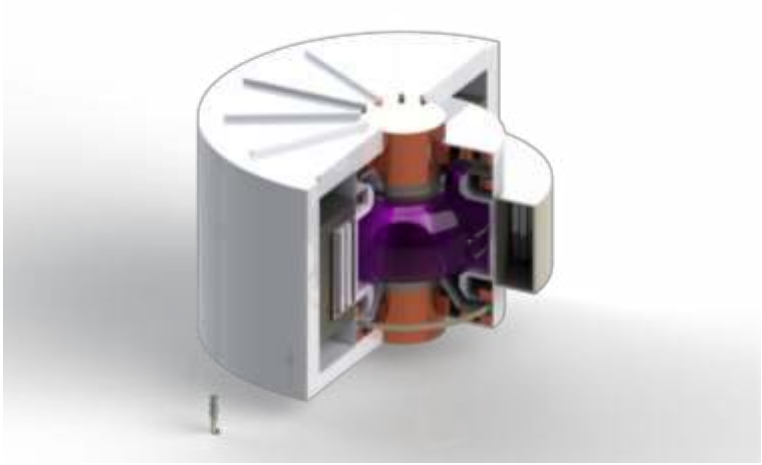

Figure 3.19. 3D render of the hybrid device based on Figure 3.17. A 6 ft. person is shown to provide scale.

3.4.3 Materials.

Once the geometry of the machine is specified, the next step is to define the materials filling the regions in Figures 3.16 and 3.17. A material is a collection of isotopes homogeneously distributed in a volume at constant density. The way a material is defined is as follows:

- Atomic fraction of each of the n elements, x_i.
- Isotopic fraction for each of the m_i isotopes of the element, y_j.
- Density of the material ρ, or density of each element ρ_i.

The molecular weight of element i is given by:

$$MW_i = \sum_{j=1}^{m_i} A_j y_j \tag{3.27}$$

where A_j is the mass number of isotope j. The average molecular weight of the material MW is then given by:

$$MW = \mu \sum_{i=1}^{n} MW_i x_i \tag{3.28}$$

For molecular materials such as Li_2O, BeO or Al_2O_3, μ represents the number of atoms per molecule. For allows and other substances that do not form a specific compound, the value of μ is unity. If the density of the material ρ is known, the density of each element in the material is given by the following expression:

$$\rho_i = \frac{\rho \mu x_i MW_i}{MW} = \frac{\rho x_i \sum_{j=1}^{m_i} A_j y_j}{\sum_{i=1}^{n} \sum_{j=1}^{m_i} A_j x_i y_j} \tag{3.29}$$

Therefore, the mass of an element M_i within a region can be calculated as:

$$M_i = \frac{V \rho x_i \sum_{j=1}^{m_i} A_j y_j}{\sum_{i=1}^{n} \sum_{j=1}^{m_i} A_j x_i y_j} \tag{3.30}$$

where V is the volume of the region, which is calculates using the second Pappus theorem and the list of vertices defining the region, as described in Appendix D.

3.4.4 Remote execution.

FFHYB makes use of the MCNP and SCALE codes, which are installed at a LINUX server physically located at the CICATA-IPN building. Any user with the adequate credentials stored in an encrypted connection file (see Table B.VI) can connect to the server by running the FFHYB program, which uses the RENCI libraries for VB.NET [80] to handle communication with the remote server. FFHYB has an interactive window (Figure 3.19) that allows the user to monitor the status of the remote machine during the execution of a scenario. The execution of commands and file exchange between the remote and local machine are completely transparent to the user.

Figure 3.20. Run monitor window in FFYB showing the run progress and the remote machine state.

3.5 Post-processing layer

Once the simulations of how the materials within the system change their composition due to the neutron irradiation, it is important to have a tool which can give access to data in an efficient way for presentation and analysis. The FFHYB system has such a tool, which can provide two types of data output for each region marked as dynamic:

- Time series for isotopes mass, total neutron flux, total mass and fission products mass.
- Snapshots at a specified time for isotopic composition or neutron flux energy distribution.

Figure 3.21 shows the overall screen for the data post processor, and Figure 3.22 shows the controls and their description. The post-processor window is available by selecting the "Analyze" option in the main application menu, which is enabled after successfully loading an existing scenario. The user can load the data associated with the scenario by pressing the LOAD DATA button; if the directories with the output data are not present, the program notifies the user that the data is not available.

A drop-down menu allows for the selection of the region that will be analyzed; the list of options will include all the regions marked as dynamic in the scenario definition. Another option for the user is to lump the assemblies in a given annular region of the fission blanket and obtain average quantities for the assemblies contained in that fission blanket zone. This averaging can only be done for fuel assemblies zones. Once a region or a fission blanket zone is selected for analysis, time series and snapshots can be generated. The data populates two output tables: the top one is for time series, and the bottom one is for snapshots. The data in this tables can be copied and pasted into plotting and data analysis programs for further processing or data presentation.

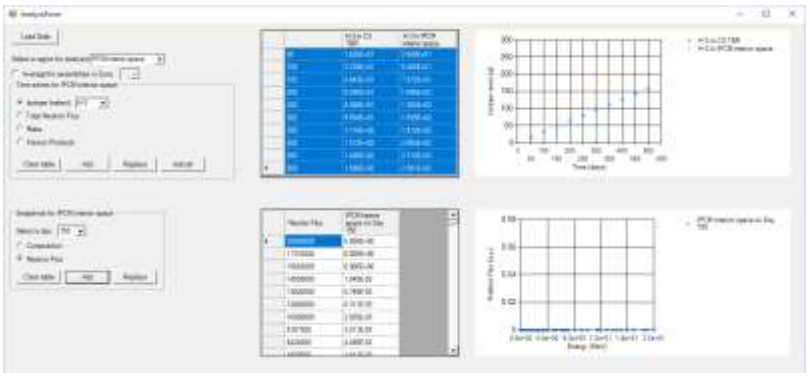

Figure 3.21. The main post-processor window.

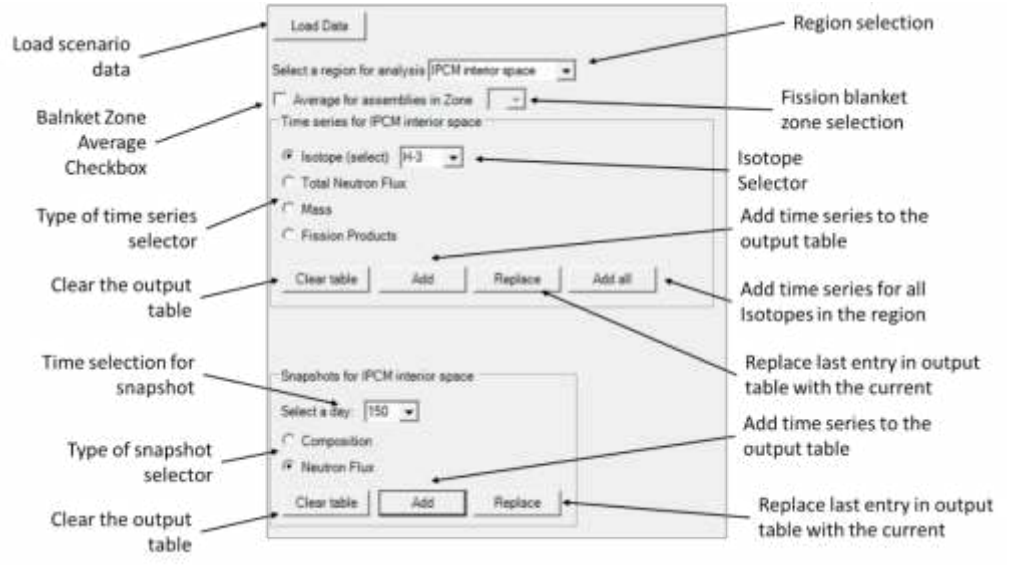

Figure 3.22. The controls in the post-processor window used to extract data from output files.

4 Results

4.1 Definition of case studies.

4.1.1 Neutron source and geometry description.

High power tokamak options (above 100 MW) have been proposed by the University of Texas at Austin (UT-A) with a primary focus on the Fusion–fission hybrid to assist the rejuvenation of nuclear energy by making fission energy greener (minimizing radio–toxic wastes) and sustainable (breeding fissile fuel U–233 from abundant fertile material Th–232) [81]. Their rather compact, lightweight, flexible, and removable fusion module, named Compact Fusion Neutron Source (CFNS), is enabled by advanced divertor configurations like the Super-X, which significantly lowers the power loads in the divertor, removing many of the power handling problems associated with the standard divertor configurations in other machines, including ITER [82]. The expected features of advanced divertors are currently being investigated experimentally on DIIID (USA); soon, new divertor configurations such as Super-X will be testbed available on the MAST–U machine [83].

Two reference plasma geometries were analyzed for this work to highlight the importance of the plasma shape in the performance of the hybrid system: one with plasma shape parameters similar to those of the JET tokamak [84], and another with plasma geometry parameters similar to those of the MAST tokamak [83]. The MAST-like configuration has smaller major radius, lower aspect ratio and higher elongation compared to the JET-like configuration. The relevant parameters for both configurations are shown in Table 4.I, and Figure 4.1presents a comparison of the two plasma cross sections, to scale. In both cases, parabolic temperature and density profiles are assumed, and the peak density value is adjusted so that both configurations have similar total neutron emission strength. Table 4.II presents the values for the dimensions in Figure 3.18 for both configurations. Notice that some dimensions need to be modified in order to accommodate the plasma volume for the two cases, while other remain unchanged for both scenarios. Figure 4.2 shows a comparison of both geometries in the same scale.

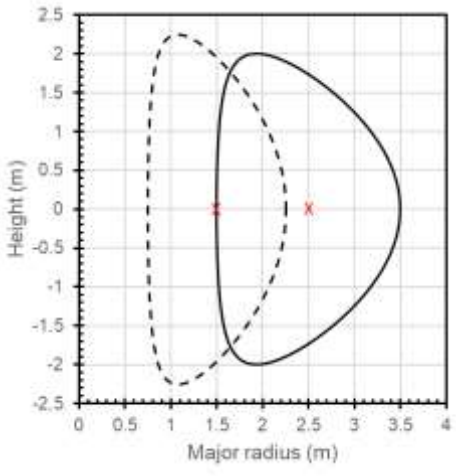

Figure 4.1. Plasma cross sections for the JET-like configuration (solid line) and the MAST-like configuration (dashed line). Red crosses indicate major radius values, 1.5 m for MAST-like and 2.5 m for JET-like.

Table 4.I. Plasma parameters for the two configurations studied in this work.

Parameter (units)	*JET-like*	*MAST-like*
Major radius, R_p (m)	*2.5*	*1.5*
Minor radius, r_p (m)	*1.0*	*0.75*
Aspect ratio, R_p/r_p	*2.5*	*2.0*
Elongation, k	*2*	*3*
Triangularity, a	*0.6*	
Plasma volume (m^3)	*89.08*	*44.43*
Peak temperature (keV)	*25*	
Edge temperature (keV)	*0.6*	
Peak density (m^{-3})	*1.5 x10^{20}*	*2.0 x10^{20}*
Edge density (m^{-3})	*1.0 x10^{18}*	
Neutron power (MW)	*250*	*224*
Tritium consumption (g/day)	*47.4*	*42.6*

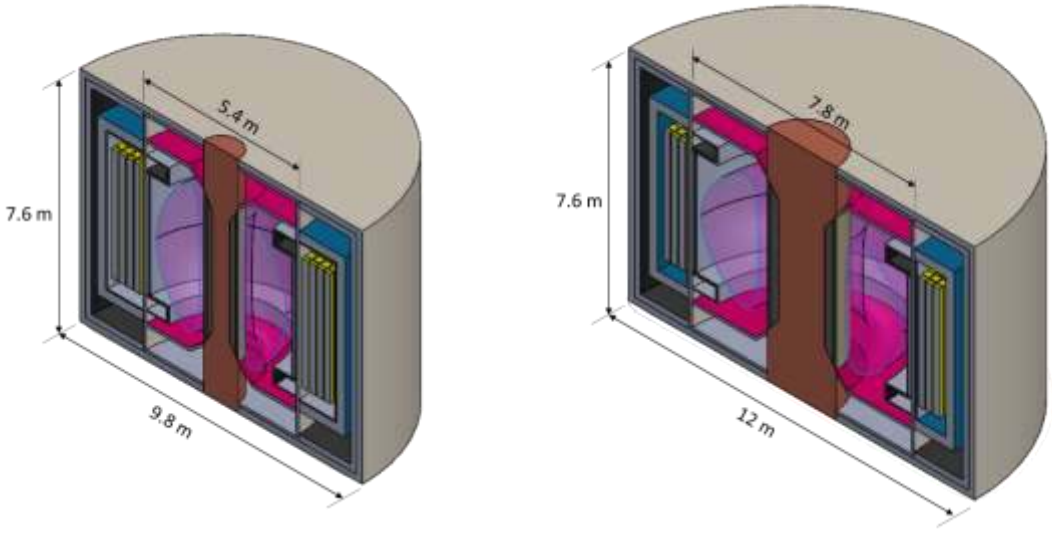

Figure 4.2. Comparison of the MAST-like (left) and JET-like (right) geometries.

Table 4.II. List of dimensions for JET-like and MAST-like configurations. Dimensions in meters.

Parameter (units)	*JET-like*	*MAST-like*
Center stack		
Overall height		*3.8*
Maximum radius	*1.2*	*0.6*
Minimum radius	*0.8*	*0.3*
Shield inner height		*1.8*
Tritium breeding region thickness		*0.1*
Tritium breeding outer height		*2.3*
Internal Poloidal Coils Module (IPCM)		
Inner radius	*2.9*	*1.8*
Height		*0.55*
Cask thickness		*0.05*
Shield thickness		*0.05*
Neutron Multipliers		
Top NM z coordinate		*2.7*
Side NM height		*1.8*
Side NM armor plate thickness		*0.05*
Side NM thickness		*0.1*
Top NM straight section length	*2.2*	*1.5*
Top NM thickness		*0.1*
Tokamak cask		
Outer radius	*3.9*	*2.7*
Side wall thickness		*0.1*
Lid thickness		*0.1*
Toroidal field coil		
Outer radius	*6*	*4.9*
Horizontal limb thickness		*0.2*
Vertical limb thickness		*0.2*
Fission blanket		
Cask outer radius	*5*	*4*
Cask height		*2.4*
Cask wall thickness		*0.05*
Tritium breeding region thickness		*0.3*
Reflector horizontal limb thickness		*0.2*
Reflector vertical limb thickness		*0.2*
Fuel assembly height		*1.95*
Number of zones	*3*	*4*

4.1.2 Materials.

Table 4.III presents the materials used to construct the hybrid system. Some materials remain unchanged throughout the study: poloidal coils and center column are made of copper, toroidal coil is made of aluminum, and all metallic walls are made of HT-9 low-activation steel [85]. For the tritium breeding regions, the reflectors, the neutron multiplier and the fission blanket coolant, the composition material was changed. The choices of materials are guided from the discussion in Sections 3.1.3 and 3.1.4. It should be mentioned that not all material combinations were explored, since it was found to have either no effect or detrimental effect to the performance of the machine,

such as in the case of a lithium-cooled fission blanket. Detailed information on the composition and density of the materials in Table 4.III can be found in Appendix C.

Table 4.III. Material choices for the different regions in the hybrid device.

Component	*Material*
Poloidal field coils	*Natural copper*
Toroidal field coil	*Natural aluminum*
Metallic walls	*HT-9 steel*
Fission blanket coolant	*Helium, Lithium*
Neutron multiplier	*Beryllium, Beryllium oxide, FLiBe*
Tritium breeder	*Lithium, Lithium oxide*
Reflectors	*Lead, Pb-Li eutectic, Pb-Bi eutectic*

The scenarios simulated using the scheme discussed in Section 3.4 are shown in Table 4.IV; these cases were pre-evaluated by simulations over a total irradiation time period of 100 days with composition updates every 5 days and using 10^6 neutron histories in MCNP. These material layout scenarios were used for both the JET-like and MAST-like neutron sources. The figures of merit used to determine which cases were relevant were the overall tritium breeding ratio, eq. (1.7), and the total irradiation time required to achieve 3% enrichment of the fuel assemblies, which can be estimated from eq. (3.21) once the simulation gives the rate of fissile material production for each zone.

Table 4.IV. Scenarios of material composition selected for quick evaluation.

Case	*Neutron Multiplier*	*Tritium breeder*	*Blanket Coolant*	*Shields*
Base	*Be*	*Li_2O*	*He*	*Pb*
A	*Be*	*Li_2O*	*He*	*Pb-Bi*
B	*FLiBe*	*Li_2O*	*He*	*Pb*
C	*FLiBe*	*Li*	*Li*	*Pb-Li*
D	*FLiBe*	*Li*	*He*	*Pb*
E	*Be*	*Li_2O*	*He*	*Pb-Li*
F	*Be*	*Li_2O*	*Li*	*Pb*

4.2 Results for the JET-like geometry.

4.2.1 Neutron flux behavior.

An important aspect to evaluate the performance of the hybrid device is to observe how neutron flux behaves in the system. MCNP flux tallies give both the total flux and the flux energy spectrum, which is necessary for the nuclear reaction kinetics calculation. The most important variation in neutron flux intensity occurs in the radial direction, and the radial profile of neutron flux is shown in Figure 4.3 for the different material configurations in Table 4.IV. The base case, case A and case E case are virtually identical, so their symbols overlap. This is an indication that the material choice between Pb, Pb-Bi and Pb-Li has very little influence on the performance of the system. Cases C and F stand out because they are consistently lower than the other cases for the blanket region (R > 4 m in the Figure), and those correspond to the cases when Li is used as coolant in the fission blanket; Case D, corresponding to a FLiBe neutron multiplier and a Li breeder, has the opposite

behavior, giving the highest flux in the blanket. Figure 4.4 presents a region map of the hybrid indicating the flux reported by the MCNP flux tally. The numbers in the figure need to be multiplied by 10^{14} to give the neutron flux in cm^{-2} s^{-1}.

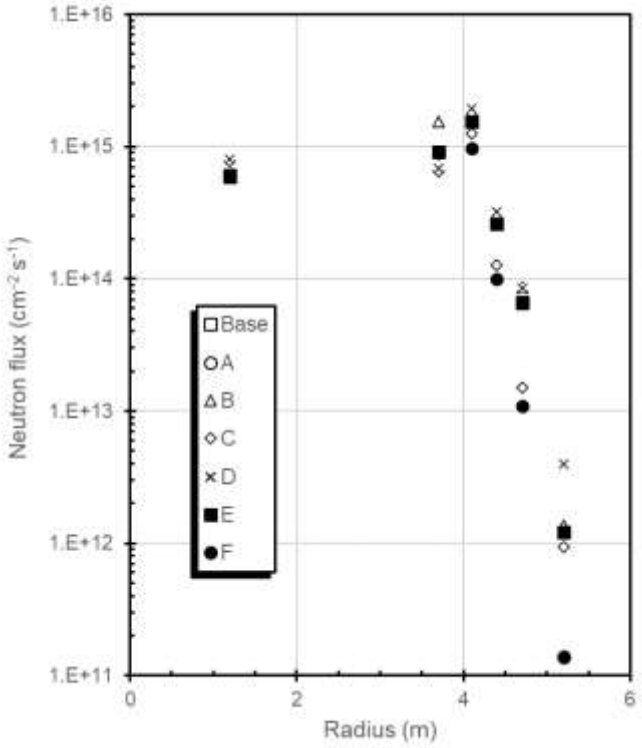

Figure 4.3. Neutron flux radial profile for the material scenarios in Table 4.IV.

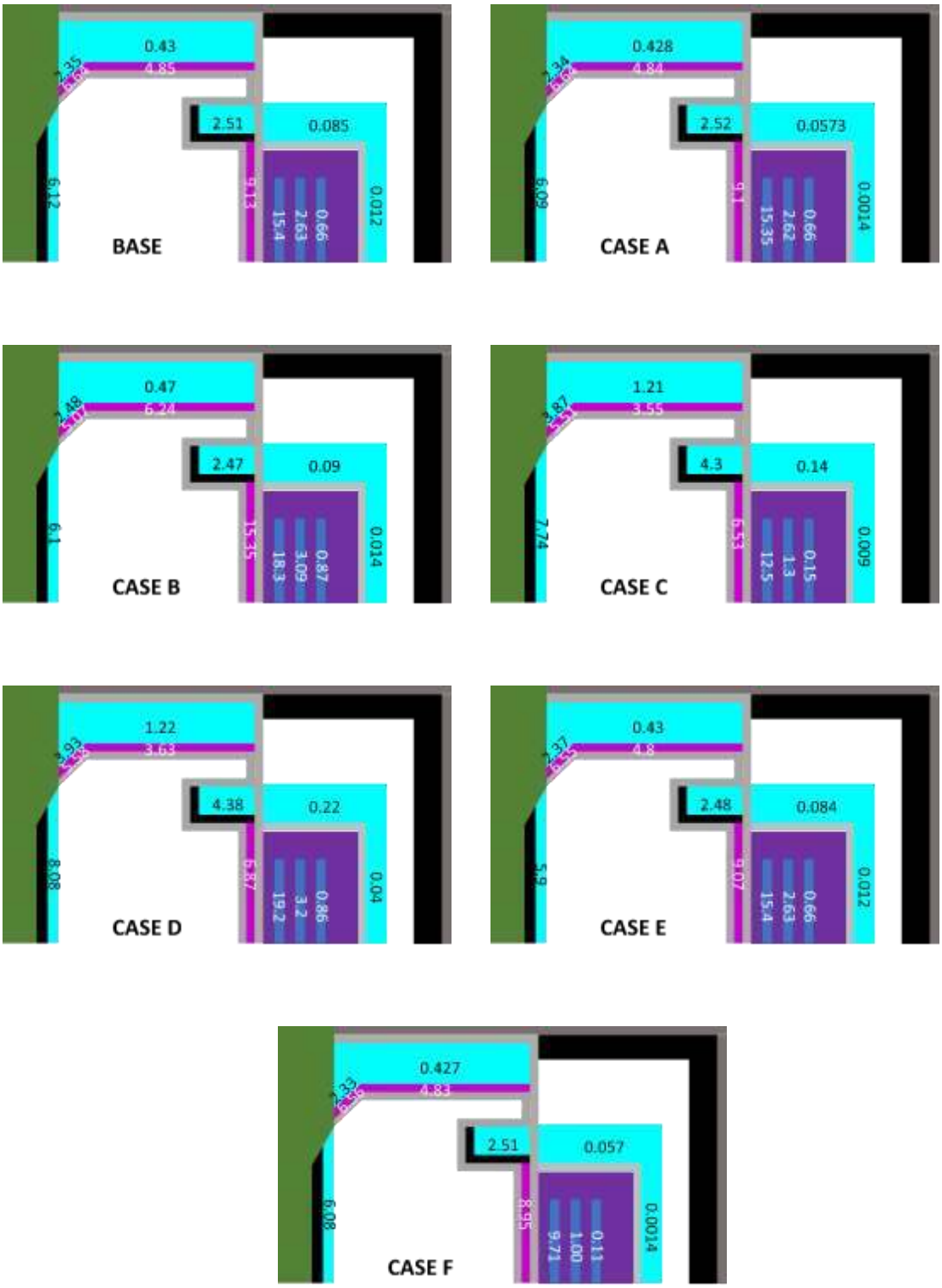

Figure 4.4. Region maps of the hybrid showing the neutron flux values for the different scenarios.

4.2.2 Tritium self-sufficiency.

Figure 4.5 presents the results for tritium production for the cases in Table 4. IV. The columns indicate in the left vertical axis the relative contribution to the total by the different regions in the system: the Internal Poloidal Coil Module (IPCM), the neutron multipliers (NM), the poloidal plenum tritium breeding region, the center stack regions (CS), the coolant the blanket tritium breeding regions and the blanket shields (see Figures 3.16 and 3.17 for reference). The solid line represents the tritium generation rate for each scenario, and it is read in the right vertical axis. As can be seen, the tritium generation rate for all cases is in the range of 65 – 80 g/day. Since the plasma in this geometry generates 250 MW (see Table 4.I), the minimum tritium generation rate according to eq. (1.7) is 47.52 g/day, so the tritium breeding ratio is between 1.4 and 1.7. The other thing to notice from the Figure is that most of the tritium production occurs on the regions belonging to the tokamak, except on the cases where lithium is used as coolant (C and F). Although attractive from the point of view of tritium generation, the use of lithium as coolant presents a disadvantage for the breeding of fissile material, as it will be seen in the next section. Cases A and E are virtually identical to the Base case, indicating the weak dependence of tritium breeding rate on shield materials. Cases B and D, which use FLiBe as neutron multiplier, present a higher production of tritium than the base case, indicating that the choice of FLiBe as neutron multiplier is an improvement with respect to the base case.

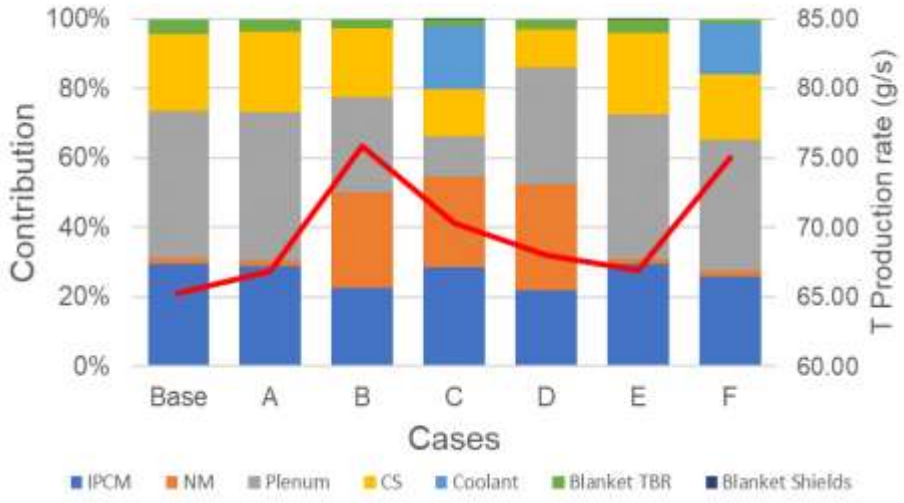

Figure 4.5. Tritium generation rate in the hybrid system for different material choices, showing the contribution from the different regions.

Presenting the data as in Figure 4.5 does not give any information about how efficiently the different regions generate tritium. For instance, the IPCM and the plenum have a comparable contribution to tritium generation in Case B, but the IPCM has a volume of 1 m^3 and the plenum region has a volume 3 times larger; therefore, the IPCM generates tritium more efficiently (with less material). Figure 4.6 is similar to Figure 4.5, but now the tritium volumetric generation rate (per unit volume) is reported. Notice that the relative contributions by each region change significantly. Clearly the center stack, the IPCM and the neutron multiplier are the key regions to achieve significant tritium production.

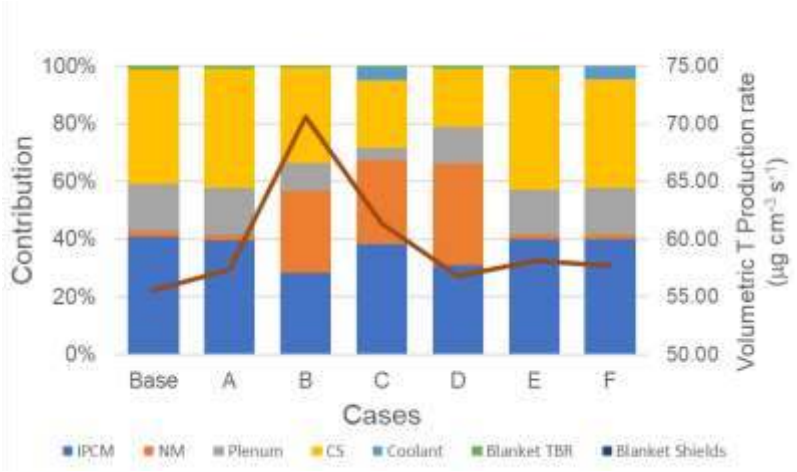

Figure 4.6. Volumetric tritium generation rate in the hybrid system for different material choices, showing the contribution from the different regions.

4.2.3 Fissile material production rates.

The fuel assemblies placed in the blanket initially contain pure ThO_2, and the expectation is that their exposure to the neutron flux coming from the tokamak neutron source produces ^{233}U to achieve a target enrichment of 3%, which is the expected commercial enrichment for thorium fuel in a hypothetical thermal reactor burning ^{233}U [86]. The simulation of the cases allows for the obtention of 233U production rates at each zone, and therefore an estimate of the irradiation time required to achieve the desired enrichment by using the method outlined in Section 3.1.5.

Table 4.V presents the obtained production rates in the blanket zones for the material scenarios, and the calculated required time to achieve 3% enrichment. The time calculation is assuming the shuffling scheme shown in Figure 3.13. The results of the table highlight the impracticality of scenarios C and F, which require 30 and 40 months to achieve the desired enrichment, respectively. This is well beyond the 18-month period between fuel recharges of thermal reactors. Cases A and E give a behavior similar to the base case again, confirming the previous finding that the system is not sensitive to the choice among the three shield materials considered in this study. It should also be noted that in addition to increasing the tritium production with respect to the base case as shown in Figure 4.5, Cases B and D show a slight reduction in the required irradiation time.

Table 4.V. Production rates in the blanket zones for the material scenarios, and the calculated required time to achieve 3% enrichment.

Case	*^{233}U production rate (g/day)*			*Time to 3% enrichment (months)*
	Zone 1	*Zone 2*	*Zone 3*	
Base	*97.32*	*17.2*	*6.5*	*19*
A	*98.67*	*17.14*	*6.44*	*19*
B	*110.84*	*20.04*	*7.68*	*17*
C	*68.6*	*8.14*	*4.66*	*29*
D	*121.4*	*22.52*	*8.1*	*15*
E	*96.44*	*17.27*	*6.32*	*19*
F	*50.12*	*6.04*	*0.84*	*41*

4.2.4 Effect of material choices in the performance of a JET-like hybrid device.

As mentioned in Section 4.1.2, the scenarios analyzed previously were run for 100 days and with 10^6 MCNP histories for the purpose of preliminary evaluation. The results of this preliminary evaluation are presented in the previous two sections. Three key findings of that preliminary evaluation are:

- The choice of reflector material between Pb, Pb-Bi and Pb-Li does not affect the performance of the machine in either tritium self-sufficiency or required irradiation time to reach a given enrichment target.
- Tritium breeding occurs primarily within the tokamak, so the material choice for the tritium breeding regions in the blanket is not relevant.
- The use of Li as coolant in the fission blanket has a positive impact on tritium production, but the required time to reach a relevant enrichment increases significantly.

Given these three conclusions from the preliminary case exploration, the next focus of the study was on scenarios where the neutron multiplier and the tritium breeder materials are changed. For neutron multiplier, Be and FLiBe are the two candidate materials; for tritium breeder, Li and Li_2O are the two candidate materials. The base case uses Li_2O and Be, so three more scenarios were explored:

- Li breeder, FLiBe neutron multiplier.
- Li2O breeder, FLiBe neutron multiplier.
- Li breeder, Be neutron multiplier.

For identifying the cases, the notation multiplier/breeder will be used. Since the most common usage for both FLiBe and Li is on the liquid state, and the most common use for Be and Li_2O is in solid form, both the breeder and the multiplier can be either solid or liquid. The scenario using the combination Li_2O/Be is labeled as S/S (solid-solid); similarly, the scenario using Li/FLiBe is L/L (liquid-liquid). The two remaining scenarios are S/L (Li_2O/FLiBe) and L/S (Li/Be). These cases were simulated for a total irradiation time of 500 days, with composition updates every 50 days, and $2x10^6$ histories for MCNP calculations.

The effect of the material choice in the neutronics behavior of the system is clear by looking at the energy distribution of the neutron flux in the neutron multipliers. Figure 4.7 shows the energy distribution function for the top and side neutron multipliers with Be and FLiBe. When the neutron multiplier is beryllium, a peak below 1 eV is clearly noticeable, which is likely caused by the neutrons resulting from the (n, 2n) reaction of Be. Most of those neutrons are likely absorbed by the wall separating the multiplier from the fission blanket, but they are definitely present in the flux that reaches the assemblies in zone 1, as can be seen in Figure 4.8.

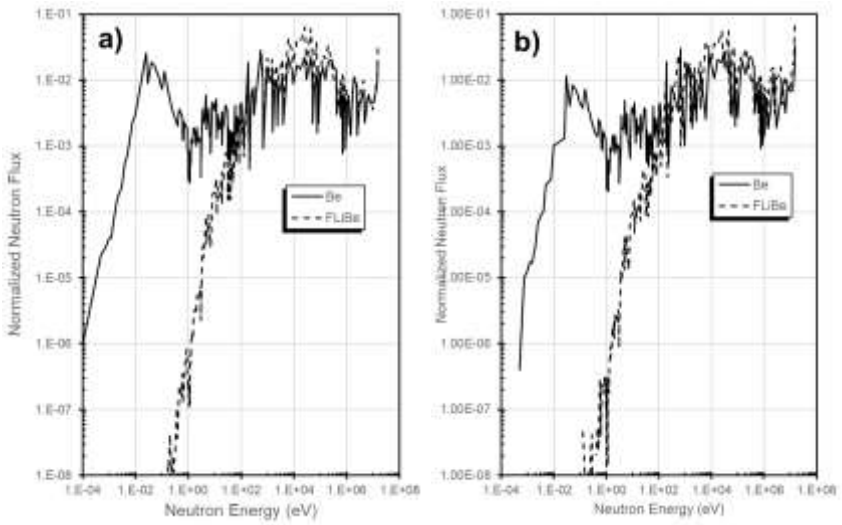

Figure 4.7. Neutron energy distribution for the a) side and b) top neutron multiplier. Two neutron multiplying materials are compared: solid curve is for beryllium; dashed curve is for FLiBe.

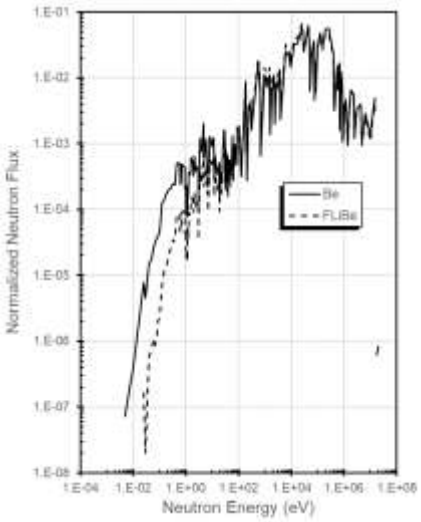

Figure 4.8. Neutron energy distribution for the a) side and b) top neutron multiplier. Two neutron multiplying materials are compared: solid curve is for beryllium; dashed curve is for FLiBe.

Neutron flux maps such as those in Figure 4.4 were generated for the 4 extended simulation cases and are shown in Figure 4.9 at the end of the simulation (500 days). Comparing the Base Case in Figure 4.4 and the S/S case in Figure 4.9, which have the exact same configuration, it can be notices that the flux values for the tokamak regions have the same flux values, but the fission blanket zones have increased by a factor of 1.5. The only difference between the cases is the irradiation time, which for Figure 4.4 is at 100 days and in Figure 4.9 is at 500 days. This is an indication that the neutron flux changes over time.

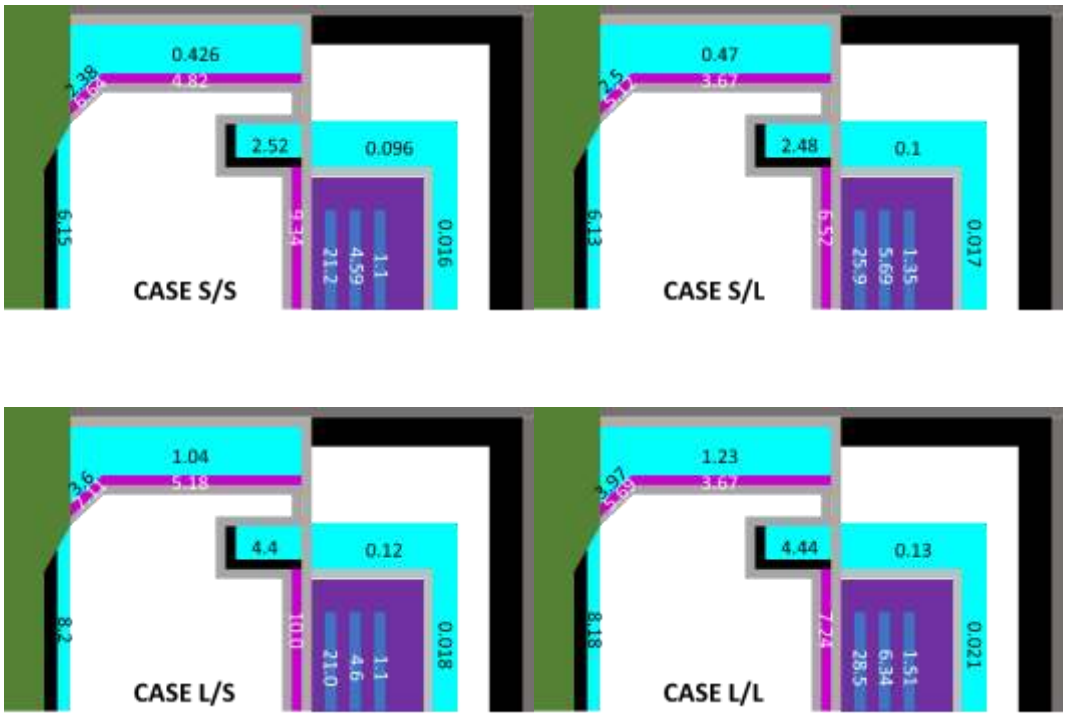

Figure 4.9. Neutron flux maps for the 4 extended simulation cases.

A plot of the neutron flux as a function of time for the three blanket zones is shown in Figure 4.10 for the S/S case. The flux shows a fairly linear increase over time, which indicates net production of neutrons due to the fissioning of some of the ^{233}U produced. This fission is an undesirable side effect in the system, since its primary function is to breed fissile material without consuming it. The energy structure of the flux is also modified, as can be seen in Figure 4.11, which presents the energy-resolved flux intensity for the first blanket zone at different times for the S/S case. A clear decrease in the low-energy neutron population (< 100 eV) is observed in Figure 4.11a, and the high-energy component (Figure 4.11b) shows an increment. The unscattered 14 MeV component remains constant for all times.

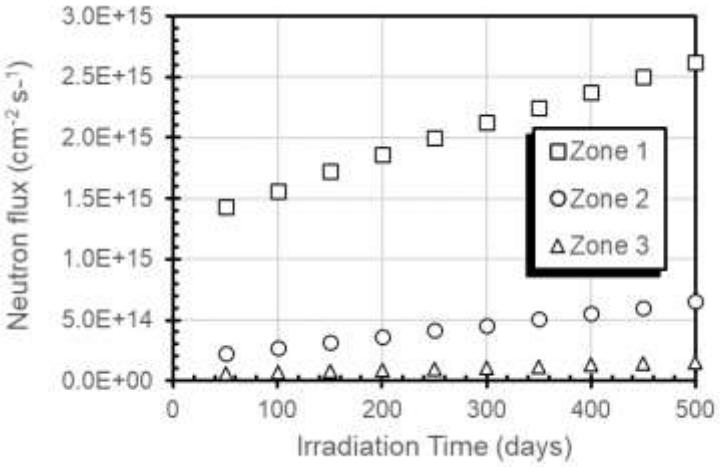

Figure 4.10. Evolution of neutron flux in the blanket zones for the S/S case.

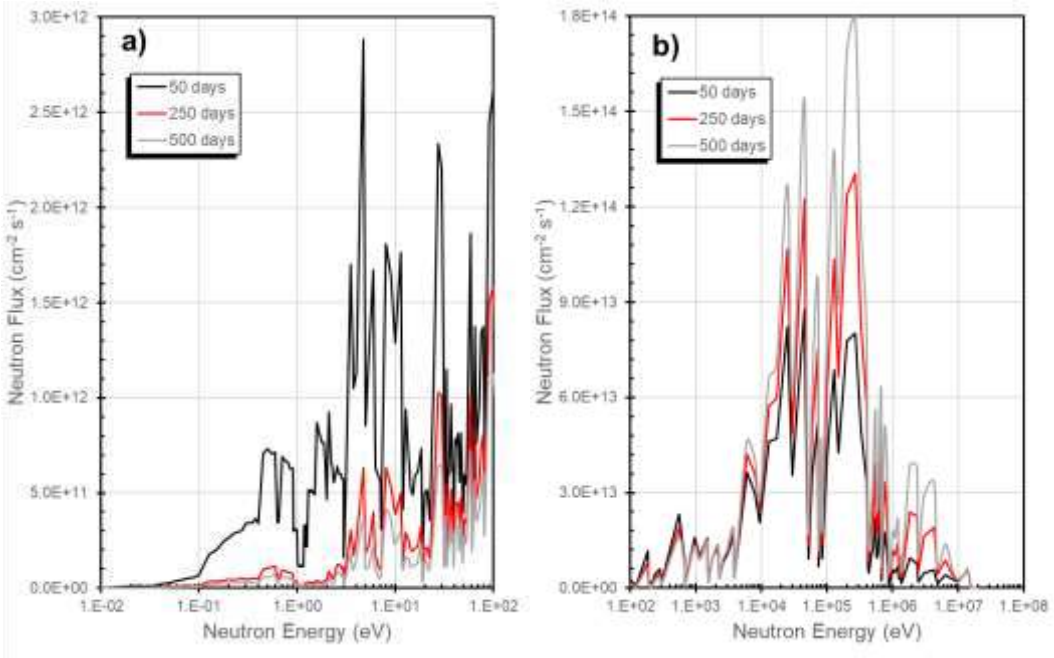

Figure 4.11. Energy structure of the neutron flux on the first fission blanket zone at 3 different times for the S/S case.

Given that the neutron flux is changing over time, it might be useful to look at the behavior of the ^{233}U mass in the three blanket zones. Figure 4.12 presents the evolution of the average ^{233}U mass on each fuel assembly as time progresses for the four cases considered. The figure includes linear fits to the mass increase, which have correlation coefficient $R > 0.99$. The production rate is not constant, since it starts at higher values and then decays over time, as can be seen on Figure 4.13 which present the evolution of the production rate over time for the S/S case. This behavior is more pronounced on the first blanket zone, which is exposed to the largest neutron flux. An increase in the

fission rate might be the cause of the decrease in the production rate over time. The other three cases present a similar behavior. Despite these variations, the constant rate is a good approximation to the accumulation of material on the fuel assemblies.

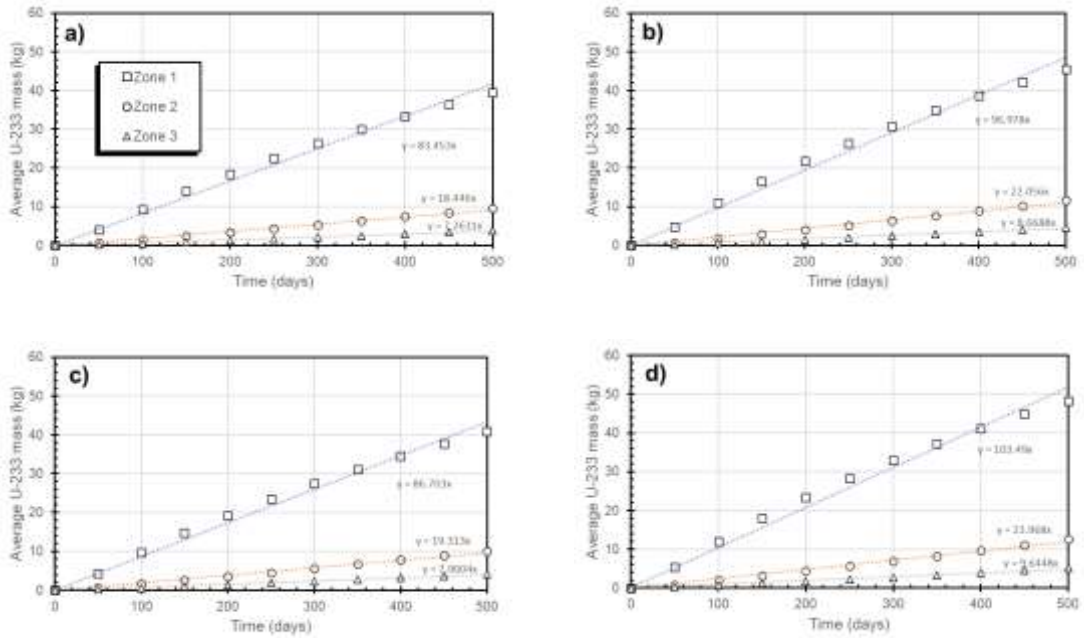

Figure 4.12. ^{233}U production rate in the blanket for four material scenarios: a) S/S, b) S/L, c) L/S and d) L/L.

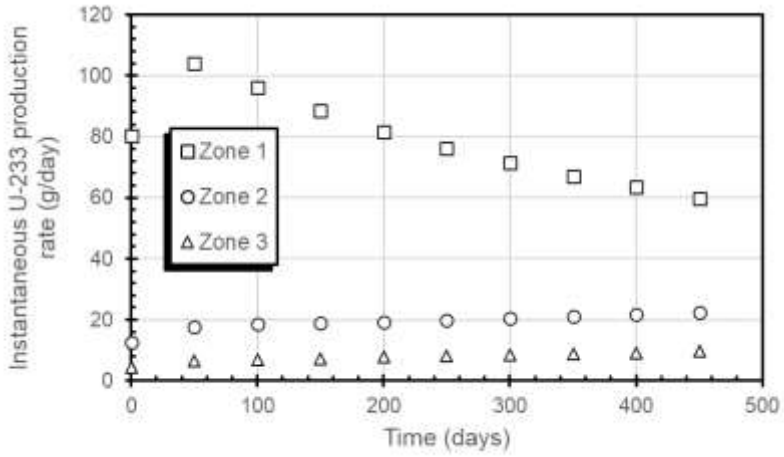

Figure 4.13. Instantaneous ^{233}U production rate in the different zones of the blanket for the S/S case.

As mentioned before, the system during these 500 days of irradiation is not in steady state in terms of flux or composition. Table 4.VI presents the average composition of assemblies at three different irradiation times in the three blanket regions for the L/L case, which is the one with the highest fissile material production. The only products with masses larger than 1 kg at the end of irradiation are U isotopes (mostly ^{233}U), fission products and Pa isotopes (mostly ^{233}Pa). On the other hand, only ^{232}Th decreases significantly during the irradiation.

Table 4.VI. Average mass composition for fuel assemblies in the different blanket zones after 50, 250 and 500 irradiation days. Data is for the L/L scenario.

Isotopes	*Mass @ 50 days (g)*			*Mass @ 250 days (g)*			*Mass @ 500 days (g)*		
	Zone 1	*Zone 2*	*Zone 3*	*Zone 1*	*Zone 2*	*Zone 3*	*Zone 1*	*Zone 2*	*Zone 3*
^{16}O	*108200*	*108200*	*108200*	*108200*	*108200*	*108200*	*108100*	*108200*	*108200*
^{232}Th	*775500*	*782300*	*783100*	*748600*	*777300*	*781200*	*717200*	*769400*	*778000*
Light isotopes[1]	*4.50*	*0.32*	*0.05*	*24.8*	*1.9*	*0.27*	*56.1*	*4.8*	*0.7*
Fission Products	*143.3*	*6.0*	*0.9*	*3230.0*	*133.7*	*18.4*	*12791*	*734.99*	*96.6*
Other Th[2]	*23.7*	*10.8*	*0.2*	*114.7*	*54.8*	*1.0*	*222.4*	*14.2*	*2.1*
Pa[3]	*2572.8*	*382.9*	*1.5*	*2673.4*	*491.8*	*7.40*	*3140.0*	*686.9*	*255.3*
^{233}U	*5277*	*815.2*	*287.4*	*28350*	*5584*	*2162*	*48270*	*12620*	*5201*
Other U[4]	*103.7*	*2.90*	*0.32*	*715.2*	*24.6*	*3.6*	*2004*	*101.2*	*15.1*
Other isotopes[5]	---	---	---	*0.013*	---	---	*0.35*	---	---

[1]Excludes ^{16}O
[2]Includes ^{228}Th, ^{229}Th and ^{230}Th
[3]Includes ^{230}Pa, ^{231}Pa, ^{233}Pa
[4]Includes ^{232}U, ^{234}U, ^{235}U and ^{236}U
[5]Includes minor actinides and heavy decay products

A utilization factor UF will be introduced as a measure of how efficiently the system converts ^{232}Th to ^{233}U, and it will be defined as the ^{233}U production rate divided by the ^{232}Th consumption rate:

$$UF = -\frac{\frac{dm_{U233}}{dt}}{\frac{dm_{Th232}}{dt}} \approx -\frac{\Delta m_{U233}}{\Delta m_{U233}} \qquad (4.1)$$

The utilization factor is a good indicator of how efficiently the system makes use of the fertile material. The presence of fission products indicates that there is a competition between generation and destruction of ^{233}U; lack of fission products after irradiation would indicate a utilization factor of nearly one. Other than fission, side channels of ^{233}Pa nuclear reactions also contribute to the decrease in the utilization factor of the system. As can be seen from Figure 4.14, the utilization factor in zones

2 and 3 of the blanket is always above 80% except at the very beginning, but for the blanket zone closest to the neutron source it decreases steadily, reaching a minimum around 0.56 - 0.6 depending on the material combination scenario. The burning increasing steadily and the breeding decreasing steadily (see Figure 4.13).

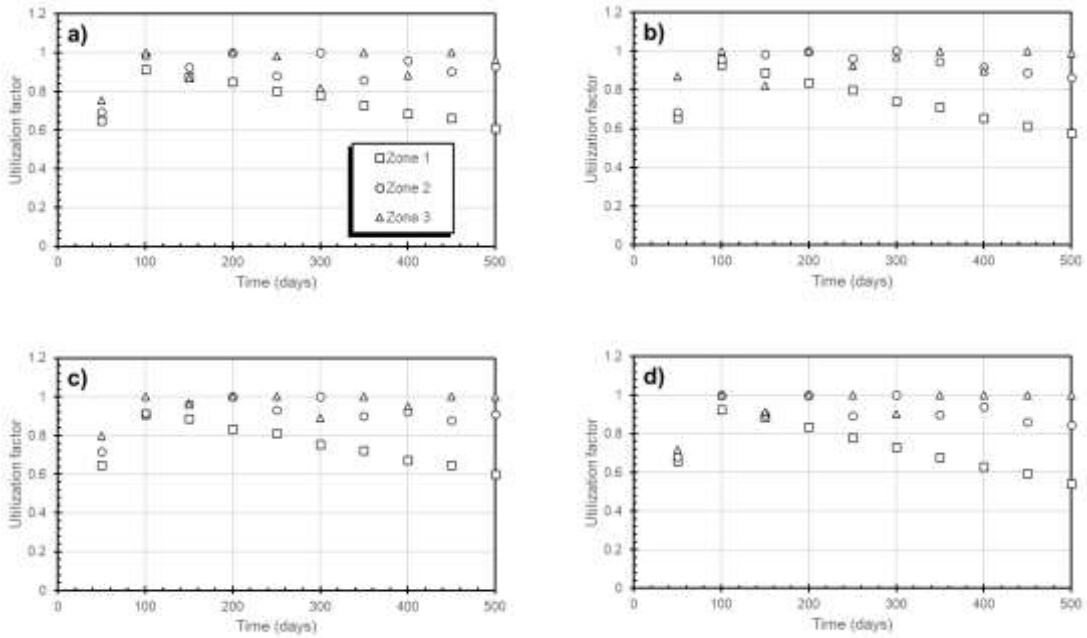

Figure 4.14. Stepwise thorium utilization factor in the fission blanket for the four analyzed cases: a) S/S, b) S/L, c) L/S, and d) L/L.

In terms of tritium breeding, the generation rate was evaluated for the four cases as well. For the tokamak regions, the neutron flux remains constant during the whole irradiation period, as can be seen in Figure 4.15 which shows the evolution of the neutron flux for some of the regions within the tokamak for the L/L case. The tritium breeding regions are indicated with white symbols, while the neutron multiplying regions are shown with dark symbols The only region where a slight increase in the flux is observed is the side wall neutron multiplier, which receives some neutron feedback from the blanket due to its proximity to the blanket region.

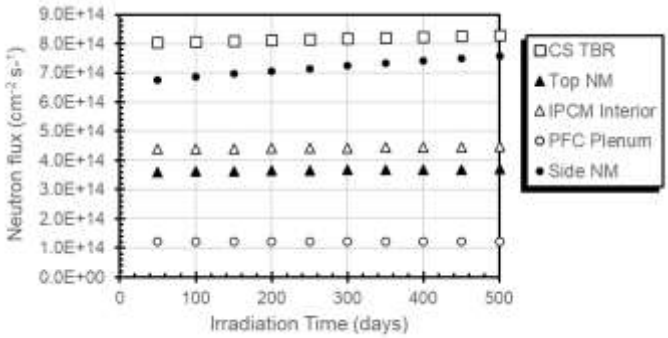

Figure 4.15. Neutron flux evolution on 5 regions of the tokamak interior for the L/L case.

Since the flux can be assumed constant and the tritium breeding isotope (6Li) is present in large amounts, the production rate in all regions remains constant over time, as can be seen in Figure 4.16 for the L/L scenario. As in the case of the preliminary evaluations discussed in the previous section, it can be observed the tritium breeding regions in the blanket have a very minor contribution to the tritium production, less than 5% contribution to the total. The total production rates and breakup by region for the four scenarios are shown in Figure 4.17. The cases with the liquid breeder have the lowest tritium breeding ratio because the changes in neutron flux cannot compensate for the difference in 6Li atomic density between metallic Li and Li2O (see Table 3.I). If a liquid breeder is desired, regions with larger volume need to be incorporated in the design.

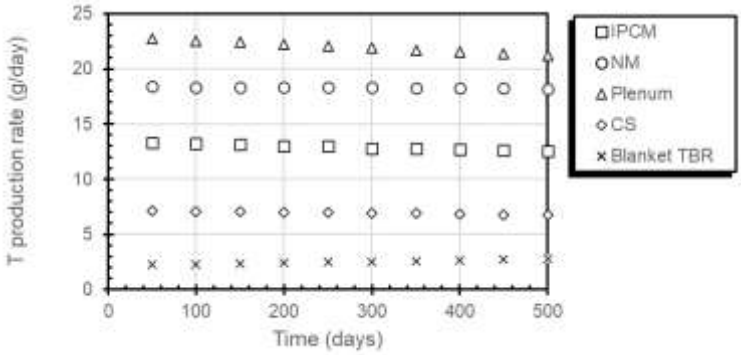

Figure 4.16. Evolution of the tritium production rate in the L/L scenario for the different regions in the tokamak and the blanket.

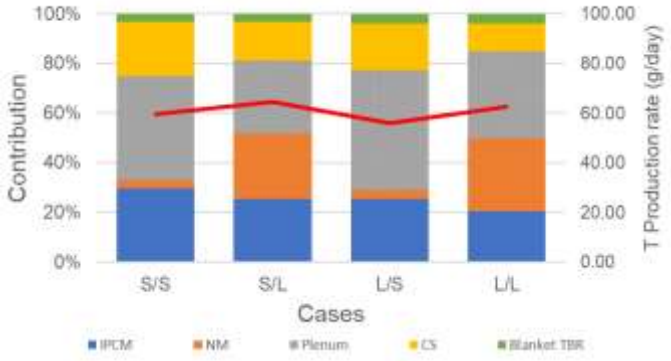

Figure 4.17. Tritium production rate for the four scenarios considered in the study. Bars indicate the contribution of each region to the generation, and the solid line indicates the T production rate.

To account for the effect of region size, the volumetric generation rate is also reported in Figure 4.18, as was done in the previous section for the exploratory simulation runs. With the aid of the values in this Figure, the thickness of the tritium breeding region to achieve a desired production rate can be estimated.

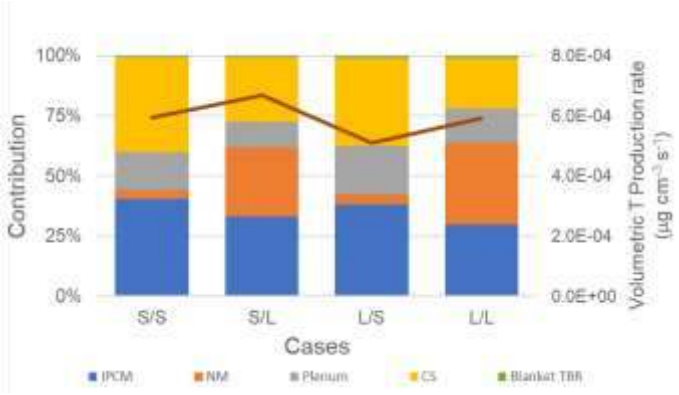

Figure 4.18. Volumetric tritium production rate for the four scenarios considered in the study. Bars indicate the contribution of each region to the generation, and the solid line indicates the volumetric production rate.

Table 4.VII presents a summary of the findings for the four scenarios considered in the JET-like geometry regarding fissile material breeding and tritium self-sufficiency. The time estimate to reach the target enrichment of 3% is calculated using the methodology described in Section 3.1.5 and taking the slopes of the linear fits in Figure 4.12 as the constant generation rates for each blanket zone. The most attractive scenario is the combination of Li2O as tritium breeder and FLiBe as neutron multiplier, which is the S/L case. This case presents the higher TBR value (1.12), gives a reasonable irradiation time to achieve 3% enrichment, comparable with the 18-month fuel recharge period of LWRs, and roughly the same utilization factor as all other cases. In the next section, the performance of this scenario with a more radially compact source configuration will be contrasted with the results in this section.

Table 4.VII. Summary of performance measures for the four material configuration cases.

Scenario	*Time to 3% enrichment (months)*	*Overall utilization factor @ Zone 1*	*Tritium generation rate (g/day)*	*Tritium breeding ratio*
S/S	*22*	*0.76*	*59.6*	*1.03*
S/L	*19*	*0.74*	*64.6*	*1.12*
L/S	*21*	*0.75*	*55.9*	*0.97*
L/L	*19*	*0.72*	*62.6*	*1.09*

4.3 Performance comparison between JET-like and MAST-like geometries.

4.3.1 Key differences between the two geometries.

Figure 4.2 and Table 4.II highlights the dimensional differences between the two configurations, but there are more subtle differences between the two configurations that are not obvious from the Table nor the Figure:

- The system geometry shrinks in the radial direction, but not in the axial direction. Regions are exposed to higher neutron fluxes in the MAST-like case because the power is similar, but the radius is smaller, as shown in Figure 4.18. The regions within the tokamak will also shrink in volume, since their thicknesses do not change. Table 4.VIII shows the change in volume for the relevant regions within the tokamak devices, which will be important when comparing volumetric tritium production rates. Volumes for the different regions are calculated using the method outlined in Appendix D.
- The blanket capacity changes. The JET-like geometry has three zones: two with 112 assemblies and one with 128 assemblies, so the capacity is 352 assemblies per batch, sufficient to fill 1.5 large PWR full cores (see the discussion in Section 1.4.2); the blanket in the MAST-like geometry, on the other hand, has two regions with 80 assemblies and two regions with 96 assemblies, giving the same capacity of 352 assemblies per batch, but with a different configuration.

Table 4.VIII. Volume of the different regions within the tokamak for the JET-like and MAST-like configurations. Table values are in m^3.

Region	*JET-like*	*MAST-like*
Internal Poloidal Coil Module	*0.43*	*0.23*
Poloidal coils upper plenum	*1.53*	*0.68*
Center stack tritium breeding region	*0.1*	*0.05*
Top neutron multiplier	*0.25*	*0.13*
Side wall neutron multiplier	*0.27*	*0.18*

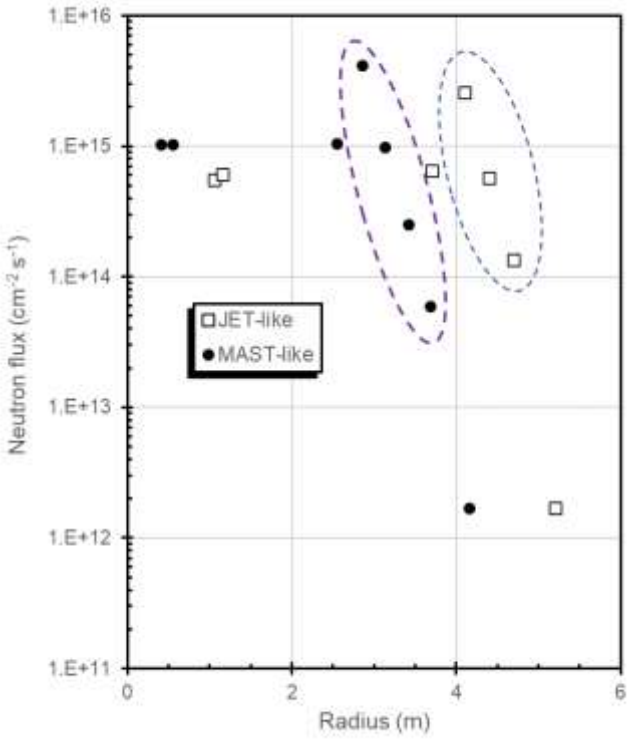

Figure 4.19. Neutron flux radial profile for the JET-like and the MAST-like geometries. Points corresponding to the blanket zones (4 for the MAST-like case, 3 for the JET-like case) are enclosed by dashed ovals.

The neutronics behavior retains most of the characteristics discussed in the previous section. The neutron flux in the tokamak regions remains fairly constant, while the blanket regions show a linear increase over time, as can be seen in Figure 4.19. Clearly the first region in the MAST-like case has a flux that, by the time the irradiation is over, is almost double of that received by the first zone in the JET-like geometry.

4.3.2 Tritium self-sufficiency.

Figure 4.19 presents a comparison between the tritium generation rates, in grams per day, for the different regions in the MAST and JET-like tokamak configurations for the Li2O/FLiBe material combination. All but one of the tritium producing regions show a decrease for the MAST-like tokamak when compared to the JET-like machine due to their reductions in volume. The only region that shows an increase are the IPCM and the blanket tritium breeding region. The cause for this increase is not clear, since the volume of this region is smaller for the MAST-like configuration, and according to Figure 4.18, this region gets the same flux for both geometry configurations. Still, the contribution from this region is small compared to the production rate within the tokamak, so the increase does not affect the TBR value significantly.

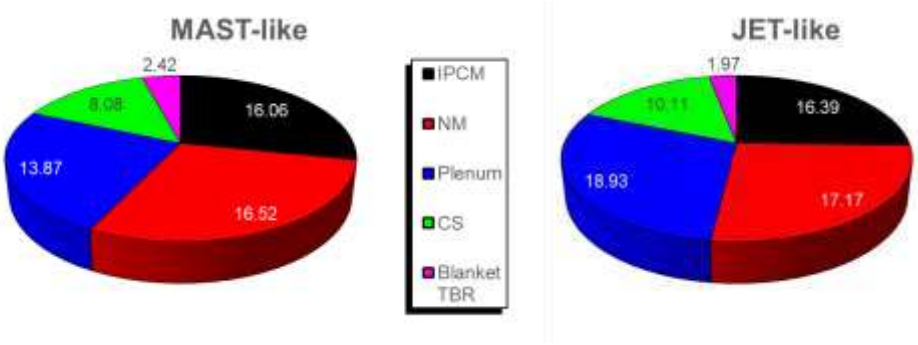

Figure 4.20. Tritium production rates for the MAST-like and the JET-like configurations. Values are in grams per day.

The comparison of the volumetric generation rates paints a completely different story. It is clear that the MAST-like geometry has a higher volumetric generation rate just by looking at Table 4.VIII and Figure 4.19. Consider the center stack tritium breeding region as an example: the volume of this region for the JET-like configuration is twice the value of this same region in the MAST-like configuration. If the volumetric production rate were constant for both cases, the production rate in the JET-like configuration would be twice that of the MAST-like configuration, and from Figure 4.19 this is clearly not the case. From the point of view of neutron flux, the situation is inverted: the flux for this region on the MAST-like device is 1 x 1015 cm-2 s-1, while for the JET scenario it is 6 x 1014 cm-2 s-1. The end production rate seems to be the balance between a reduction in the volume and an increase in the neutron flux. Figure 4.20 presents the difference between the volumetric production rate for all relevant tritium production regions in both scenarios.

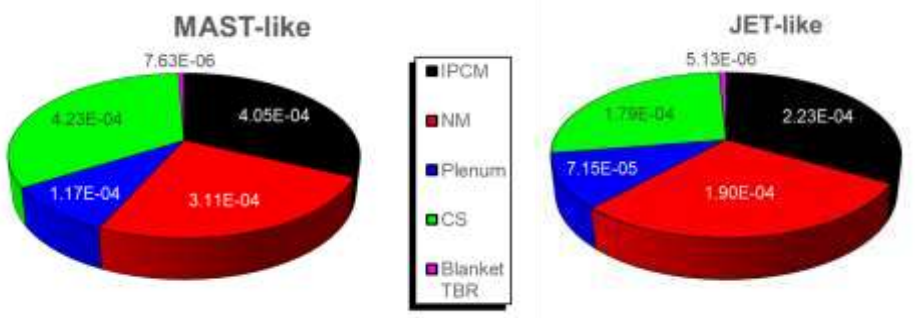

Figure 4.21. Volumetric tritium production rates for the MAST-like and the JET-like configurations. Values are in $\mu g\ s^{-1}\ m^{-3}$.

The tritium breeding ratio ends up being 1.08 for the MAST-like configuration, versus 1.12 in the JET-like configuration. It follows that form the point of view of tritium generation, both cases are nearly equivalent. Although the tritium generation rate for the MAST configuration is smaller, the tritium requirement to achieve self-sufficiency is also smaller due to the difference in neutron power: 275 MW in the MAST-like machine vs 300 MW for the JET-like machine, a power difference that translates in a tritium generation rate difference of 4 g/day.

4.3.3 Blanket breeding performance comparison.

Figure 4.21presents a comparison between the ^{233}U generation rates in the different blanket zones of the two geometry configurations. Zone 1 has 50% more production in the MAST-like configuration, and Zones 2 and 3 almost double in production rate. This will represent a definite advantage for the MAST-like configuration, since the total irradiation time to reach the 3% enrichment established as target is lowered by 2 months, as can be seen in Table 4.IX. A further reduction would be achieved if the MAST-like source power is increased to 300 MW. To calculate the irradiation time, the slope of the linear fit is used as the average production rate for each zone to construct the shuffling matrix. The downside of the MAST-like configuration is that, given that it has 4 zones, the current shuffling strategy would require four movements during the irradiation.

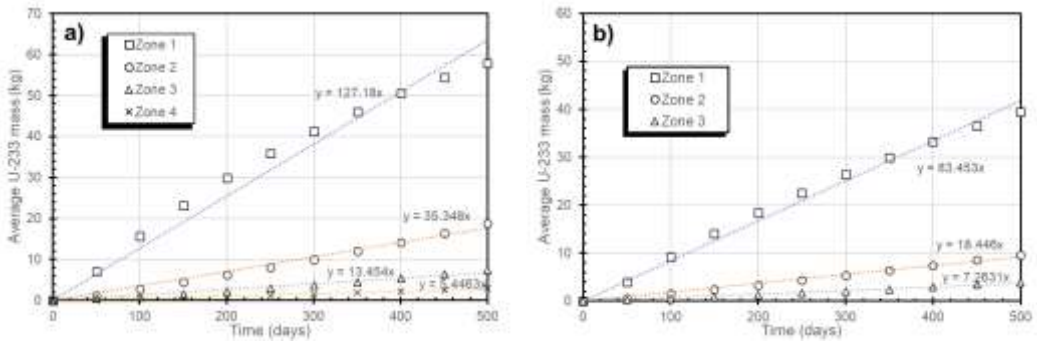

Figure 4.22. Evolution of average ^{233}U mass on each assembly in the different blanket zones. a) MAST-like geometry; b) JET-like geometry.

The other important aspect to compare is fertile material utilization. The faster production of ^{233}U has the unfortunate side effect of promoting fission reactions, therefore reducing the ^{232}Th utilization efficiency. The evolution of the utilization factor for the MAST-like geometry is not too different from the curves shown in Figure 4.14, but a better comparison is obtained by plotting the utilization factor vs ^{233}U mass as in Figure 4.22, since the amount of ^{233}U at various times is very different for the two cases. The UF as a function of ^{233}U mass for blanket zone 1 of both JET-like and MAST-like geometries is presented in Figure 4.23. Clearly the curves follow the same trend, despite the differences in flux shown in Figure 4.18. This independence of the utilization factor from the flux can be explained by starting from the definition of the utilization factor, eq. (4.1):

$$UF = -\frac{\frac{dm_{U233}}{dt}}{\frac{dm_{Th232}}{dt}} = \frac{k_1\phi m_{Th232} - k_3\phi m_{U233}}{k_1\phi m_{Th232} + k_2\phi m_{Th232}} = \frac{k_1 m_{Th232} - k_3 m_{U233}}{k_1 m_{Th232} + k_2 m_{Th232}} \qquad (4.2)$$

The utilization factor in eq. (4.2) has now been written in terms of two second-order kinetic expressions: the rate of ^{232}Th consumption due to radiative capture of a neutron to produce ^{233}U, with rate constant k_1; the rate of ^{232}Th consumption from other neutron reactions, with rate constant k_2; and the ^{233}U destruction rate due to neutron-induced fission, with rate constant k_3. Since all rates involve the neutron flux ϕ, it can be factored, and the result will be independent of neutron flux. With respect to the mass of ^{233}U, eq. (4.2) is a straight line with negative slope, which is what is observed in Figure 4.23.

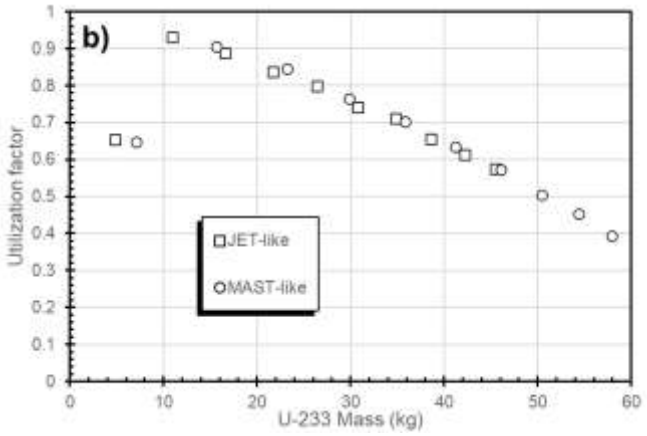

Figure 4.23. Th utilization factor as a function of ^{233}U mass.

Table 4.IX. Irradiation time and utilization factor comparison for the two geometry configurations.

Scenario	*Time to 3% enrichment (months)*	*Overall utilization factor @ Zone 1*
JET-lke	*19*	*0.74*
MAST-like	*17*	*0.64*

5 Conclusions and Future Work.

Present work is a compilation of the use of several computational tools that make possible to model a hybrid nuclear reactor and build several cases as an overall system for enhancing fusion analysis allowing the improvement of the capabilities that brings the use of fast neutrons to enforce the fission industry. In the first chapter an overall analysis of the nuclear industry was presented. There are several nuclear power plants running around the world (~440), proving that fission reactions is a matured technology. Natural ^{235}U reserves also were mentioned as an interesting window of time to develop a breeding fissile material strategy by the use of advanced nuclear cycles to augment the fissile isotopes reserves, even if these are anthropomorphic generated.

As per recent advances in the nuclear fusion research and experience, referenced in various published development articles, in the chapter three, first, it was explained a possible concept of a compact but intense source of neutrons design, CFNS, based in copper, low weighting, as a replaceable and removable module (king of a plug and play item with a surrounding fission blanket) permitting that damaged parts by neutron collisions can be removed periodically in a remote zone. Also, as the whole idea, the concept of having a fusion –fission hybrid reactor is presented, utilizing computational tools like MCNP, SCALE and the own developed tool to make a communication task between codes and data, easy and efficient. It was clear that with these tools is possible to build a complete model of the hybrid reactor and simulate its behavior for several cases to figure it out an optimum case that permits make interesting conclusions.

Chapter four is as such the model of a referenced specific reactor that permits the simulation of different cases, changing its material compositions to analyze its behavior, taking into account the neutron flux in the reactor zones as well as the tritium and ^{233}U production basically. Results shows that by changing the reactor geometry and the fixed material compositions, big differences can be obtained. In the case of tritium production, it is clear that the MAST-like geometry has a higher volumetric generation. Considering the center stack tritium breeding region as an example: the volume of this region for the JET-like configuration is twice the value of this same region in the MAST-like configuration. If the volumetric production rate were constant for both cases, the production rate in the JET-like configuration would be twice that of the MAST-like configuration. From the point of view of neutron flux, the situation is inverted: the flux for this region on the MAST-like device is 1 x 1015 cm-2 s-1, while for the JET scenario it is 6 x 1014 cm-2 s-1. The end production rate seems to be the balance between a reduction in the volume and an increase in the neutron flux.

Four cases were analyzed, all of them had a TBR > 1, and this assures at least that the main objective of the present work was achieved. Accordantly with the model developed and the materials chose, an excess of neutrons is attained permitting the generation of fissile material in the fission blanket. Different material compositions change reactor behavior in a very interesting way, beryllium element plays an important role in the reactor behavior because it is an efficient neutron multiplier. Those material configurations where Be is more present, have a better response in neutron production, and hence in the production of fissile material.

This project is the base for several research in the future plane, as was mentioned the concept of the ReFree cycle is also much more efficient, for a future work it can be proved, for the same thermal power, many thermal fission reactors can be fed by only one hybrid reactor. Burning actinides is also a future research that can be tested using this development. One of the more challenging problems that nuclear energy needs to face is the disposition of the highly radioactive waste generated

at nuclear power plants, transmuting these radioisotopes into a lower radioactivity levels is a task that can be analyzed with present tool, in fact, the tool can be configured to run for both purposes, burning actinides and breeding fissile materials, in a dual function manner. Finally, this tool can be used in the shuffling processes of nuclear fuel assemblies in the nuclear reactor core. In the case of the hybrid reactor, a shuffling analysis is an important task because of the burn of assemblies varies depending on the zone position in the fission blanket. In other words, this hybrid reactor model can be used to save time and money in the cumbersome shuffling tasks.

6 References

[1] The History of Nuclear Energy. U. S. Department of Energy. Office of Nuclear Energy, Science and Technology. Washington D. C. 20585. DOE/NE-0088.
[2] https://www.world-nuclear.org/information-library/current-and-futuregeneration/outline-history-of-nuclear-energy.aspx
[3] https://www.world-nuclear.org/information-library/current-and-future-generation/nuclear-power-in-the-world-today.aspx
[4] https://www.world-nuclear.org/information-library/current-and-future-generation/world-energy-needs-and-nuclear-power.aspx
[5] https://www.world-nuclear.org/information-library/nuclear-fuel-cycle/nuclear-waste/storage-and-disposal-of-radioactive-waste.aspx
[6] https://www.energy.gov/ne/articles/advantages-and-challenges-nuclear-energy
[7] Englert, Matthias & Krall, Lindsay & Ewing, R.. (2012). Is nuclear fission a sustainable source of energy?. MRS Bulletin. 37. 10.1557/mrs.2012.6.
[8] J. R. Lamarsh and A. J. Baratta, Introduction to Nuclear Engineering, 3rd ed., Prentice-Hall, New Jersey, USA, 2001.
[9] Englert, Matthias & Krall, Lindsay & Ewing, R.. (2012). Is nuclear fission a sustainable source of energy?. MRS Bulletin. 37. 10.1557/mrs.2012.6.
[10] https://www-pub.iaea.org/MTCD/publications/PDF/Pub1415_web.pdf
[11] http://www.jaif.or.jp/ja/wnu_si_intro/document/2009/m_salvatores_advanced_nfc.pdf
[12] https://en.wikipedia.org/wiki/File:Radioactive_decay_chains_diagram.svg
[13] https://www.world-nuclear.org/information-library/nuclear-fuel-cycle/introduction/physics-of-nuclear-energy.aspx
[14] https://en.wikipedia.org/wiki/Spent_fuel_pool
[15] https://www.vpr.org/post/psb-oks-second-fuel-storage-pad-vermont-yankee#stream/0
[16] https://www.intera.com/intera-solutions/regulatory-review-of-post-closure-safety-analysis-for-a-spent-nuclear-fuel-geological-repository-in-sweden/
[17] https://www.world-nuclear.org/information-library/current-and-future-generation/fast-neutron-reactors.aspx
[18] Walter Mitchell, III, and Stanley E. Turner. Breeder Reactors. United States Atomic Energy Commission. Division of Technical Information, Library of Congress Catalog Card Number: 76-611325. 1971.
[19] MYCLE SCHNEIDER (2009) Fast Breeder Reactors in France, Science & Global Security, 17:1, 36-53, DOI: 10.1080/08929880902953013
[20] https://www.world-nuclear.org/information-library/nuclear-fuel-cycle/nuclear-wastes/radioactive-waste-management.aspx
[21] Radioactive effluents from nuclear power stations and nuclear fuel reprocessing plants in the European Community. COMMISSION OF THE EUROPEAN COMMUNITIES, DISCHARGE DATA 1976 TO 1980 RADIOLOGICAL ASPECTS. MARCH 1983
[22] Guidelines for Pressure Relief and Effluent Handling Systems. By CCPS (Center for Chemical Process Safety) of The American Institute of Chemical Engineers. 1998.
[23] Silvawalker, Storm. (2019). Hypothetical Direct Electron Beam Inertial Electrostatic Confinement Nuclear Fusion Reactor.
[24] R. J. Barrett R. W. Hardie. The Fusion-Fission Hybrid as an Alternative to the Fast Breeder Reactor. LA-8503-MS Informal Report UC-80 Issued: September 1980.
[25] Colonna, N. & Belloni, Francesca & Berthoumieux, E. & Calviani, Marco & Domingo-Pardo, C. & Guerrero, C. & Karadimos, D. & Lederer, C. & Massimi, Cristian & Paradela, Carlos & Plag, R. & Praena, Javier & Sarmento, R.. (2010). Advanced nuclear energy systems and the need of accurate nuclear data: The n-TOF project at CERN. Energy Environ. Sci.. 3. 1910-1917. 10.1039/C0EE00108B.
[26] Mahdavi, Mohammad & Shahbahrami, Maryam. (2013). Multiplication of Fast Neutrons Source Flux by Using Deuterium-Helium-3 Plasma. ISRN High Energy Physics. 2013. 10.1155/2013/689739.

[27] Jeffery Lewins, Martin Becker. Advances in Nuclear Science and Technology: Volume 16. Library of Congress Catalog Card Number 62-13039. 1984 Plenum Press, New York.
[28] L. Lidsky, "Fusion–fission systems: hybrid, symbiotic, and augean," Nucl. Fus., 15, 151–173 (1975).
[29] Energy in Transition, 1985-2010: Final Report of the Committee on Nuclear and Alternative Energy Systems (1980). Chapter: 7 Controlled Nuclear Fusion
[30] The hybrid returns. Vol 460|2 July 2009. https://www.nature.com/news/2009/090701/pdf/460025a.pdf
[31] Research Needs for Fusion-Fission Hybrid Systems. Report of the Research Needs Workshop (ReNeW). Gaithersburg, Maryland Sept 30 – Oct 2, 2009
[32] Wallace Manheimer. Fusion Breeding for Mid-Century Sustainable Power. J Fusion Energy (2014) 33:199–234 DOI 10.1007/s10894-014-9690-9.
[33] W.M. Stacey et al., Fusion Sci. Technol. 47, 1210 (2005)
[34] 2827 NUCLEAR FUSION AND FISSION IN TH E SAME REACTOR . Freiburg , D . Elektron International ; No . 11 , 338 (1980) .
[35] R.A. Tinguely1,∗ , et al. White MIT Plasma Science and Fusion Center, Cambridge, MA, USA 02139. Neutron diagnostics for the physics of a high-field, compact, $Q \geq 1$ tokamak
[36] Mohamed A. Abdou (1985) Overview of Finesse Effort on Fusion Nuclear Technology, Fusion Technology, 8:1P2B, 1081-1090, DOI: 10.13182/FST85-A39916
[37] Peng Y. -K M., et al. A component test facility based on the spherical tokamak. Plasma Phys. Control. Fusion. 2005;47:263. doi: 10.1088/0741-3335/47/12B/S20.
[38] A.W. Morris, R.J. Akers, G.F. Counsell, T.C. Hender, B. Lloyd, A. Sykes, G.M. Voss, H.R. Wilson, Fusion Eng. Des. 74 (2005) 67.
[39] Y. Wu, H. Chen, J. Jiang, S. et al. The Fusion-Fission Hybrid Reactor for Energy Production: A Practical Path to Fusion Application. P.O. Box 1126, Hefei, Anhui, 230031, China.
[40] Gazi University, Faculty Arts & Science, Dept. of Physics, Ankara, Turkey. TRISO Fuel with LWR Spent Fuel in Fusion-Fission Hybrid Reactor System.
[41] Marques, Renato V.A.; Velasquez, Carlos E. et al. Liquid metal coolants for fusion-fission hybrid system: A neutronic analysis. Departamento de Engenharia Nuclear; Barros, Graiciany P. [ComissÃ£o Nacional de Energia Nuclear (CNEN), Rio de Janeiro, RJ (Brazil) 2017-07-01
[42] H. Salazar-Cravioto ; M. Nieto-Perez. Et al. Modeling of a Spherical Tokamak as an Extended Neutron Source Using ASTRA and MCNP.
[43] M. Kotschenreuther, P. Valanju and S. Mahajan, "Reprocessing free nuclear fuel production via fusion fission hybrids", Fusion Engineering and Design 4, pp. 303-317 (2012).
[44] S. C. Xiao, J. Zhao, X. Heng, X. Y. Sheng, Z. Zhou and Y. Yang, "Burn-up study of an innovative natural uranium-thorium fueled reprocessing-free fusion-fission hybrid reactor blanket with closed thorium-uranium fuel cycle", Fusion Science and Technology 68, n. 3, pp. 566-572 (2015).
[45] M. Kotschenreuther, P. Valanju, S. Mahajan, B. Covele, and D. Raj, "Deterministically Safe Highly Sub-Critical Fission-Fusion Hybrid Reactors", presented at the 24th IAEA Fusion Energy Conference, paper FTP/P7–08, San Diego, CA, Oct 8 – 13, 2012.
[46] R. Bari, L-Y Cheng, J. Phillips, J. Pilat, G. Rochau, I. Therios, R. Wigeland, E. Wonder, M. Zentner, Proliferation Risk Reduction Study of Alternative Spent Fuel Processing, Brookhaven National Laboratory Report BNL- 90264-2009-CP, 2009.
[47] H.G. Wood, A. Glaser, R. Scott Kemp, The gas centrifuge and nuclear weapons proliferation, Phys. Today (September) (2008).
[48] M.Perez-Gamboa M.Nieto-Pereza, et al. A 232Th closed fuel cycle utilizing both a thermal and hybrid nuclear systems. Progress in Nuclear Energy. Volume 83, August 2015, Pages 135-143
[49] Perez-Gamboa, M.L. & Nieto-Perez, M. & Mahajan, S. & Valanju, P.. (2013). Optimization of fusion-fission hybrid reactor fuel composition. 2013 IEEE 25th Symposium on Fusion Engineering, SOFE 2013. 1-5. 10.1109/SOFE.2013.6635505.
[50] J.l. François, j.j. Dorantes, c. Martín-del-campo, j.j.e. Herrera. "lwr spent fuel transmutation with hybrid fusion-fission reactors". Progress in nuclear energy. Vol. 65, pp. 50-55, 2013.
[51] V.P. Smirnov. Nuclear Fusion Institute, RRC 'Kurchatov Institute', Moscow, Russia. IOP PUBLISHING and INTERNATIONAL ATOMIC ENERGY AGENCY. NUCLEAR FUSION. "Tokamak foundation in USSR/Russia 1950–1990". Nucl. Fusion 50 (2010) 014003 (8pp).
[52] https://doi.org/10.1016/j.fusengdes.2015.03.002

[53] R Abraham, J E Marsden, and T Ratiu. Manifolds, Tensor Analysis, and Applications. volume 75 of Applied Mathematical Sciences. Springer, 2001.
[54] MULTIPLIER, MODERATOR, AND REFLECTOR MATERIALS FOR ADVANCED LITHIUM-VANADIUM FUSION BLANKETS. Y. Gohar and D. L. Smith Fusion Power Program, Argonne National Laboratory, 9700 S. Cass Avenue, Argonne, IL 60439, USA.
[55] Westinghouse Technology Manual. Chapter 17.0. Plant Operations. Nuclear Regulatory Commission (NRC) Documents.
[56] Physics and Engineering of the EPR. Keith Ardron. UK Licensing Manager, AREVA NP UK. Presentation to IOP Nuclear Industry Group Birchwood Park, Warrington UK, November 10 2010.
[57] Mike Kotschenreuther1, Prashant Valanaju1, Swadesh Mahajan1, Brent Covele1, Devesh Raj. Deterministically Safe Highly Sub-Critical Fission-Fusion Hybrid Reactors. FTP/P7-08
[58] Graignic, Pascal & Vosgien, Thomas & Jankovic, Marija & Tuloup, Vincent & Berquet, Jennifer & Troussier, Nadège. (2013). Complex System Simulation: Proposition of a MBSE Framework for Design-Analysis Integration. Procedia Computer Science. 16. 59–68. 10.1016/j.procs.2013.01.007.
[59] J. A. Wesson, P. Kirby, and M. F. Nave, in Plasma Physics and Controlled Nuclear Fusion Research 1986, Kyoto (IAEA, Vienna, 1987), Vol. 2, p. 3.
[60] De Tommasi, Gianmaria. (2018). Plasma Magnetic Control in Tokamak Devices. Journal of Fusion Energy. 10.1007/s10894-018-0162-5.
[61] https://www.iter.org/mach/Magnets

[62] William R. Ellis. LTPR A Linear Theta-Pinch Neutron Source. UC-20 Reporting Date: July 1975. LOS ALAMOS.
[63] Sykes, A. & Cunningham, G. & Gryaznevich, M. & Hood, M. & McArdle, Graham & Alladio, Franco & Costa, P. & Mancuso, A. & Micozzi, P. & Dnestrovskij, A.. (2004). Plasma formation without a central solenoid in a Spherical Tokamak.
[64] JB Lister, Y Martin, JM Moret. On locating the poloidal field coils for tokamak vertical position control.
[65] R Martin and MAST Team, IAEA Fusion Energy Conference, 2014, paper FIP/P8-26.
[66] J.E. Menard, T. Brown, L. El-Guebaly, M. Boyer, J. Canik, B. Colling, R. Raman, Z. Wang, Y. Zhai. Fusion nuclear science facilities and pilot plants based on the spherical tokamak.
[67] G. V. Pereverzev, P. N. Yushmanov. Automated System for TRansport Analysis. ASTRA. MAX-PLANCK-INSTITUT FUR PLASMAPHYSIK. IPP 5/98 February 2002.
[68] A.D. Turnbull, T.S. Taylor, M.S. Chu, R.L. Miller and Y.R. Lin-Liu. Synergism between cross-section and profile shaping in beta optimization of tokamak equilibria with negative central shear
[69] H.S. Bosch and G.M. Hale "Improved Formulas for Fusion Cross-sections and Thermal Reactivities" Nuclear Fusion, Vol. 32 No. 4, 1992, pp. 611-631.
[70] G. W. Hollenberg, Westinghouse Hanford Company C. E. Johnson, Argonne National Laboratory M. Abdou, University of California at Los Angeles. TRITIUM BREEDING MATERIALS.
[71] Shanliang, Zheng & Yican, Wu. (2006). Neutronic Comparison of Tritium-Breeding Performance of Candidate Tritium-Breeding Materials. Plasma Science and Technology. 5. 1995. 10.1088/1009-0630/5/5/011.
[72] P. Chiovaro and P.A. Di Maio. Assessment of the importance of neutron multiplication for tritium production. 17 November 2016 • © 2016 IAEA, Vienna
[73] Rubel, M. Fusion Neutrons: Tritium Breeding and Impact on Wall Materials and Components of Diagnostic Systems. J Fusion Energ 38, 315–329 (2019).
[74] High-resolution X-Ray diagnostic upgrade for ITER-like wall experiments at JET Amy Shumack ADAS workshop 29/9/14.
[75] T. A. Tomberlin. "Beryllium – A Unique Material In Nuclear Applications". Idaho National Engineering and Environmental Laboratory. November 15, 2004. 36th International SAMPE Technical Conference
[76] Journal of NUCLEAR SCIENCE and TECHNOLOGY, 25[1], pp.72~80 (January 1988). TECHNICAL REPORT
[77] MCNP — A General Monte Carlo N-Particle Transport Code, Version xx. Volume II: User's Guide. April 24, 2003. Los Alamos National Laboratory.
[78] SCALE 6.2. A Comprehensive Modeling and Simulation Suite for Nuclear Safety

Analysis and Design; Includes ORIGEN and AMPX. OAK RIDGE NATIONAL LABORATORY. RSICC COMPUTER CODE COLLECTION
[79] TRELLUE, HOLLY R. ; POSTON, DAVID I. USER'S MANUAL, VERSION 2.0 FOR MONTEBURNS, VERSION 5B. Los Alamos. September 1, 1999.
[80] https://codebeta.com/renci-ssh-for-net-5e07641f5851
[81] P.M. Valanju, M. Kotschenreuther, S.M. Mahajan, J. Reprocessing free nuclear fuel production via fusion fission hybrids. Fusion Engineering and Design 87 (2012) 303– 317
[82] https://www.iter.org/
[83] https://ccfe.ukaea.uk/research/mast-upgrade/
[84] https://www.euro-fusion.org/devices/jet/
[85] D. S. Gelles, J. Nuc. Mat. 239, p. 99, 1996
[86] https://www.world-nuclear.org/information-library/nuclear-fuel-cycle/conversion-enrichment-and-fabrication/uranium-enrichment.aspx
[87] https://mathworld.wolfram.com/PappussCentroidTheorem.html
[88] http://wwwf.imperial.ac.uk/~rn/centroid.pdf

Appendix A. Calculation of the plasma volume from the Turnbull expressions of the cross section.

The starting point will be the expressions for the "D" shaped plasma cross section, eq. (3.5), which is repeated here:

$$\frac{r}{R_p} = 1 + \varepsilon\, cos(\theta + \alpha sin\theta) \tag{A.1a}$$

$$\frac{z}{R_p} = \kappa\, \varepsilon\, sin\theta \tag{A.1b}$$

Recalling that there is an expression for the volume of revolution defined by a parametric closed contour [52], the volume of revolution for the 2D contour defined by the parametric equations (3.2a) and (3.2b) around the z axis for a given value of ε is:

$$V(\varepsilon) = \pi \int_0^{2\pi} r^2 \frac{dz}{d\theta} d\theta \tag{A.2}$$

Substituting the expressions for r and z and assuming equatorial symmetry, the integral in eq. (3.5) can be written as:

$$V(\varepsilon) = 2\pi R_p^3 \kappa \int_0^{\pi} [1 + \varepsilon\, cos(\theta + \alpha sin\theta)]^2 \varepsilon\, \cos\theta\, d\theta \tag{A.3}$$

The integral (A.3) can be broken down into three separate integrals:

$$\begin{aligned} V(\varepsilon) = 2\pi R_p^3 \kappa \Bigg[& \int_0^{\pi} \varepsilon\, \cos\theta\, d\theta \\ & + 2\int_0^{\pi} \varepsilon^2\, \cos(\theta + \alpha \sin\theta)\cos\theta\, d\theta \\ & + \int_0^{\pi} \varepsilon^3 \cos^2(\theta + \alpha sin\theta)\, \cos\theta\, d\theta \Bigg] \end{aligned} \tag{A.4}$$

The first integral in the RHS of (A.4) is trivial and gives zero. The other two integrals are only analytically solvable if $\alpha = 0$. Eq. (A.4) can be written as:

$$V(\varepsilon) = 2\pi R_p^3 \kappa\, (2\varepsilon^2 I_1 + \varepsilon^3 I_2) \tag{A.5}$$

The integrals I_1 and I_2 are numbers which depend only on the value of α, and they are given by:

$$\begin{aligned} I_1 &= \int_0^{\pi} \cos(\theta + \alpha\, \sin\theta)\cos\theta\, d\theta \\ I_2 &= \int_0^{\pi} \cos^2(\theta + \alpha\, \sin\theta)\cos\theta\, d\theta \end{aligned} \tag{A.6}$$

Figure A.1 presents the values of the two integrals as a function of α obtained by performing Simpson integration. The derivative of the volume with respect to the parameter ε can now be readily obtained from eq. (A.5):

$$\frac{dV}{d\varepsilon} = 2\pi R_p^3 \kappa \, (4\varepsilon I_1 + 3\varepsilon^2 I_2) \tag{A.7}$$

Equation (A.7) can now be inserted into eq. (3.8) for the calculation of the neutron source strength for the plasma volume up to the isobar line given by the upper limit in the integral (3.8).

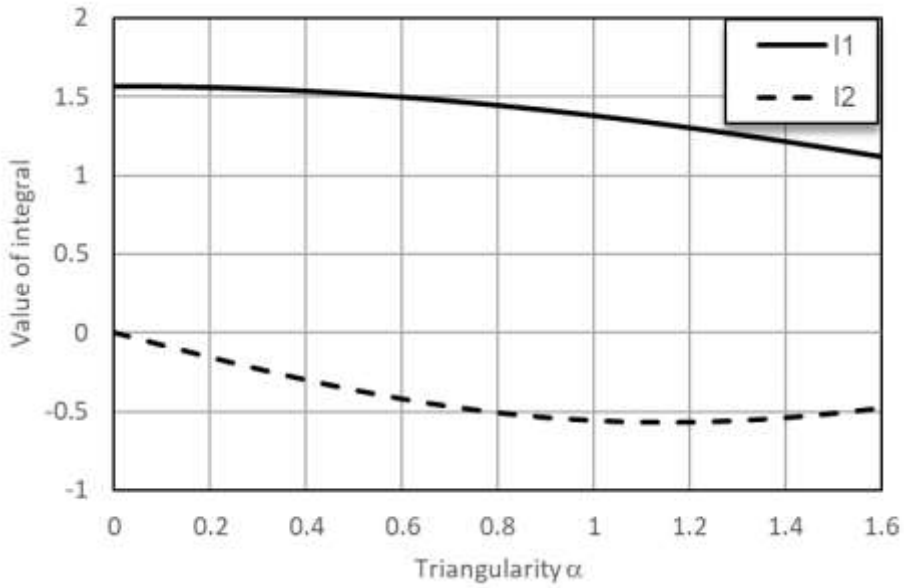

Figure A.1. Values of the integrals I_1 (solid line) and I_2 (dashed line) in eq. (A.6) as a function of the triangularity parameter α.

Appendix B. Structure of text input files for FFHYB.

Table B.I. Structure of the plasma source input file

Line	*Description*
1	*Date and time stamp for file creation*
2	*Blank line*
3	*Plasma geometry parameters header*
4	*Major radius (m)*
5	*Minor radius (m)*
6	*Elongation*
7	*Triangularity*
8	*Blank line*
9	*Profiles section header*
10	*Number of points in the profile*
11	*Column headers*
From 12 until end	*Values of ε, kT (keV) and n (m^{-3}), tab separated*

Table B.II. Definition of the tokamak file.

Line	*Description*
1	*Date and time stamp for file creation*
2	*Blank line*
3	*Center stack parameters section header*
4	*Height (m)*
5	*Maximum radius (m)*
6	*Minimum radius (m)*
7	*Toroidal field coil contact height (m)*
8	*Shield inner height (m)*
9	*Inboard tritium breeding region outer height (m)*
10	*Inboard tritium breeding region thickness (m)*
11	*Blank line*
12	*Tokamak cask section header*
13	*Side wall thickness (m)*
14	*Lid thickness (m)*
15	*Outer radius (m)*
16	*Blank line*
17	*Internal poloidal coil module (IPCM) section header*
18	*Height (m)*
19	*Inner radius (m)*
20	*Clad thickness (m)*
21	*Shield thickness (m)*
22	*Blank line*
23	*Neutron multipliers section header*
24	*Top multiplier thickness (m)*
25	*Length of top multiplier straight section (m)*
26	*z coordinate of top multiplier (m)*
27	*Side wall multiplier thickness (m)*
28	*Side wall multiplier height (m)*
29	*Side multiplier armor plate thickness (m)*
30	*Blank line*
31	*Poloidal field coils section header*
32	*Number of poloidal field coils*
From 33 until end	*Each line has the inner radius, outer radius, height and z coordinate for a poloidal field coil, tab separated*

Table B.III. Definition of the fission blanket file.

Line	*Description*
1	*Date and time stamp for file creation*
2	*Blank line*
3	*Blanket cask parameters section header*
4	*Height (m)*
5	*Inner radius (m)*
6	*Outer radius (m)*
7	*Wall thickness (m)*
8	*Blank line*
9	*Toroidal field coil section header*
10	*Coil height (m)*
11	*Outer radius (m)*
12	*Horizontal limb thickness (m)*
13	*Vertical limb thickness (m)*
14	*Blank line*
15	*Reflector and tritium breeding section header*
16	*Reflector horizontal limb thickness (m)*
17	*Reflector vertical limb thickness (m)*
18	*Tritium breeding region thickness (m)*
19	*Blank line*
20	*Fuel assemblies section header*
21	*Fuel assembly side length (m)*
22	*Assembly height (m)*
23	*Minimum gap between assemblies (m)*
24	*Assembly type*

Table B.IV. Definition of the materials collection file.

Line	Description
1	Date and time stamp for file creation
2	Blank line
3	Material list section header
4	Number of materials, *n*
5 – 4+*n*	Names of files for each material [a]
5+*n*	Blank line
6+*n*	Materials assignment section header
7+*n*	Poloidal field coil material [b]
8+*n*	Toroidal field coil material
9+*n*	Center stack material
10+*n*	Internal poloidal coil module cask material
11+*n*	Tokamak cask material
13+*n*	Fission blanket cask material
14+*n*	Side neutron multiplier armor plate material
15+*n*	Internal poloidal coil module shield material
16+*n*	Center stack shield material
17+*n*	Fission blanket reflector material
18+*n*	Side wall neutron multiplier material
19+*n*	Top neutron multiplier material
20+*n*	Tritium breeding material (tokamak interior)
21+*n*	Tritium breeding material (fission blanket)
22+*n*	Fission blanket coolant material
From 22+*n* to end	Fission blanket zones materials

[a] Individual material files must be placed in a "Materials" folder created within the folder for the Scenario.

[b] For material assignments, the number corresponding to the material in the list of materials that starts in line 5 should be provided.

Table B.V. Definition of the single material file.

Line	*Description*
1	*Date and time stamp for file creation*
2	*Blank line*
3	*Material name*
4	*Indicates if material is a molecular compound*
5	*Atoms per molecule (1 if not molecular compound)*
6	*Material density (g/cm^3)*
7	*Number of elements in the material*
From 8 to end	*Element specification as follows: symbol, density in g/cm^3, atomic fraction, atomic number of isotope 1, isotopic fraction of isotope 1, zero, atomic number of isotope 2, isotopic fraction of isotope 2, zero, atomic number of isotope 3, isotopic fraction of isotope 3, zero, and so on for all isotopes of the element*

Table B.VI. Definition of the remote connection information file [a].

Line	***Description***
1	*Server IP address*
2	*User name*
3	*Password*
4	*Connection port*
5	*Remote work directory*

[a] This file is encrypted, it cannot be edited manually, and a password is necessary for FFHYB to open it. User is prompted for the password when the program tires to read this file.

Table B.VII. Definition of the run parameters file.

Line	*Description*
1	*Date and time stamp for file creation*
2	*Blank line*
3	[illegible] *sym)*
4	*Number of MCNP histories per calculation*
5	*Total time for simulation (days)*
6	*Time step (days)*
7	*Number of neutron energy groups (96 or 238)*
8	*Threshold atomic fraction (isotope ignored if below this number)*
9	*Neutron multiplier dynamic flag*
10	*Neutron reflectors and shields dynamic flag*
11	*Tritium breeding regions dynamic flag*
12	*Center stack dynamic flag*
13	*Metallic walls dynamic flag*
14	*Poloidal field coils dynamic flag*
15	*Toroidal field coil dynamic flag*
16	*Poloidal coils plenum dynamic flag*
17	*IPCM interior volume dynamic flag*
18	*Coolant dynamic flag*

Table B.VIII. Definition of the scenario definition file.

Line	*Description*
1	*Date and time stamp for file creation*
2	*Blank line*
3	*Source definition file name*
4	*Tokamak geometry definition file name*
5	*Blanket geometry definition file name*
6	*Material list/material assignment file name*
7	*Remote connection parameters file name*
8	*Run parameters file name*

Appendix C. Density and composition of materials used for the hybrid device simulations.

Name	Elemental Composition	Density (g/cm^3)	Isotopes
Aluminum	Al (100%)	2.7	^{27}Al (100.0%)
Beryllium	Be (100%)	1.85	^{9}Be (100.0%)
Beryllium Oxide	Be (50%) O (50%)	3.02	^{9}Be (100.0%) ^{16}O (100.0%)
Copper	Cu (100%)	8.96	^{63}Cu (69.17%) ^{65}Cu (30.83%)
FLiBe	F (57.14%) Li (28.57%) Be (14.29%)	1.94	^{19}F (100.0%) ^{6}Li (7.59%), ^{7}Li (92.41%) ^{9}Be (100.0%)
HT-9 Steel	Fe (84.83%)	7.78	^{54}Fe (5.85%), ^{56}Fe (91.75%), ^{57}Fe (2.12%), ^{58}Fe (0.28%)
	Cr (12.78%)		^{50}Cr (4.35%), ^{52}Cr (83.79%), ^{53}Cr (9.50%), ^{54}Cr (2.36%)
	Mo (0.58%)		^{92}Mo (14.84%), ^{94}Mo (9.25%), ^{95}Mo (15.92%), ^{96}Mo (16.68%), ^{97}Mo (9.55%), ^{98}Mo (24.13%), ^{100}Mo (9.63%)
	W (0.15%)		^{180}W (0.12%), ^{182}W (26.50%), ^{183}W (14.31%), ^{184}W (30.64%), ^{186}W (28.43%)
	Ni (0.47%)		^{58}Ni (68.08%), ^{60}Ni (26.22%), ^{61}Ni (1.14%), ^{62}Ni (3.63%), ^{64}Ni (0.93%)
	V (0.27%)		^{50}V (0.25%), ^{51}V (99.75%)
	C (0.92%)		^{12}C(98.93%), ^{13}C (1.07%)
Lead	Pb (100.0%)	10.42	^{204}Pb (1.4%), ^{206}Pb (24.1%), ^{207}Pb (22.1%), ^{208}Pb (52.4%)
Lead-Bismuth eutectic	Pb (44.71%)	10.418	^{204}Pb (1.4%), ^{206}Pb (24.1%), ^{207}Pb (22.1%), ^{208}Pb (52.4%)
	Bi (55.29%)		^{209}Bi (100.0%)
Lead-Lithium eutectic	Pb (17%)	9.97	^{204}Pb (1.4%), ^{206}Pb (24.1%), ^{207}Pb (22.1%), ^{208}Pb (52.4%)
	Li (83%)		^{6}Li (7.59%), ^{7}Li (92.41%)
Lithium	Li (100.0%)	0.5	^{6}Li (7.59%), ^{7}Li (92.41%)
Lithium oxide	Li (66.67%) O (33.33%)	2.13	^{6}Li (7.59%), ^{7}Li (92.41%) ^{16}O (100.0%)
Thorium Oxide	Th (33.33%) O (66.67%)	10	^{232}Th (100.0%) ^{16}O (100.0%)

Appendix D. Calculation of region volume for the revolution of arbitrary convex polygons.

Consider a collection of n 2D points $\mathbf{p}_1$, $\mathbf{p}_2$,.., $\mathbf{p}_n$ defining a simple closed polygon, either convex or concave. The polygon will be rotated around the y axis to generate a solid of revolution, and it is of interest to calculate the volume of such solid.

The starting point is the second Theorem of Pappus [87], which states that the volume V of the solid of revolution generated by the revolution of a contour about an external axis is equal to the product of the area A of the polygon and the length of the path described by the centroid due to the rotation:

$$V = 2\pi A d \tag{D.1}$$

Here, d is the perpendicular distance of the contour's centroid point to the axis of rotation. The application of the second Pappus theorem requires knowledge of the polygon centroid's x coordinate c_x (since that is the perpendicular distance to the y axis, which is the axis of rotation) and the area enclosed by the polygon. The expressions for the area and the centroid x coordinate c_x, assuming the vertices are ordered sequentially counterclockwise, are given by [88]:

$$A = \frac{1}{2}\sum_{i=0}^{n-1}(x_i y_{i+1} - x_{i+1} y_i) \tag{D.2}$$

$$c_x = \frac{1}{6A}\left(\sum_{i=0}^{n-1}(x_i + x_{i+1})(x_i y_{i+1} - -x_{i+1} y_i)\right) \tag{D.3}$$

The volume of revolution V is therefore given by the following expression as a function of the polygon's vertices, ordered counterclockwise:

$$V = \frac{1}{6}\sum_{i=0}^{n-1}(x_i + x_{i+1})(x_i y_{i+1} - -x_{i+1} y_i) \tag{D.3}$$